

NAVAL POSTGRADUATE SCHOOL

Monterey, California



THESIS

DETECTION OF BINARY PHASE-SHIFT KEYING SIGNAL IN MULTIPATH PROPAGATION

by

Du San Jung

June 2002

Thesis Advisor:
Second Reader:

Charles W. Therrien
Murali Tummala

Approved for public release; distribution is unlimited

THIS PAGE INTENTIONALLY LEFT BLANK

REPORT DOCUMENTATION PAGE			<i>Form Approved OMB No. 0704-0188</i>	
Public reporting burden for this collection of information is estimated to average 1 hour per response, including the time for reviewing instruction, searching existing data sources, gathering and maintaining the data needed, and completing and reviewing the collection of information. Send comments regarding this burden estimate or any other aspect of this collection of information, including suggestions for reducing this burden, to Washington headquarters Services, Directorate for Information Operations and Reports, 1215 Jefferson Davis Highway, Suite 1204, Arlington, VA 22202-4302, and to the Office of Management and Budget, Paperwork Reduction Project (0704-0188) Washington DC 20503.				
1. AGENCY USE ONLY (Leave blank)		2. REPORT DATE June 2002	3. REPORT TYPE AND DATES COVERED Master's Thesis	
4. TITLE AND SUBTITLE: Detection of Binary Phase-Shift Keying Signal in Multipath Propagation			5. FUNDING NUMBERS	
6. AUTHOR(S) Jung, Du San				
7. PERFORMING ORGANIZATION NAME(S) AND ADDRESS(ES) Naval Postgraduate School Monterey, CA 93943-5000			8. PERFORMING ORGANIZATION REPORT NUMBER	
9. SPONSORING /MONITORING AGENCY NAME(S) AND ADDRESS(ES) N/A			10. SPONSORING/MONITORING AGENCY REPORT NUMBER	
11. SUPPLEMENTARY NOTES The views expressed in this thesis are those of the author and do not reflect the official policy or position of the Department of Defense or the U.S. Government.				
12a. DISTRIBUTION / AVAILABILITY STATEMENT Approved for public release; distribution unlimited			12b. DISTRIBUTION CODE	
13. ABSTRACT (maximum 200 words) <p>Time-varying dispersion and multipath propagation in a shallow underwater environment causes intersymbol interference in underwater communication. This thesis investigates a mitigation procedure for communication using a Binary Phase-Shift Keying (BPSK) signal. The method employed uses the time-reversed ocean impulse response to mitigate the degradation of the bit error rate performance. All results were achieved by the use of computer simulation of typical shallow water environments.</p>				
14. SUBJECT TERMS Binary Phase-Shift Keying, underwater acoustics, acoustic communication, underwater communication, BPSK, MMPE, parabolic equation			15. NUMBER OF PAGES 105	
			16. PRICE CODE	
17. SECURITY CLASSIFICATION OF REPORT Unclassified	18. SECURITY CLASSIFICATION OF THIS PAGE Unclassified	19. SECURITY CLASSIFICATION OF ABSTRACT Unclassified	20. LIMITATION OF ABSTRACT UL	

THIS PAGE INTENTIONALLY LEFT BLANK

Approved for public release; distribution is unlimited

**DETECTION OF BINARY PHASE-SHIFT KEYING SIGNAL IN MULTIPATH
PROPAGATION**

Du San Jung
Lieutenant, Korean Navy
B.S., Republic of Korea Naval Academy, 1993

Submitted in partial fulfillment of the
requirements for the degree of

MASTER OF SCIENCE IN ENGINEERING ACOUSTICS

from the

**NAVAL POSTGRADUATE SCHOOL
June 2002**

Author: Du San Jung

Approved by: Charles W. Therrien, Thesis Advisor

Murali Tummala, Second Reader

Kevin B. Smith, Chairman
Engineering Acoustics Academic Committee

THIS PAGE INTENTIONALLY LEFT BLANK

ABSTRACT

Time-varying dispersion and multipath propagation in a shallow underwater environment causes intersymbol interference in underwater communication. This thesis investigates a mitigation procedure for communication using a Binary Phase-Shift Keying (BPSK) signal. The method employed uses the time-reversed ocean impulse response to mitigate the degradation of the bit error rate performance. All results were achieved by the use of computer simulation of typical shallow water environments.

THIS PAGE INTENTIONALLY LEFT BLANK

TABLE OF CONTENTS

I.	INTRODUCTION.....	1
A.	GENERAL.....	1
B.	OBJECTIVE	1
C.	ORGANIZATION	1
II.	BINARY PHASE-SHIFT KEYING.....	3
A.	BINARY PHASE-SHIFT KEYING.....	3
B.	SIGNAL CONSTELLATION FOR BPSK.....	5
C.	PROBABILITY OF BIT ERROR FOR BPSK.....	5
D.	BIT ERROR PROBABILITY CONVERGENCE.....	10
E.	TWO TYPES OF BIT ERROR PERFORMANCE DEGRADATION	12
III.	EXPERIMENTAL DESCRIPTION	15
A.	BPSK SIGNAL GENERATION	15
B.	MMPE MODEL DESCRIPTION	18
1.	A Brief Description of the MMPE Model.....	18
2.	Signal Representation in MMPE	25
a.	<i>Time Windowing</i>	<i>27</i>
b.	<i>Processing of Bandpass Signals.....</i>	<i>28</i>
3.	Input Parameters for the MMPE Model.....	31
C.	OCEAN ENVIRONMENTAL CHARACTERIZATION.....	33
1.	Case 1: Positive SSP Gradient	33
2.	Case 2: Strong Negative SSP Gradient	34
3.	Case 3: Negative SSP Gradient Below Surface Duct.....	36
D.	BPSK DEMODULATION AND DETECTION	36
1.	Correlation Receiver.....	36
E.	MULTIPATH MITIGATION	39
IV.	SIMULATION RESULTS	43
A.	EVALUATION OF BIT ERROR PROBABILITY FOR BPSK SIGNAL	43
1.	Evaluation for BPSK Parameters	43
2.	Influence of AWGN on Bit Error Probability.....	48
B.	BIT ERROR DEGRADATION AND MULTIPATH MITIGATION FOR BPSK SIGNAL IN A SHALLOW WATER ENVIRONMENT	50
1.	Bit Error Performance Results for a Positive SSP Gradient.....	50
a.	<i>Investigation Of The One Specific Case</i>	<i>50</i>
b.	<i>Results For Many Chosen Ranges and Depths</i>	<i>58</i>
2.	Bit Error Performance Results for a Strong Negative SSP Gradient	60
3.	Bit Error Performance Results for a Negative SSP Gradient below Surface Duct	62

V.	CONCLUSIONS AND RECOMMENDATIONS.....	65
A.	CONCLUSIONS	65
B.	RECOMMENDATIONS.....	65
APPENDIX A. MMPE INPUT FILES FOR THREE DIFFERENT OCEAN ENVIRONMENTAL CASES		
A.	MMPE INPUT FILES FOR POSITIVE SSP GRADIENT	67
1.	pefiles.inp File of the Main Input File	67
2.	pesrc.inp File of the Source Data.....	67
3.	pessp.inp File of the Environmental Data	68
4.	pebath.inp File of the Environmental Data	68
5.	pebotprop.inp File of the Environmental Data	69
6.	pedbath.inp File of the Environmental Data	69
7.	pefiles.inp File of the Environmental Data	69
B.	MMPE INPUT FILES FOR STRONG NEGATIVE SSP GRADIENT ..	70
1.	pefiles.inp File of the Main Input File	70
2.	pessp.inp File of the Environmental Data	70
C.	MMPE INPUT FILES FOR NEGATIVE SSP GRADIENT BELOW SURFACE DUCT	71
1.	pefiles.inp File of the Main Input File	71
2.	pessp.inp File of the Environmental Data	71
APPENDIX B. DETAILED SIGNAL PROCESSING STEPS.....		
A.	RANDOM BINARY DATA GENERATION	73
B.	FILTERING	74
C.	GENERATION OF BPSK SIGNAL	74
D.	DEMODULATION OF BPSK SIGNAL, FILTERING.....	75
E.	BER COUNTING	76
APPENDIX C. COMPLETE PROCEDURES TO GENERATE THE PASSBAND OCEAN IMPULSE RESPONSE AND FREQUENCY RESPONSE FROM THE MMPE MODEL		
A.	MODIFIED OCEAN FREQUENCY RESPONSE AND OCEAN IMPULSE RESPONSE FROM MMPE MODEL	79
B.	BASEBAND OCEAN IMPULSE RESPONSE BY PADDING ZEROS ..	79
C.	FILTERING AND PRE-ENVELOPE OF THE OCEAN IMPULSE RESPONSE	81
D.	PASSBAND OCEAN IMPULSE RESPONSE.....	82
LIST OF REFERENCES		83
INITIAL DISTRIBUTION LIST		85

LIST OF FIGURES

Figure 2.1.	BPSK Signal in the Time Domain.	3
Figure 2.2.	BPSK Signal in Frequency Domain.	4
Figure 2.3.	Signal Constellation for BPSK.	5
Figure 2.4.	Conditional Probability Density Functions: $p(z s_1)$, $p(z s_2)$	8
Figure 2.5.	General Shape of the P_B versus E_b/N_o Curve.....	11
Figure 2.6.	(a) Loss in E_b/N_o . (b) Irreducible P_B Caused by Distortion.	13
Figure 3.1.	BPSK Signal Generation.	15
Figure 3.2.	Three Stages to Extract Ocean Response from MMPE Model.	18
Figure 3.3.	Pulse Arriving after Propagation Delay t	26
Figure 3.4.	Spectrum of Bandpass Signal.	27
Figure 3.5	Spectrum of a Complex Valued Lowpass Signal Corresponding to Bandpass Signal of Figure 3.4.	29
Figure 3.6.	pefiles.inp File of the Main Input File.....	31
Figure 3.7.	pesrc.inp File of the Source Data.	32
Figure 3.8.	pessp.inp File of the Environmental Data.	33
Figure 3.9.	(a) Positive SSP (b) Sound Propagation at Frequency 400 Hz, Source 5 m...34	
Figure 3.10.	(a) Negative SSP (b) Sound Propagation at Frequency 400 Hz, Source 30 m.....	35
Figure 3.11.	(a) SSP (b) Sound Propagation at Frequency 400 Hz, Source 5 m.	36
Figure 3.12.	Two Basic Steps in the Demodulation/Detection of the Received Signal.	37
Figure 3.13.	Correlator Receiver.	38
Figure 3.14	Multipath Mitigation for the Distorted Signal in Underwater Environment. ..	40
Figure 4.1.	The Power Spectral Density for BPSK Signal.....	44
Figure 4.2.	General FIR Filter (Hamming Window Design).	46
Figure 4.3.	Frequency Response for BPSK Signal Sampled by Null-to-null Bandwidth.	47
Figure 4.4.	Frequency Response for BPSK Signal Sampled by Power Bandwidth.	47
Figure 4.5.	BER versus $SNR_{(dB)}$	49
Figure 4.6.	BPSK Signal in Time Domain and Frequency Domain.	51
Figure 4.7.	Passband Ocean Frequency Response (Magnitude and Phase) and Ocean Impulse Response.	52
Figure 4.8.	Received Signal in Time Domain and Frequency Domain.	53
Figure 4.9.	Comparison of Recovered Binary Data with Transmitted Binary Data for the Received Signal.	54
Figure 4.10.	Time Reversed Ocean Frequency Response (Magnitude and Phase) and Ocean Impulse Response.	55
Figure 4.11.	Mitigated Ocean Impulse Response and Frequency Response.....	56
Figure 4.12.	Mitigated Signal in Time and Frequency Domain.....	57
Figure 4.13.	Comparison of Recovered Binary Data with Transmitted Binary Data for Mitigated Signal Showing Zero Error.....	57

Figure 4.14.	Bit Error Performance for Received Signal at Chosen Depths 5 to 95 m and Ranges 0.5 to 9.5 km for a Positive SSP Gradient.	59
Figure 4.15.	Bit Error Performance for Mitigated Signal at Chosen Depths 5 to 95 m and Ranges 0.5 to 9.5 km for a Positive SSP Gradient.	60
Figure 4.16.	Bit Error Performance for Received Signal at Chosen Depths 5 to 95 m and Ranges 0.5 to 9.5 km for a Strong Negative SSP Gradient.	61
Figure 4.17.	Bit Error Performance for Mitigated Signal at Chosen Depths 5 to 95 m and Ranges 0.5 to 9.5 km for a Strong Negative SSP Gradient.	62
Figure 4.18.	Bit Error Performance for Received Signal at Chosen Depths 5 to 95 m and Ranges 0.5 to 9.5 km for a Negative SSP Gradient below Surface Duct.	63
Figure 4.19.	Bit Error Performance for Mitigated Signal at Chosen Depths 5 to 95 m and Ranges 0.5 to 9.5 km for a Negative SSP Gradient below Surface Duct.	64
Figure B-1.	Random Binary Data in Time Domain and Frequency Domain.	73
Figure B-2.	Frequency Response of the FIR Filter and the Filtered Binary Data.	74
Figure B-3.	BPSK Signal $s[n]$ in Time Domain and Frequency Domain.	75
Figure B-4.	Demodulated BPSK Signal $y[n]$ in Frequency Domain.	76
Figure B-5.	Demodulated and Filtered BPSK Signal in Time and Frequency Domain.	76
Figure B-6.	Comparison between Recovered Binary Data and Transmitted Binary Data.	77
Figure C-1.	Modified Ocean Frequency Response $H'(f)$ and Impulse Response $h'[n]$	80
Figure C-2.	Baseband Ocean Frequency Response $H_o(f)$ and Impulse Response $h_o[n]$	80
Figure C-3.	Frequency Response of FIR Filter and Filtered Baseband Ocean Frequency Response.	81
Figure C-4.	Pre-Envelope Ocean Frequency Response $H_p(f)$	82
Figure C-5.	Passband Ocean Frequency Response $H_b(f)$	82

LIST OF VARIABLES

AWGN	additive white Gaussian noise
A_c	sinusoidal carrier amplitude
$\{a_n\}$	message data or a set of random variables with $a_n = \pm 1$
BPSK	binary phase-shift keying
$b(t)$	random binary signal
$B_T(f)$	Fourier transform of the truncated signal, $b_T(t)$
$B(f)$	Fourier transform of a random binary signal
$b_T(t)$	truncated signal of $b(t)$
$b[n]$	discrete random binary data
$b_f[n]$	filtered random binary data
$c(\bar{x})$	sound speed
c_0	reference sound speed
DFT	Discrete Fourier Transform
$d[n]$	cosine demodulating signal
E_b	average energy per bit
f_c	center frequency or carrier frequency
f_s	sampling frequency
f_s'	up-sampling frequency
$FT[\cdot]$	Fourier transform
$FT^{-1}[\cdot]$	inverse Fourier transform
$g(t - nT_b)$	rectangular pulse with bit time duration, T_b
$G(f)$	Fourier transform for a rectangular pulse

$h(t)$	ocean impulse response
$h(-t)$	time-reversed ocean impulse response
$H(f)$	ocean frequency response
$H'(f)$	modified ocean frequency response
$h[n]$	discrete ocean impulse response
$h'[n]$	modified ocean impulse response
$h_b[n]$	passband ocean impulse response
$H_b(f)$	passband ocean frequency response
$h_t[n]$	time-reversed ocean impulse response
$h_m[n]$	mitigated ocean impulse response
$h_o[n]$	baseband ocean impulse response
$H_o(f)$	baseband ocean frequency response
$h_p[n]$	pre-envelope of passband ocean impulse response
$H_p(f)$	pre-envelope of passband ocean frequency response
$h_{LPF}[n]$	FIR lowpass filter
ISI	intersymbol interference
I	interpolation factor
$k[n]$	cosine modulating signal
k_o	reference wavenumber
L	number of time and frequency samples used in the transform
l	index of refraction
$n(t)$	additive white Gaussian noise
n_o	noise component of the output of the correlator
N_{bit}	number of bits in the transmitted binary data
$N_o/2$	two-sided noise power spectral density
N_o	noise power spectral density
N	noise power
N_{sb}	number of samples per bit

P_B	probability of bit error
P_E	probability of symbol error
$P(s_i s_j)$	conditional probabilities
$p(z s_j)$	conditional probability density function
$P(s_i)$	prior probability of the symbols
pdf	probability density function
PSD	power spectral density
$P_b(f)$	PSD for a random binary signal with a rectangular pulse
$P_s(f)$	PSD of BPSK signal
$p(\vec{x}, t)$	acoustic pressure as a function of position \vec{x} and time t
$P_{BPSK}^+(f)$	single-sided power spectral density
$q(t)$	received signal
$q[n]$	discrete time received signal
$Q(\cdot)$	complementary error function
r	range
R	bit rate (<i>bits/sec</i>)
s_{BPSK}	BPSK signal set
$s(t)$	BPSK signal
$s_b(t)$	continuous-time real bandpass signal
$s[n]$	discrete time BPSK signal
$s_p(t)$	“in-phase” modulation components
$s_q(t)$	“quadrature” modulation components
$\tilde{s}(t)$	complex envelope of BPSK signal
$\hat{s}(t)$	mitigated signal
$\hat{s}[n]$	discrete time mitigated signal
$S[k]$	DFT coefficient of $s[n]$
S	signal power
SNR	average signal power to average noise power ratio

$SNR_{\text{(dB)}}$	SNR in decibels
$s(\vec{x}, t)$	sound source distribution as a function of position \vec{x} and time t
$\tilde{S}(f)$	frequency spectrum of a complex valued low-pass signal
$S_b(f)$	frequency spectrum of bandpass signal
Δt	sampling interval
T_b	bit time duration or symbol time duration
t	time
t'	reduced time
TL	transmission loss
v_i	signal component of the output of the correlator
$w_1(t)$	single waveform for the BPSK signal set
W	bandwidth
\mathbf{w}	digital frequency
\vec{x}	spatial position at which the pressure signal is measured
$y(t)$	recovered signal
$y[n]$	discrete time recovered signal
$z(T_b)$	correlator output or decision statistic at bit time duration T_b
z	depth
\mathbf{g}_o	decision threshold
\mathbf{s}_o^2	white Gaussian noise variance
$\mathbf{f}(t)$	sinusoidal carrier

$\Phi(f)$ Fourier transform of a sinusoidal carrier $\mathbf{f}(t)$

$\mathbf{d}(\cdot)$ delta function

$\Psi(r, z, \mathbf{j}, f)$ PE field function

t gross propagation delay
 t_o propagation delay

\mathbf{j} azimuthal angle

$\Theta_i(t)$ phase term of transmitted BPSK signal

THIS PAGE INTENTIONALLY LEFT BLANK

ACKNOWLEDGMENTS

I wish to give recognition to:

My thesis advisor, Professor Charles W. Therrien, for his time and support in past one year. His expertise advice, directions and great help were an enormous support to me in achieving this thesis.

My second reader, Professor Murali Tummala, for his time and help. Especially discussing the results with him was a great help to me.

Professor, Kevin B. Smith, for valuable comments

My wife, Sug Hyun Park, for her love, devotion and encouragement throughout my tour at the Naval Postgraduate School. Thanks to her outstanding skills as a mother and a wife. I will always love you, perhaps some days more than others.

My two sons, Sung Yeop and Sung Moon. Although they are probably too young to realize, they constantly kept my daily life in the correct perspective.

My parents, Tae Young Jung and Cha Soon Cho, for their never-ending love and encouragement for me.

My country and Republic of Korea Navy for sending me to NPS to have this education and opportunity. NPS not only gave me a good technical knowledge but also awarded me a different way of looking at life.

THIS PAGE INTENTIONALLY LEFT BLANK

I. INTRODUCTION

A. GENERAL

The underwater environment is the most challenging region of the battle space in which to communicate effectively. Sound propagation in an underwater communication channel becomes a very difficult task due to numerous constraints and limitations imposed by the nature of the medium and the environment. The most important characteristics of the underwater environment that put limitations on the performance of underwater communication are dispersion caused by the spatial and temporal variability and multipath propagation. Multipath propagation produces intersymbol interference (ISI) and severe degradation of the bit error performance in digital communication. The specific investigation in this thesis is the demodulation of Binary Phase-Shift Keying (BPSK) in three different shallow water ocean acoustic channels.

B. OBJECTIVE

The objective of this thesis was to study the possibility of using the time-reversed ocean impulse response prior to the demodulation of a BPSK signal to mitigate the degradation of the bit error performance in multipath propagation. The thesis evaluates the bit error performance of the mitigated signal compared to the bit error performance of the received signal distorted by the intersymbol interference in three different ocean environments in the absence of noise.

C. ORGANIZATION

The remainder of this thesis is organized as follows. Chapter II gives the general theory related to BPSK binary communication. This describes the definition, waveform and constellation of the BPSK signal, the theoretical convergence of the bit error probability, and two types of the bit error degradation factors. Chapter III describes the experiments and simulation procedure used in this thesis. This includes a time-domain and frequency-domain BPSK representation, Power Spectral Density (PSD) for BPSK, a description of the Monterey-Miami Parabolic Equation (MMPE) model, the ocean impulse response extraction from MMPE model, BPSK demodulation and multipath mitigation. Chapter IV provides the main results of the simulation. Included in the results are the evaluation for the bit error performance of the BPSK signal, bit error degradation

and multipath mitigation for BPSK signal in three different shallow water acoustic channels.

II. BINARY PHASE-SHIFT KEYING

This chapter describes the general theory related to binary phase-shift keying (BPSK). First, the definition, waveform and its constellation for BPSK modulation are explained. Next, as an important criterion of performance in digital communication, the probability of bit error is defined and the theoretical convergence of the bit error probability is described. Finally, two types of the bit error degradation factors are presented.

A. BINARY PHASE-SHIFT KEYING

In binary phase-shift keying (BPSK), the phase of a constant-amplitude carrier signal is switched between two values according to the two possible “messages” m_1 and m_2 corresponding to binary 1 and 0, respectively. Normally, the two phases are separated by 180 degrees. If the sinusoidal carrier has amplitude A_c , then the average energy per bit is $E_b = \frac{1}{2} A_c^2 T_b$ where T_b is the bit time duration, and the transmitted BPSK signal can be represented as:

$$s_i(t) = \sqrt{\frac{2E_b}{T_b}} \cos[2\pi f_c t + \Theta_i(t)] \quad \begin{matrix} 0 \leq t \leq T_b \\ i = 1, 2 \end{matrix} \quad (2.1)$$

where the phase term, $\Theta_i(t)$, will have two discrete values, given by $\Theta_1=0$ and $\Theta_2=\pi$. In other words, in BPSK modulation, the modulating data signal shifts the phase of the waveform $s_i(t)$ to one of two states, either zero or $\pi(180^\circ)$. Instead of using a rectangular shaped pulse as shown in Figure 2.1, we can use non-rectangular shaped pulses by applying hanning, hamming, and Gaussian windows. However, we shall adhere to the simplest case of a rectangular pulse in this thesis.

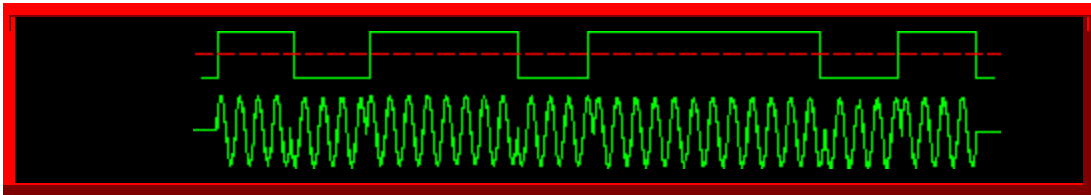


Figure 2.1. BPSK Signal in the Time Domain.

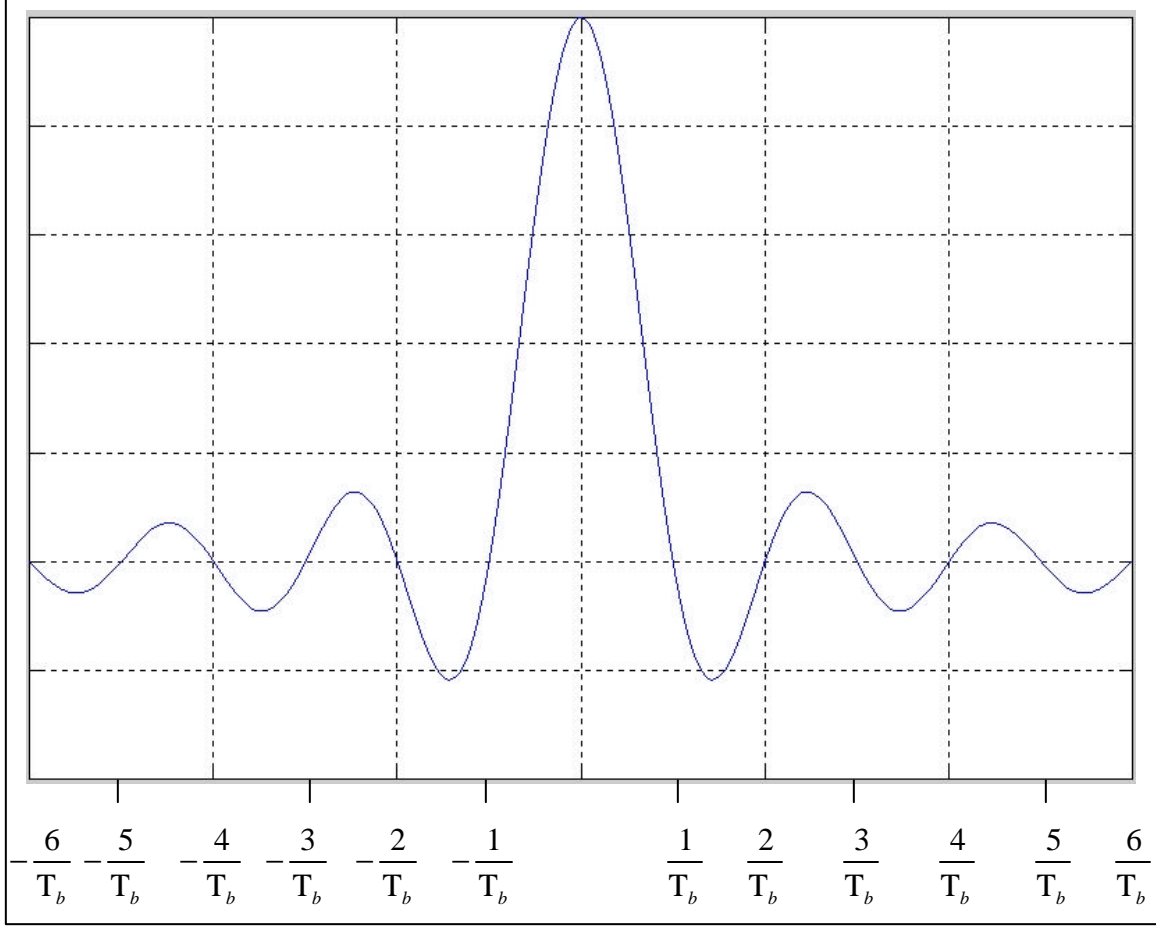


Figure 2.2. BPSK Signal in Frequency Domain.

Figure 2.1 shows a typical BPSK waveform in the time domain with its abrupt phase changes at the symbol transitions. The sketch in Figure 2.2 shows the spectrum of the BPSK waveform in frequency domain. For this signal set, the single waveform

$$w_1(t) = \sqrt{\frac{2}{T_b}} \cos(2\pi f_c t) \quad 0 \leq t \leq T_b \quad (2.2)$$

can be defined. Using this signal, the BPSK signal set can be represented as

$$s_{BPSK} = \left\{ \sqrt{E_b} w_1(t), -\sqrt{E_b} w_1(t) \right\} \quad (2.3)$$

B. SIGNAL CONSTELLATION FOR BPSK

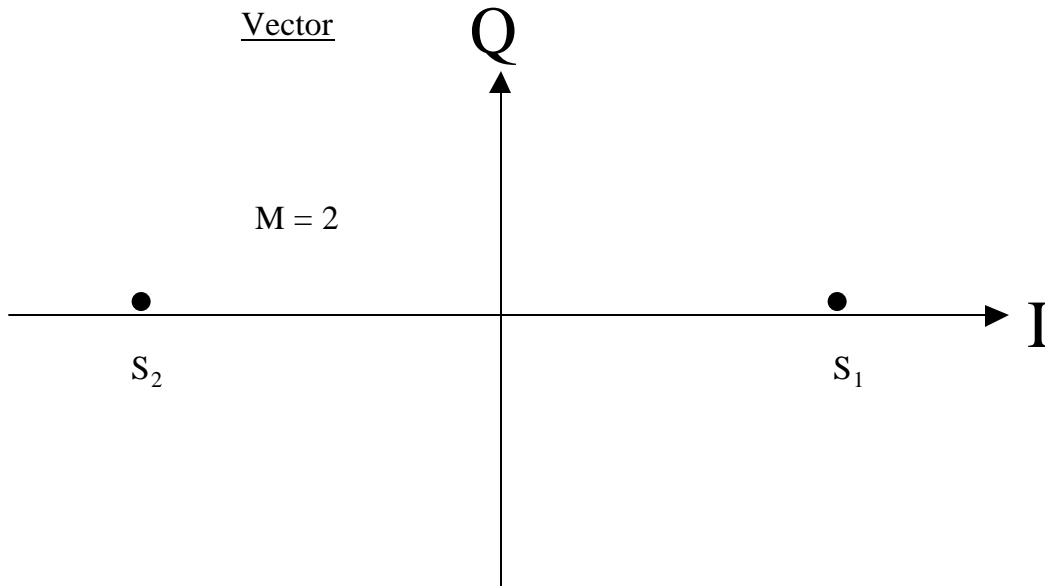


Figure 2.3. Signal Constellation for BPSK.

A BPSK signal waveform, as shown in Figure 2.3, can be geometrically represented as vectors or phasors on a polar plot; the vector length corresponds to the signal amplitude, and the vector direction corresponds to the phase. Such a representation is referred to as the symbol constellation and provides a graphical representation of the complex envelope of a BPSK signal for the two possible symbols. The I-axis of the constellation diagram represents the “in-phase” component of the complex envelope, and the Q-axis represents the “quadrature” component of the complex envelope. The distance between the signals on a constellation diagram measures separation of the modulation waveforms and determines how well a receiver can differentiate between all possible symbols when random noise is present. The larger the signal distance, the better the chance of correct symbol detection.

C. PROBABILITY OF BIT ERROR FOR BPSK

An important measure of performance used for digital modulation is the probability of symbol error, P_E . It is often convenient to specify system performance by

the probability of bit error P_B , even when decisions are made on the basis of symbols rather than bits. The relationship between P_B and P_E for orthogonal signaling is:

$$P_B = \frac{P_E}{\log_2 M} \quad (2.4)$$

where M is the number of symbols.

For BPSK modulation ($M=2$), the symbol error probability is equal to the bit error probability. When the signals are assumed equally likely and signal $s_i(t)$ ($i=1,2$) is transmitted, the received signal, $q(t)$, is equal to $s_i(t) + n(t)$, where $n(t)$ is modeled as additive white Gaussian noise (AWGN). The antipodal signals (signals of equal amplitude and opposite polarity) $s_1(t)$ and $s_2(t)$ are [cf. Eq. (2.3)]:

$$s_1(t) = \sqrt{E_b} w_1(t) \quad 0 \leq t \leq T_b \quad (2.5)$$

$$s_2(t) = -\sqrt{E_b} w_1(t) \quad 0 \leq t \leq T_b \quad (2.6)$$

The detection and demodulation of the received signal involves a correlation with each of the antipodal signals, as explained in Chapter 3. At the end of each symbol duration T_b , the output of the correlator yields a sample $z(T_b)$, called the detection statistic given by

$$z(T_b) = v_i(T_b) + n_o(T_b) \quad i=1,2 \quad (2.7)$$

where $v_i(T_b)$ is the desired signal component and $n_o(T_b)$ is the noise component. The noise component is a zero mean Gaussian random variable, and thus $z(T_b)$ is a Gaussian

random variable with a mean of either v_1 or v_2 depending on whether $s_1(t)$ or $s_2(t)$ was sent.

The decision stage of the detector will choose the $s_i(t)$ with the largest correlator output $z_i(t)$, or in this case of equal-energy antipodal signals, the detector, using the decision rules, decides:

$$s_1(t) \quad \text{if} \quad z(T_b) > g_o \quad (2.8)$$

$$s_2(t) \quad \text{otherwise} \quad (2.9)$$

where g_o denotes the decision threshold (equal to 0 for equally probable antipodal signals) and $z(T_b)$ is the correlator output at time T_b . Two types of detection errors can be made. The first type of error takes place if $s_1(t)$ is transmitted but the detector measures a negative value for $z(T_b)$ and decides (incorrectly) that signal $s_2(t)$ was sent. The second type of error takes place if signal $s_2(t)$ is transmitted but the detector measures a positive value for $z(T_b)$ and decides (again incorrectly) that signal $s_1(t)$ was sent. Therefore, the probability of bit error, P_B , is the sum:

$$P_B = P(s_2|s_1)P(s_1) + P(s_1|s_2)P(s_2) \quad (2.10)$$

where $P(s_i|s_j)$ are the conditional probabilities and $P(s_i)$ are the prior probability of the symbols. For the case when the symbols are equally likely (which is mostly the case):

$$P(s_1) = P(s_2) = \frac{1}{2} \quad (2.11)$$

The expression for the bit error probability then becomes:

$$P_B = \frac{1}{2} P(s_2|s_1) + \frac{1}{2} P(s_1|s_2) \quad (2.12)$$

The conditional probabilities $P(s_2|s_1)$ and $P(s_1|s_2)$ are found by integrating the conditional probability density function (pdf) of the output of the correlator which is depicted in Figure 2.4

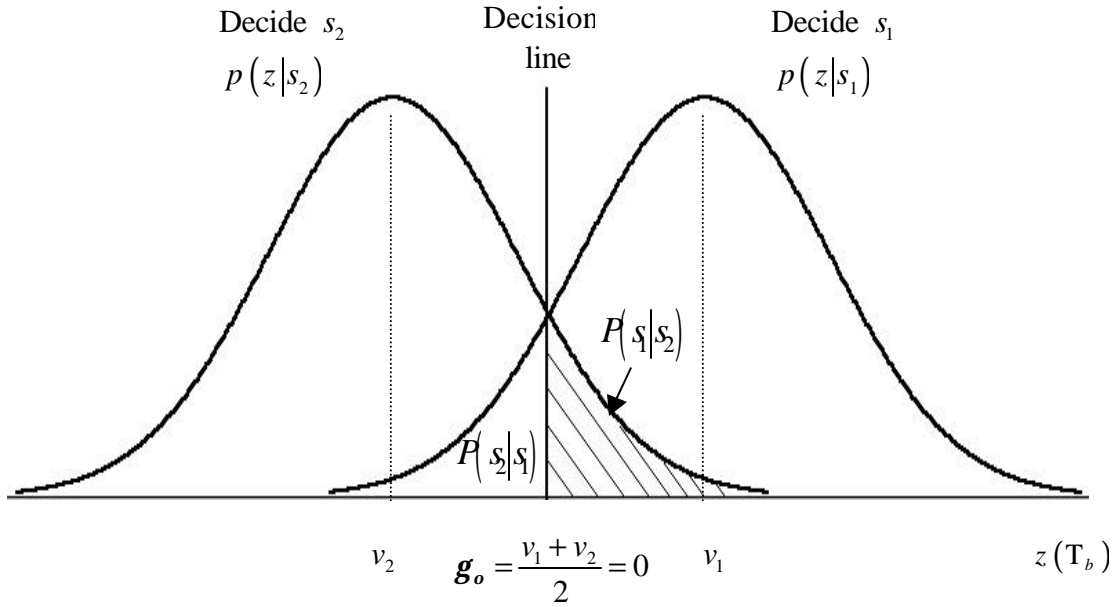


Figure 2.4 Conditional Probability Density Functions: $p(z|s_1)$, $p(z|s_2)$

The conditional probability density functions (pdf's) of the signal with an additive white Gaussian noise (AWGN) are:

$$p(z|s_i) = \frac{1}{\sqrt{2\pi s_o}} \exp \left[-\left(\frac{z - v_i}{\sqrt{2s_o}} \right)^2 \right] \quad i = 1, 2 \quad (2.13)$$

i.e., the conditional pdf's $p(z|s_i)$ ($i=1,2$) are Gaussian with mean value v_i , and variance \mathbf{s}_o^2 where \mathbf{s}_o^2 corresponds to the noise variance at the output of the correlator. Because of the symmetry of $p(z|s_i)$, the bit error probability of Eq. (2.12) reduces to:

$$P_B = P(s_2|s_1) = P(s_1|s_2) \quad (2.14)$$

Thus, the probability of a BPSK bit error P_B is numerically equal to the area under the “tail” of either pdf $p(z|s_1)$ or $p(z|s_2)$ that falls on the incorrect side of the threshold. We can therefore compute P_B by either integrating $p(z|s_1)$ between the limits $-\infty$ and g_o or by integrating $p(z|s_2)$ between the limits g_o and ∞ , where $g_o = (v_1 + v_2)/2$ is the optimum threshold. Hence,

$$P_B = \int_{g_o}^{\infty} p(z|s_2) dz \quad (2.15)$$

Using Eq. (2.13), the probability of bit error for BPSK is:

$$P_B = \int_{g_o}^{\infty} \frac{1}{\mathbf{s}_o \sqrt{2\mathbf{p}}} \exp \left[-\frac{1}{2} \left(\frac{z - v_2}{\mathbf{s}_o} \right)^2 \right] dz \quad (2.16)$$

If we introduce $u = \frac{z - v_2}{\mathbf{s}_o}$ and $\mathbf{s}_o du = dz$, the integral simplifies to

$$P_B = \int_{(v_1 - v_2)/2\mathbf{s}_o}^{\infty} \frac{1}{\sqrt{2\mathbf{p}}} \exp \left(-\frac{u^2}{2} \right) du = Q \left(\frac{v_1 - v_2}{2\mathbf{s}_o} \right) \quad (2.17)$$

where $Q(\cdot)$ is the complementary error function defined as:

$$Q(x) = \frac{1}{\sqrt{2\pi}} \int_x^\infty \exp\left(-\frac{u^2}{2}\right) du \quad (2.18)$$

For equal energy antipodal signaling, such as the BPSK format in Eq. (2.3), the receiver output signal components are $v_1 = \sqrt{E_b}$ when $s_1(t)$ is sent and $v_2 = -\sqrt{E_b}$ when $s_2(t)$ is sent. For AWGN, the noise variance σ_o^2 of the correlator output can be written as $N_o/2$, where $N_o/2$ is two-sided power spectral density of the noise. Thus, we can rewrite probability of bit error as follows:

$$P_B = \int_{\sqrt{2E_b}/N_o}^\infty \frac{1}{\sqrt{2\pi}} \exp\left(-\frac{u^2}{2}\right) du = Q\left(\sqrt{\frac{2E_b}{N_o}}\right) \quad (2.19)$$

D. BIT ERROR PROBABILITY CONVERGENCE

In digital communications, we more often use E_b/N_o , a normalized version of average signal power to average noise power ratio (S/N or SNR), as a figure of merit. E_b is bit energy and can be described as signal power S times the bit time T_b . N_o is noise power spectral density, and can be described as noise power N divided by bandwidth W . Since the bit time and bit rate R_b are reciprocal, we can replace T_b with $1/R_b$ and write

$$\frac{E_b}{N_o} = \frac{ST_b}{N/W} = \frac{S/R_b}{N/W} \quad (2.20)$$

If we use R instead of R_b to represent bits/sec, and we rewrite Equation (2.20) to emphasize that E_b/N_o is just a version of S/N normalized by bandwidth and bit rate, we obtain:

$$\frac{E_b}{N_o} = \frac{S}{N} \left(\frac{W}{R} \right) \quad (2.21)$$

One of the most important metrics of performance in a digital communication system terms is a plot of the bit error probability P_B versus E_b/N_o . Figure 2.5 shows the “waterfall-like” shape of most such curves.

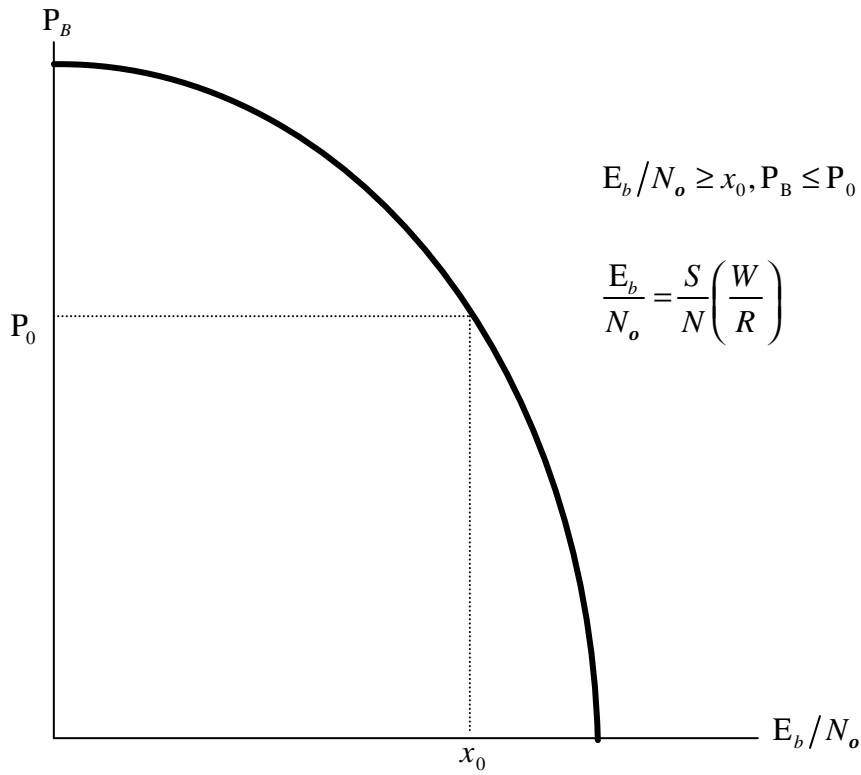


Figure 2.5. General Shape of the P_B versus E_b/N_o Curve.

For $E_b/N_o \geq x_0, P_B \leq P_0$. The dimensionless ratio E_b/N_o is a standard quality measure for digital communications system performance. Therefore, the smaller the required E_b/N_o , the more efficient is the detection process for a given probability of error.

To optimize (minimize) P_B in the context of an AWGN channel and the receiver, we need to select the optimum receiving filter and the optimum decision threshold. For the binary case, the optimum decision threshold is $g_o = (v_1 + v_2)/2$ and it was shown in Equation (2.17) that this threshold results in $P_B = Q[(v_1 - v_2)/2s_o]$. Next, for minimizing P_B , it is necessary to maximize the argument of $Q(x)$. Thus, we need to maximize $(v_1 - v_2)/2s_o$ or equivalently, maximize

$$SNR = \frac{(v_1 - v_2)^2}{s_o^2} \quad (2.22)$$

where $(v_1 - v_2)$ is the difference of the desired signal components at the filter output at time $t = T_b$, and the square of this difference signal is the instantaneous power of the difference signal. The SNR can also be maximized by minimizing s_o^2 ; however, s_o^2 is usually not under our control.

E. TWO TYPES OF BIT ERROR PERFORMANCE DEGRADATION

The effects of bit error performance degradation can be partitioned into two categories. The first is due to a decrease in received signal power or an increase in noise or interference power, giving rise to a loss in signal-to-noise ratio or E_b/N_o . The second is due to signal distortion, such as might be caused by intersymbol interference (ISI) where the tail of a pulse can “smear” into adjacent symbol intervals, thereby interfering with the detection process and degrading the error performance. Even in the absence of noise, the effects of filtering and channel-induced distortion lead to ISI. Figure 2.6a shows the effect of a loss in E_b/N_o ; the solid-line corresponds to the theoretical P_B versus E_b/N_o curve and the dashed-line corresponds to a degradation effect brought about by a loss in E_b/N_o . Figure 2.6b shows an irreducible P_B caused by distortion (ISI). The solid-line corresponds to the theoretical P_B versus E_b/N_o curve and the dashed-line corresponds to a degradation effect brought about by ISI instead of a simple

loss in signal-to-noise ratio. The bit error rate in this case cannot further be reduced by increasing the signal power.

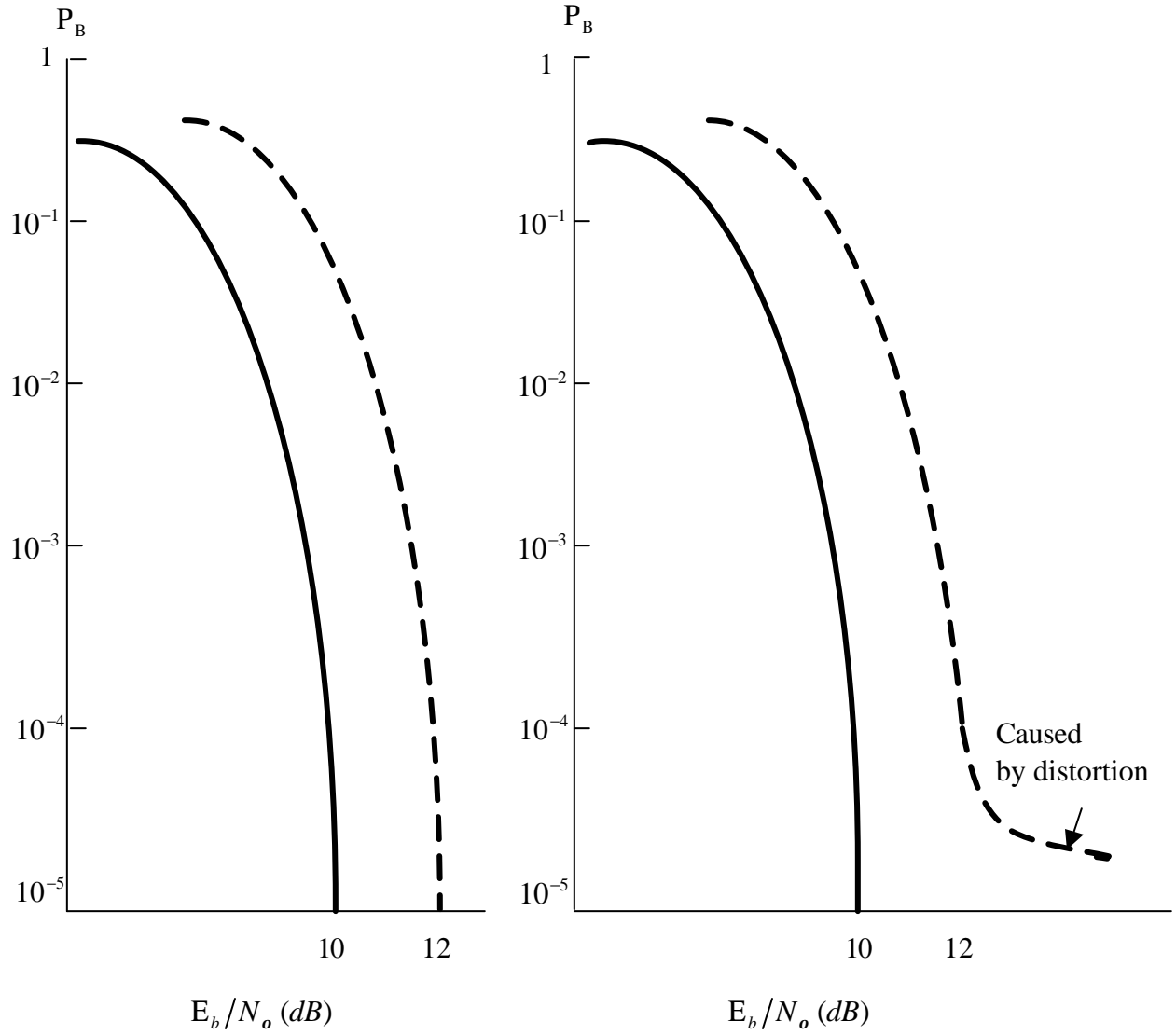


Figure 2.6. (a) Loss in E_b/N_o . (b) Irreducible P_B Caused by Distortion.

THIS PAGE INTENTIONALLY LEFT BLANK

III. EXPERIMENTAL DESCRIPTION

In this chapter, we describe the experiments and simulation procedure used in this thesis. First, as a part of BPSK signal generation, time-domain and frequency-domain BPSK representations and Power Spectral Density (PSD) for BPSK are analytically derived. Second, we describe the Monterey-Miami Parabolic Equation (MMPE) acoustic simulation model and how to generate the ocean responses in the time-domain and frequency-domain from the MMPE model. Third, we describe the ocean environment for our simulations and the input data for the MMPE model. Finally, we present the results of BPSK demodulation and multi-path mitigation.

A. BPSK SIGNAL GENERATION

In Chapter II, we described the properties of BPSK. In this section, time-domain and frequency-domain representations for the BPSK waveform are described and related to the ocean impulse response, and the power spectral density of the received signal. Figure 3.1 shows a diagram for BPSK signal generation. The quantity $b(t)$ is a random binary signal at baseband. The message data, $\{a_n\}$ represent a set of random variables with $a_n = \pm 1$ and probabilities $P(a_n = 1) = P(a_n = -1) = \frac{1}{2}$. The function $g(t - nT_b)$ is a shaped pulse in general; however we will take it to be a rectangular pulse with bit time duration, T_b . The signal $f(t)$ is a sinusoidal carrier with center frequency f_c and amplitude A_c . The output $s(t)$ is the modulated BPSK signal.

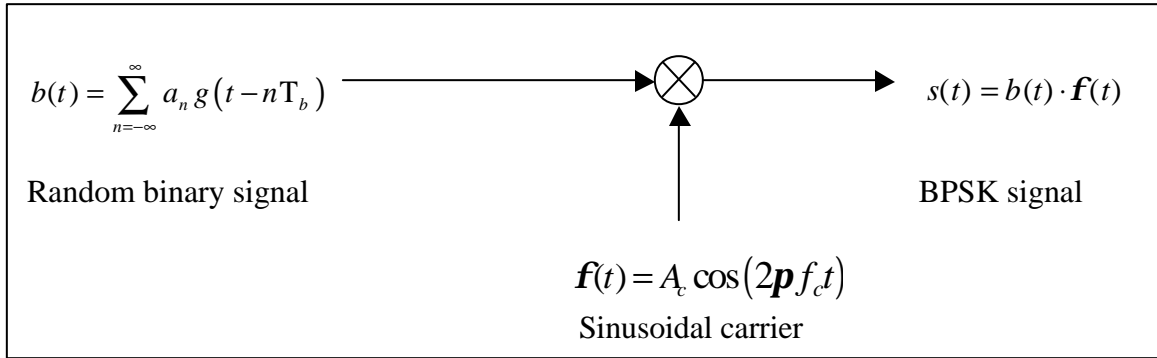


Figure 3.1. BPSK Signal Generation.

The Fourier transform for a rectangular pulse with amplitude one and bit duration T_b is given by:

$$G(f) = \int_{-\frac{T_b}{2}}^{\frac{T_b}{2}} g(t) e^{-j2\pi f t} dt = T_b \frac{\sin(\pi f T_b)}{\pi f T_b} \quad (3.1)$$

The Power Spectral Density (PSD) for a random binary signal, $b(t)$, will be evaluated by first truncating $b(t)$ as follows:

$$b_T(t) = \sum_{n=-N}^{n=N} a_n g(t - nT_b), \quad -T_o/2 \leq t \leq T_o/2 \quad (3.2)$$

where $b_T(t)$ is the truncated signal and $T_o/2 = (N + 1/2) T_b$. The Fourier transform of the truncated signal, $b_T(t)$, is then,

$$\begin{aligned} B_T(f) &= FT[b_T(t)] = \sum_{n=-N}^N a_n FT[g(t - nT_b)] = \sum_{n=-N}^N a_n G(f) e^{-j\pi n T_b f} \\ &= G(f) \sum_{n=-N}^N a_n e^{-j\pi n T_b f} \end{aligned} \quad (3.3)$$

where the notation $FT[\cdot]$ represents the Fourier transform operation and $G(f)$ is the resulting Fourier transform of $g(t)$.

The PSD for the random signal $b(t)$ can be defined by [Ref 3]

$$P_b(f) = \lim_{T_o \rightarrow \infty} \left(\frac{\overline{|B_T(f)|^2}}{T_o} \right) \quad (3.4)$$

where $B_T(f)$ represents the Fourier transform of the corresponding truncated signal and the overbar represents statistical expectation. Upon substituting (3.3) into (3.4), the PSD of $b(t)$ becomes

$$P_b(f) = \lim_{T_o \rightarrow \infty} \left(\frac{1}{T_o} |G(f)|^2 \overline{\left| \sum_{n=-N}^N a_n e^{-j\omega n T_b} \right|^2} \right) = |G(f)|^2 \lim_{T_o \rightarrow \infty} \left(\frac{1}{T_o} \sum_{n=-N}^N 1 \right) = |G(f)|^2 \lim_{T_o \rightarrow \infty} \frac{2N+1}{T_o}$$

where we have assumed that the a_n are statistically independent. Now, using $T_o = 2(N+1/2)T_b$, we obtain

$$P_b(f) = |G(f)|^2 \lim_{N \rightarrow \infty} \left[\frac{2N+1}{(2N+1)T_b} \right] = \frac{1}{T_b} |G(f)|^2 = T_b \left[\frac{\sin(\mathbf{p}f T_b)}{\mathbf{p}f T_b} \right]^2 \quad (3.5)$$

where Eq. (3.1) has been used for $G(f)$. This is the PSD of the signal at “baseband.”

For the modulated BPSK signal we have

$$s(t) = b(t)A_c \cos(2\mathbf{p}f_c t) \quad (3.6)$$

The corresponding PSD is given by

$$P_s(f) = \frac{A_c^2}{4} P_b(f + f_c) + \frac{A_c^2}{4} P_b(f - f_c) \quad (3.7)$$

(see Ref 3), where P_b is the PSD of the baseband signal $b(t)$. Upon substituting (3.5) into (3.7) we obtain

$$\begin{aligned}
P_s(f) &= \frac{A_c^2 T_b}{4} \left[|G(f + f_c)|^2 + |G(f - f_c)|^2 \right] \\
&= \frac{A_c^2 T_b}{4} \left\{ \left[\frac{\sin \mathbf{p}(f + f_c) T_b}{\mathbf{p}(f + f_c) T_b} \right]^2 + \left[\frac{\sin \mathbf{p}(f - f_c) T_b}{\mathbf{p}(f - f_c) T_b} \right]^2 \right\}
\end{aligned} \tag{3.8}$$

B. MMPE MODEL DESCRIPTION

The Parabolic Equation (PE) method was introduced into underwater acoustics in the early 1970's by Tappert [Ref 8]. The Monterey-Miami Parabolic Equation (MMPE) model [Ref 9] is a numerical model to solve acoustic wave propagation problems in the ocean using the PE method. The MMPE Model is used to compute the response at the receiver location of a signal transmitted from a source and traveling through the ocean. Figure 3.2 shows the three stages of using this model. In the first stage, we characterize the input parameters; in the second, we run the model; and in the last stage, we extract the frequency response and ocean impulse response from the outputs of the MMPE model.

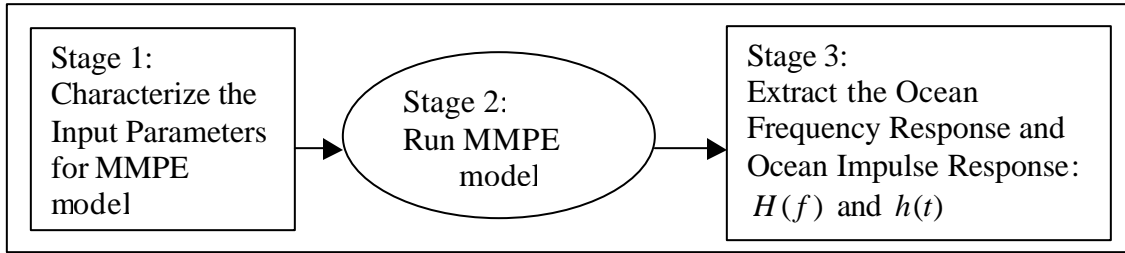


Figure 3.2. Three Stages to Extract Ocean Response from MMPE Model.

1. A Brief Description of the MMPE Model

In order to derive the frequency-domain and time-domain response of the ocean underwater communication channel, the general theory behind the parabolic equation model will be introduced. Its implementation - the split-step Fourier algorithm for solving the PE (PE/SSF) method [Ref 10] is also briefly described.

In ocean communication, all signals such as $p(t)$ represent acoustic pressure as a function of time, and are typically denoted by $p(\vec{x}, t)$ where \vec{x} represents the ocean coordinates at which the pressure signal is measured. The quantity $p(\vec{x}, t)$ is often

referred to as a space-time signal, since it is a function of the spatial parameters \vec{x} and time t . When measured at a fixed (receiver) location (say $\vec{x} = \vec{x}_1$) it becomes a function of time only. It is transformed into an electrical signal by an acoustic transducer or hydrophone.

The inhomogeneous wave (Helmholtz) equation for the acoustic pressure $p(\vec{x}, t)$ in a medium with sound speed $c(\vec{x})$ and density $\rho(\vec{x})$ can be expressed as

$$\rho(\vec{x}) \nabla \cdot \left(\frac{\nabla p(\vec{x}, t)}{\rho(\vec{x})} \right) - \frac{1}{c(\vec{x})^2} \frac{\partial^2 p(\vec{x}, t)}{\partial t^2} = S(\vec{x}, t) \quad (3.9)$$

where $S(\vec{x}, t)$ represents the sound source distribution as a function of both position \vec{x} and time t . In our application (as in most) there is a single source at a particular location $\vec{x} = \vec{x}_o$. Hence $S(\vec{x}, t)$ is formally a spatial “impulse” at \vec{x}_o with time dependence $s(t)$ corresponding to the transmitted waveform.

The parabolic equation model is based on an approximation of the Helmholtz wave equation in a cylindrical coordinate system. Because of the ocean’s relative shallowness compared to horizontal propagation distance for the majority of environments, it is well suited for a description in cylindrical coordinates.

The signals of interest in underwater communications such as BPSK have complicated time dependence; thus analytical solution to the wave equation (3.9) would be impossible. However the equation is linear, and a solution can be computed relatively easily for sources that have time dependence of the form $e^{j2\pi ft}$ for a single frequency f . Thus for a source with a time dependence of the form $Ae^{j2\pi ft}$, the output at a point $\vec{x} = \vec{x}_1$ is dependent on f and can be written as $H_{x_1}(f)e^{j2\pi ft}$. This is referred to by people working in ocean acoustics as a “time harmonic” solution to the wave equation. The quantity $H_{x_1}(f)$ is the ocean frequency response and its inverse Fourier transform is the

ocean impulse response (Green's function). The time harmonic solution forms the basis of computing the response due to a source with arbitrary time dependence by using Fourier analysis/synthesis methods.

From this point forward the analysis will be carried out in discrete time. This is appropriate since numerical techniques (i.e., the DFT) are used to perform the computations in both the time and frequency domains. We focus first on the analysis of low-pass signals at baseband $-W/2 \leq f \leq W/2$ and later extend the discussion to the case of bandpass signals such as BPSK centered around some higher carrier frequency. In particular, let us sample a signal $s(t)$ at times $t=0, T, 2T, \dots$ and represent the resulting discrete-time signal $s[n]=s(nT)$ in terms of its Discrete Fourier Transform (DFT):

$$s[n] = \frac{1}{L} \sum_{k=0}^{L-1} S[k] e^{j \frac{2\pi kn}{L}} \quad (3.10)$$

Here $S[k]$ is the DFT coefficient representing the frequency component of the signal at frequency $f = k/LT$:

$$S[k] = \sum_{n=0}^{L-1} s[n] e^{-j \frac{2\pi kn}{L}} \quad (3.11)$$

and L is the number of time and frequency samples used in the transform. The number of samples L and time interval T must of course be chosen to cover the time duration and bandwidth of the signal.

With the representation Eq. (3.10) for the source waveform, the output waveform at a point \vec{x}_1 can be computed from

$$q[n] = \frac{1}{L} \sum_{k=0}^{L-1} H_{x_1} \left(\frac{2pk}{L} \right) S[k] e^{j \frac{2pkn}{L}} \quad (3.12)$$

where the ocean frequency response has been evaluated at the frequency $f = 2pk/L$ and multiplied by the Fourier coefficient $S[k]$ for the source.

The ocean frequency response terms that need to be computed by MMPE are

$$H_x \left(\frac{2pk}{L} \right) \quad k = 0, 1, 2, \dots, \frac{L}{2} - 1 \quad (3.13)$$

which represent frequencies up to the Nyquist “fold-over” frequency $f_s/2 = \frac{1}{2T}$. The other terms in the transform represent the “negative” frequencies and may be computed from

$$H_x \left(\frac{2pk}{L} \right) = H_x^* \left(\frac{2p(L-k)}{L} \right) \quad k = \frac{L}{2}, \frac{L}{2} + 1, \dots, \frac{L}{2} - 1 \quad (3.14)$$

Both the forward DFT in Eq. (3.11) needed to compute the frequency coefficients $S[k]$ of the source signal and the inverse DFT represented in Eq. (3.12) are performed using an FFT program.

To compute $H_x(f)$ we proceed as follows. Assuming a time harmonic solution, the Helmholtz equation takes the form

$$\begin{aligned} \frac{1}{r} \frac{\partial}{\partial r} \left(r \frac{\partial p(r, z, \mathbf{j}, f)}{\partial r} \right) + \frac{1}{r^2} \frac{\partial^2 p(r, z, \mathbf{j}, f)}{\partial \mathbf{j}^2} + \frac{\partial^2 p(r, z, \mathbf{j}, f)}{\partial z^2} \\ + k_0^2 \ell^2(r, z, \mathbf{j}) p(r, z, \mathbf{j}, f) = -4 \mathbf{p} P_0 \mathbf{d} (\vec{r} - \vec{r}_s), \end{aligned} \quad (3.15)$$

where

$$p(r, z, \mathbf{j}, f) = p(r, z, \mathbf{j}) e^{-j 2 \mathbf{p} \cdot \mathbf{f}} \quad (3.16)$$

The reference wavenumber k_0 is related to a reference sound speed, c_0 , by

$$k_0 = \frac{2 \mathbf{p} f}{c_0}, \quad (3.17)$$

and the acoustic index of refraction is defined by

$$l = \frac{c_0}{c(r, z, \mathbf{j})}. \quad (3.18)$$

Note that in this derivation the density variances are neglected. By defining the effective index of refraction which contains the appropriate addition terms, the influence of the density differences at the water-bottom interface can be included [Ref 8].

By assuming that the ocean acts as a waveguide with a cylindrical coordinate system, acoustic energy is mainly propagated outward from a source in the horizontal direction. Therefore, the pressure field can be approximated by

$$p(r, z, \mathbf{j}, f) = \Psi(r, z, \mathbf{j}, f) H_0^{(1)}(k_0 r) \quad (3.19)$$

where $\Psi(r, z, \mathbf{j}, f)$ is a slowly varying envelope function, or PE field function and $H_0^{(1)}(k_0 r)$ is the zero-th order Hankel function of the first kind of the outgoing acoustic wave. Taking advantage of the far-field ($k_0 r \gg 1$) asymptotic approximation of the Hankel function, Eq. (3.19) can be rewritten as

$$p(r, z, \mathbf{j}, f) = \frac{P_0 R_0}{\sqrt{r}} \Psi(r, z, \mathbf{j}, f) e^{jk_0 r}, \quad (3.20)$$

normalized such that at the reference range $r = R_0$, $|p| = P_0$. Substituting Eq. (3.20) into Eq. (3.15) and dropping the source term on the right hand side gives

$$\frac{\partial^2 \Psi}{\partial r^2} + j2k_0 \frac{\partial \Psi}{\partial r} + \frac{1}{r^2} \frac{\partial^2 \Psi}{\partial \mathbf{j}^2} + \frac{\partial^2 \Psi}{\partial z^2} + \left[k_0^2 (l^2 - 1) + \frac{1}{4r^2} \right] \Psi = 0. \quad (3.21)$$

Neglecting the azimuthal coupling and the far-field terms, and dropping the first term due to the slow modulation of the envelope function, Eq. (3.21) can be rewritten as

$$\frac{j}{k_0} \frac{\partial \Psi}{\partial r} = -\frac{1}{2k_0^2} \frac{\partial^2 \Psi}{\partial z^2} - \frac{1}{2} (l^2 - 1) \Psi. \quad (3.22)$$

Now, by defining the operators

$$T_{op} = -\frac{1}{2k_0^2} \left(\frac{\partial^2}{\partial z^2} \right) \quad (3.23)$$

and

$$U_{op} = -\frac{1}{2}(l^2 - 1) , \quad (3.24)$$

Eq. (3.22) can be rewritten as

$$\frac{j}{k_0} \frac{\partial \Psi}{\partial r} = (T_{op} + U_{op}) \Psi . \quad (3.25)$$

Equation (3.25) is known as the “standard” parabolic equation (SPE) [Ref 8], with accurate solutions limited to a half width of $\pm 15^\circ$ for the propagation angle and represents the complete description of the outgoing acoustic energy propagation in the waveguide. In order to extend this limit to $\pm 40^\circ$, a higher order wide-angle parabolic equation (WAPE) approximation [Ref 11] is used. Its operators are defined by

$$T_{WAPE} = 1 - \sqrt{1 + \frac{1}{k_0^2} \frac{\partial^2}{\partial z^2}} , \quad (3.26)$$

and

$$U_{WAPE} = -(l-1) . \quad (3.27)$$

The MMPE uses the split-step Fourier (SSF) method in order to solve the parabolic equation numerically. This algorithm integrates the solution in range by applying the T_{WAPE} and the U_{WAPE} operators in the wavenumber (k_z)-domain and the

spatial (z)-domain, respectively, where each operator is a scalar multiplier. In the k_z -space, the wide angle \hat{T}_{WAPE} operator to simplify calculation is defined as

$$\hat{T}_{WAPE} = 1 - \sqrt{1 - \frac{k_z^2}{k_0^2}}. \quad (3.28)$$

The field function at range $r + \Delta r$ is expressed as

$$\Psi(r + \Delta r, z, f) = e^{-jk_0 \frac{\Delta r}{2} U_{WAPE}(r + \Delta r)} FT \left\{ e^{-jk_0 \Delta r \hat{T}_{WAPE}(k_z)} FT^{-1} \left[e^{-jk_0 \frac{\Delta r}{2} U_{WAPE}(r, z)} \Psi(r, z) \right] \right\}. \quad (3.29)$$

Since the output data of the MMPE model is the field function in the form of equation (3.29), we substitute Eq. (3.29) into Eq. (3.20). The ocean frequency response (with respect to pressure) at range r and depth z is then given by

$$H_{(r,z)}(f) = p(r, z, f) = \frac{1}{\sqrt{r}} \Psi(r, z, f) e^{jk_0 r}. \quad (3.30)$$

As described earlier, for broadband signals, the output results require knowing $H_{(r,z)}(f)$ for all frequencies in the bandwidth of the signal [see Eq. (3.12)]. Thus the MMPE model must be run for all frequencies within the band. The model produces frequency domain results which are written to an output file. A post processing program performs the synthesis specified in Eq. (3.12).

2. Signal Representation in MMPE

The time intervals encountered in ocean acoustics can be large. In particular the time due to propagation delay from source to receiver during which no sound is heard at

the receiver can be very large compared to the duration of the signal when it finally arrives (see Figure 3.3)

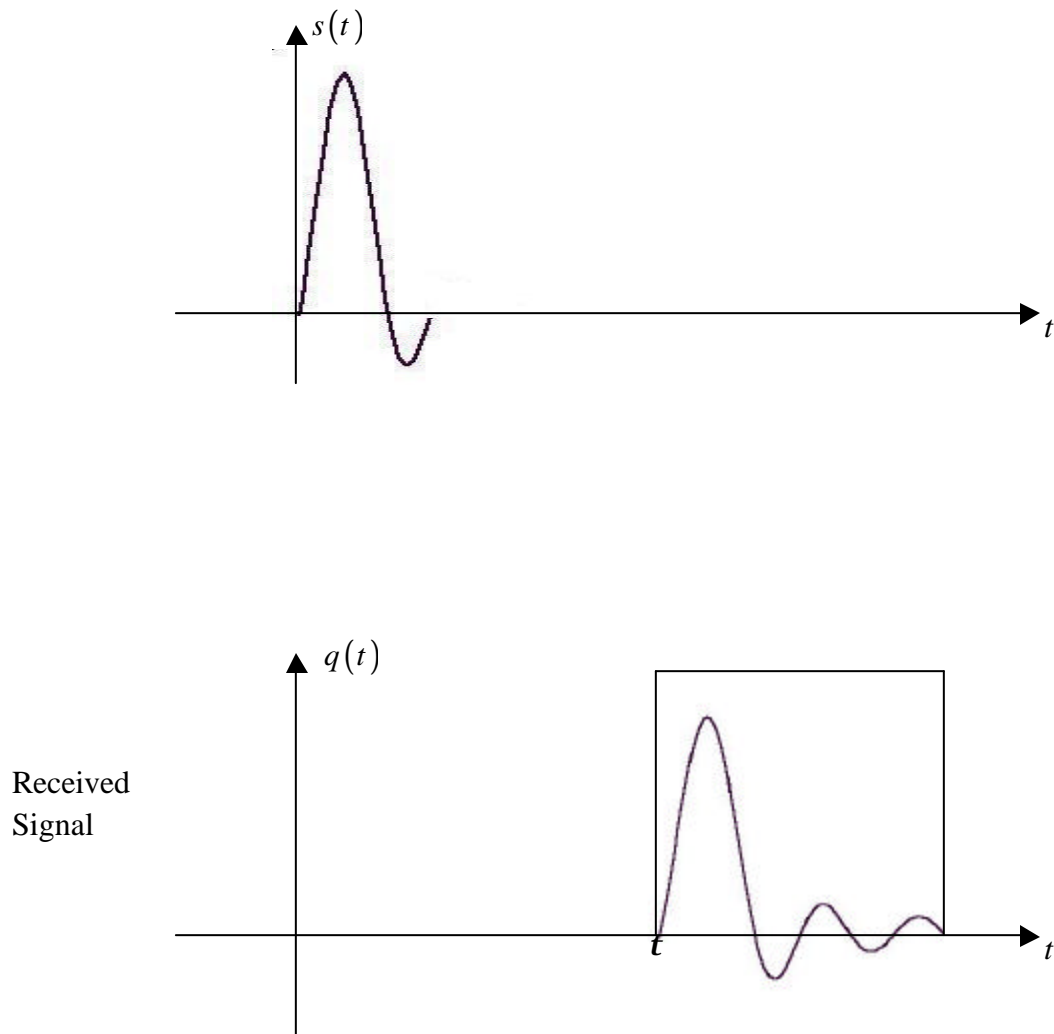


Figure 3.3. Pulse Arriving after Propagation Delay t .

To obtain the most accurate results, the analysis time needs to be focused in a small time window surrounding the received signal as shown in Figure 3.3.

The signals of interest are also often restricted in frequency as well as time. For example, a BPSK transmission has a frequency spectrum similar to that shown in Figure 3.4.

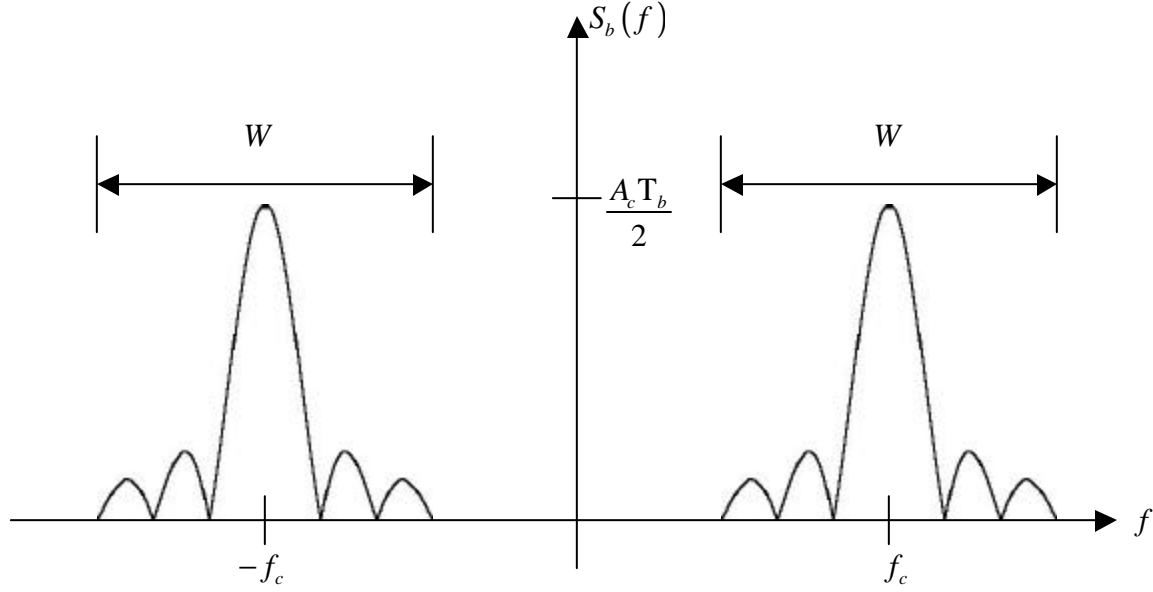


Figure 3.4. Spectrum of Bandpass Signal.

Such signals are referred to as bandpass signals; the spectral power is assumed negligible outside of an interval $\pm W/2$ around the center frequency or carrier frequency f_c . Again, for accuracy and reduced computation in processing, it is most appropriate to focus in a *frequency window* (frequency band) where the spectrum is non-zero.

MMPE deals with the signal processing in an efficient way by permitting the user to specify a time window and frequency band for the processing. The formulation for such processing is described below.

a. Time Windowing

The time windowing in MMPE is relatively simple to explain. The frequency response $H_{(r,z)}(f)$ of Eq. (3.30) contains a term $e^{jk_o r} = e^{j2\pi f \frac{r}{c_o}}$ which

corresponds to the gross propagation delay $t = r/c_o$ from source to receiver in the ocean. MMPE drops this term, so that the modified frequency response is given by

$$H'_{(r,z)}(f) = \frac{1}{\sqrt{r}} \Psi(r, z, f) \quad (3.31)$$

The time domain signals resulting from this modified frequency response correspond to a reduced time scale t' defined as

$$t' = t - t = t - \frac{r}{c_o} \quad (3.32)$$

and referred to as *reduced time*. MMPE uses this reduced time for its output results. Absolute time (relative to the source) can be obtained by adding back in the gross propagation delay $t = r/c_o$.

Without the modification to the frequency response specified in Eq. (3.31), some time response would be produced within the analysis window of the DFT. However, this response would appear as a circularly shifted version of the true correct response and the time scale would not be correct. This effect is known as “time aliasing.”

b. Processing of Bandpass Signals

A continuous-time real bandpass signal such as that depicted in Figure 3.4 can be written in the general form

$$s_b(t) = s_p(t) \cos 2\pi f_c t - s_q(t) \sin 2\pi f_c t$$

Here $s_p(t)$ and $s_q(t)$ are known as the “in-phase” and “quadrature” modulation components. The bandpass signal can be equivalently expressed as

$$s_b(t) = \text{Re} \left[\tilde{s}(t) e^{j2\pi f_c t} \right] \quad (3.33)$$

where

$$\tilde{s}(t) = s_p(t) + js_q(t)$$

is known as the *complex envelope*. The complex envelope is a complex-valued low-pass signal with spectrum as depicted in Figure 3.5.

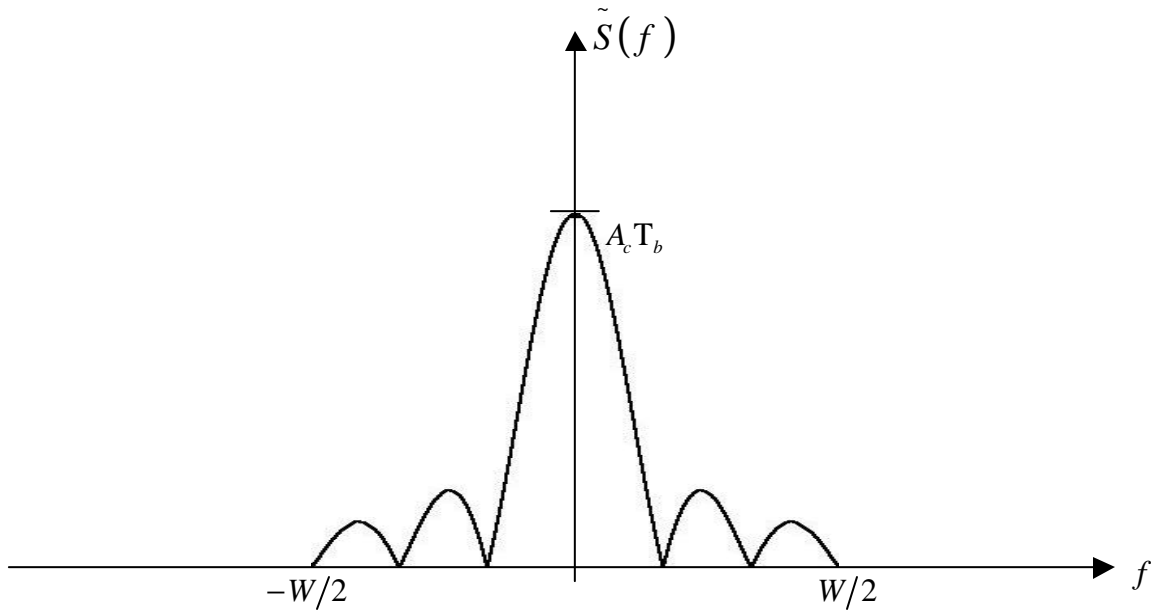


Figure 3.5 Spectrum of a Complex Valued Lowpass Signal Corresponding to Bandpass Signal of Figure 3.4.

The *complex envelope* may be obtained from the original bandpass signal by discarding the negative-frequency part of the spectrum, moving the positive-frequency part of the spectrum from a center point of $f = f_c$ to $f = 0$ (“baseband”) and scaling by a factor of 2.

The advantage of using complex envelope representation for the bandpass signal is that the processing can be focused in the bandpass region by processing the complex envelope at baseband. Let us denote the sampled version of the *complex envelope* as

$$s[n] = \tilde{s}(nT) = s_p(nT) + js_q(nT)$$

(The notation $s[n]$ was previously used to denote a sampled real band-limited baseband signal; the only difference now is that $s[n]$ is complex.) The complex baseband signal can be represented as in Eq. (3.10) where $S[k]$ are the frequency components at baseband defined by Eq. (3.11). However a frequency in the DFT of $2pk/L$ represents an actual frequency in the ocean of $2pk/L + f_c$. Hence the ocean frequency response $H_{x_1}(f)$ must be computed by MMPE at this higher frequency ($2pk/L + f_c$). The time-sampled complex envelope of the received signal is then given by

$$q[n] = \frac{1}{L} \sum_{k=0}^{L-1} H_{x_1} \left(\frac{2pk}{L} + f_c \right) S[k] e^{j \frac{2pkn}{L}} \quad (3.34)$$

(Compare this to Eq. (3.12)). The sampled real bandpass signal at the receiver is thus given by

$$q_b[n] = 2\text{Re}\left[q[n]e^{j2p f_p^T}\right] \quad (3.35)$$

3. Input Parameters for the MMPE Model

The input data for the MMPE model fall into three main categories: the main input file, the source data, and the environmental data. Each of these is described below.

The main input file is called `pefiles.inp`: it is the only filename that *must* exist. All other input files are specified in this file. Figure 3.6 shows that the first several entries of this main file simply define the other input files. Line 1 specifies the source data file. Lines 2 to 6 specify files that provide the environmental data, while line 7 specifies the output data file (a binary file). Following these data files, the user specifies the number of points in depth, minimum depth, maximum depth (at line 8), the number of points in range, minimum range, maximum range (at line 9). The final line in this file represents the vertical FFT size, the range step, the maximum depth of the calculation, and the reference sound speed.

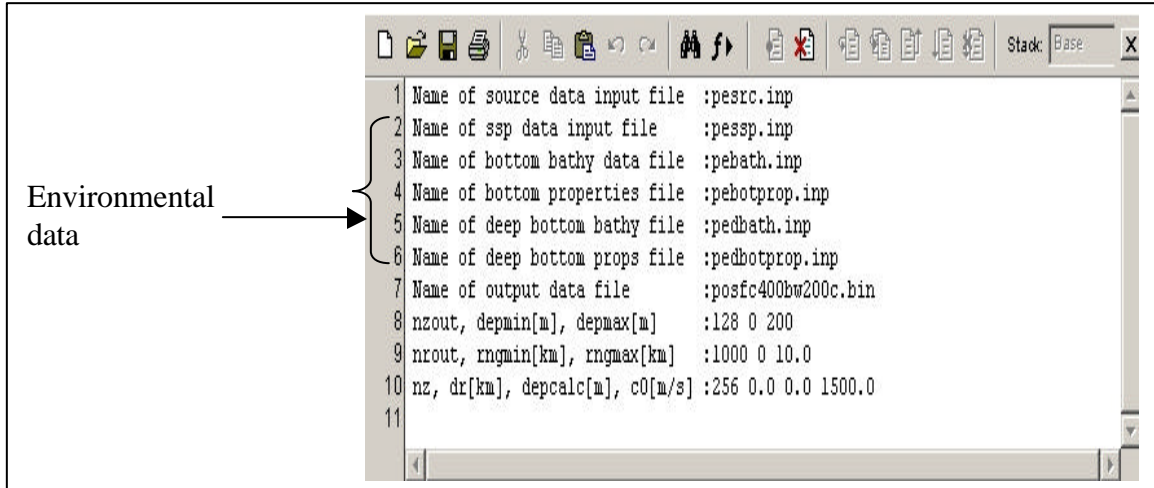


Figure 3.6. `pefiles.inp` File of the Main Input File.

The source data input file depicted in Figure 3.7 defines all of the source information. There are two source types which are available: a wide-angle source which approximates a point source, and a vertical line array which approximates a continuous line array. For this work, we will use the wide-angle point source approximation. The

first line in Figure 3.7 represents the source depth. The second line denotes the array length; an array length of zero indicates a point source. For a wide-angle source, the D/E angle is ignored since a point source cannot be steered. The remaining lines represent the center frequency, the bandwidth, and the number of the frequencies at which the ocean response is to be evaluated (size of the DFT). This number must be a power of two.

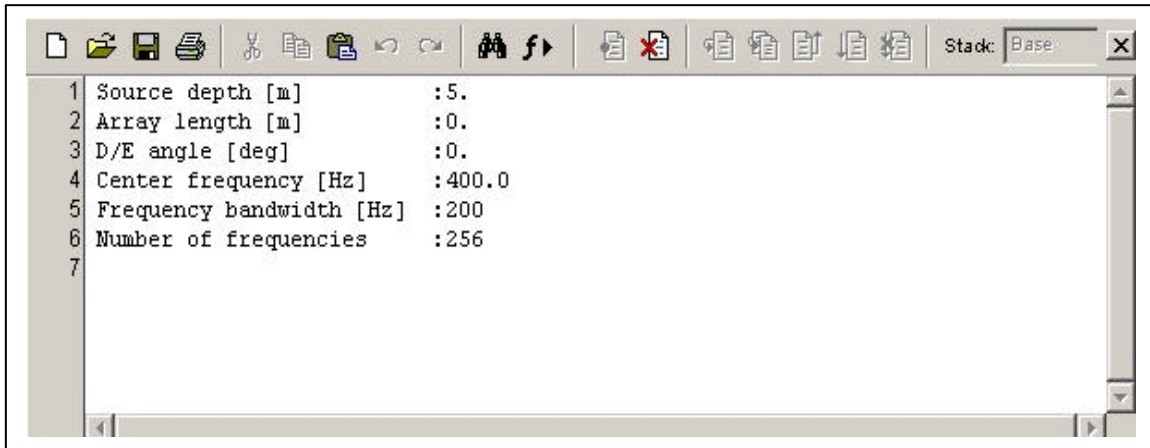


Figure 3.7. pesrc.inp File of the Source Data.

The environmental data consists of five input files. The pessp.inp file contains the sound speed profile data and is illustrated in Figure 3.8. As shown there, the first line contains two numbers indicating the number of azimuthal radials and the total azimuthal aperture. The second line contains a single number indicating the number of sound speed profiles. The following line denotes the range of the current profile and the number of sound speed values. Finally, the profile is defined by pairs of the depth and sound speed.

The other environmental files are similar in structure. Their detailed descriptions are contained in the Ocean Acoustic Library web page <http://oalib.saic.com/PE/mmpe.html> which is supported by the U.S. Office of Naval Research. The pebath.inp file contains the bathymetry of the water/bottom interface; the pebotprop.inp file contains the acoustics parameters of the medium just below the water/bottom interface; the pedbath.inp file defines the “deep” layer bathymetry

beneath the water/sediment interface; and finally, the `pedbotprop.inp` file contains the acoustic properties of the deep layer.

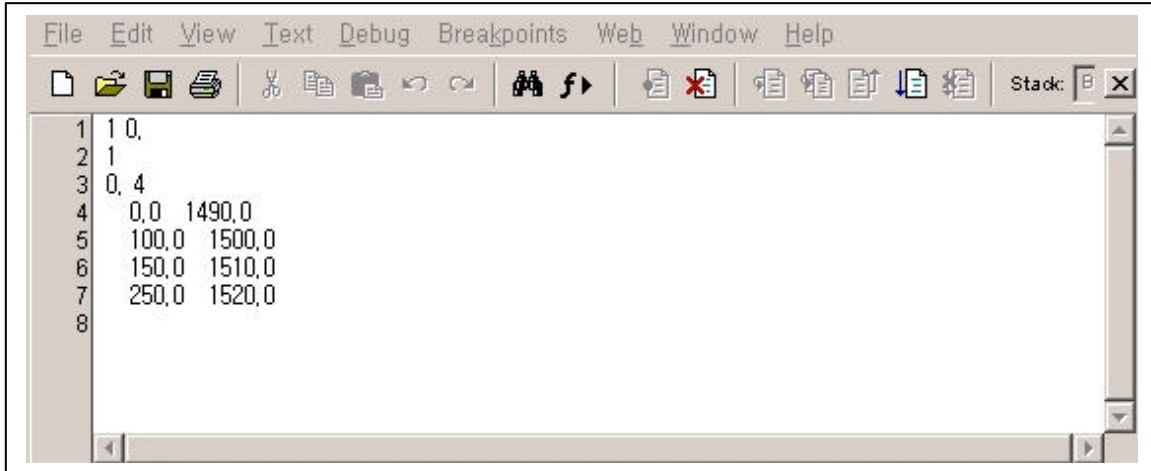


Figure 3.8. `pessp.inp` File of the Environmental Data.

The last file, the output data file is a binary file produced by MMPE. It is read by the postprocessing program to produce final results

C. OCEAN ENVIRONMENTAL CHARACTERIZATION

For our simulation studies of underwater communication, we focused on shallow water environments. Three different ocean environments which have three different sound speed profiles (SSP) were simulated to test the performance of underwater communication using a BPSK signal. The complete set of MMPE input files for all three cases are given in Appendix A.

1. Case 1: Positive SSP Gradient

For this case, the source is located at a range of 0 m and at a depth of 5 m. The sound speed is range-independent with a positive, linear gradient SSP of 1497 m/s at the surface and 1499 m/s at a depth of 100m. The density of water is assumed to be 1.0 g/cm^3 . The bottom is chosen to be a ‘bumpy’ bottom with the following depths: 102m at 0 km; 101 m at 2.5 km; 99m at 5 km; 102 m at 7.5 km; and 99 m at 10 km. Its compressional sound speed is 1700 m/s, the sound speed gradient 1 s^{-1} , density 1.5 g/cm^3 , and compressional attenuation 0.1 dB/km/Hz. Figure 3.9 shows the positive sound speed profile versus depth and the corresponding sound transmission loss plot

(versus range and depth) for a source at depth 5 m and frequency of 400 Hz. Transmission loss is defined as

$$TL = 20\log[p(1, z_s)/p(r, z)] \quad (3.36)$$

where $p(r, z)$ is the acoustic pressure amplitude and $p(1, z_s)$ is the reference acoustic pressure amplitude measured at range 1 m (from the source) and at the source depth z_s . The color in Figure 3.9 represents the transmission loss in dB according to the scale shown on the right.

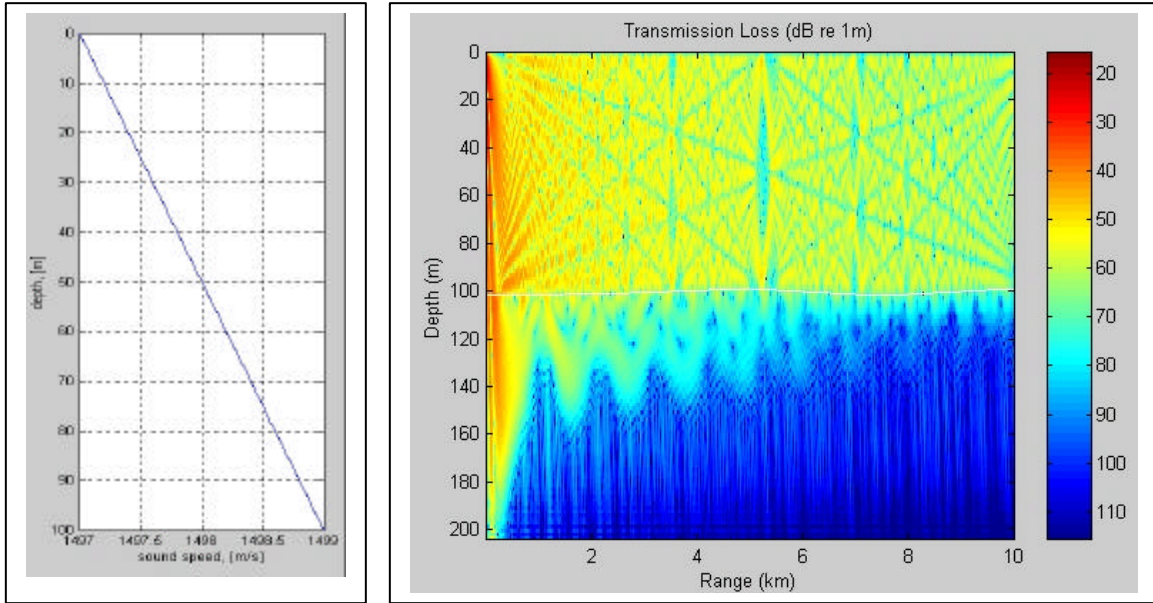


Figure 3.9. (a) Positive SSP (b) Sound Propagation at Frequency 400 Hz, Source 5 m.

2. Case 2: Strong Negative SSP Gradient

For this case, the source is located at a range of 0 m and at a depth of 30 m. The sound speed is range-independent with a strong negative, bilinear gradient (downward refraction) sound speed profile of 1528 m/s at the surface and 1510 m/s at a depth of 50m, and 1489 m/s at the depth of 100 m. The density of water is assumed to be 1.0 g/cm³. The bottom is chosen to be a ‘bumpy’ bottom with the same depths as in the

previous case. Its compressional sound speed is 1700 m/s, the sound speed gradient 1 s^{-1} , density 1.5 g/cm^3 , and compressional attenuation 0.1 dB/km/Hz . Figure 3.10 shows the strong negative sound speed profile versus depth and the sound transmission loss for a source at depth 30 m, and frequency of 400 Hz.

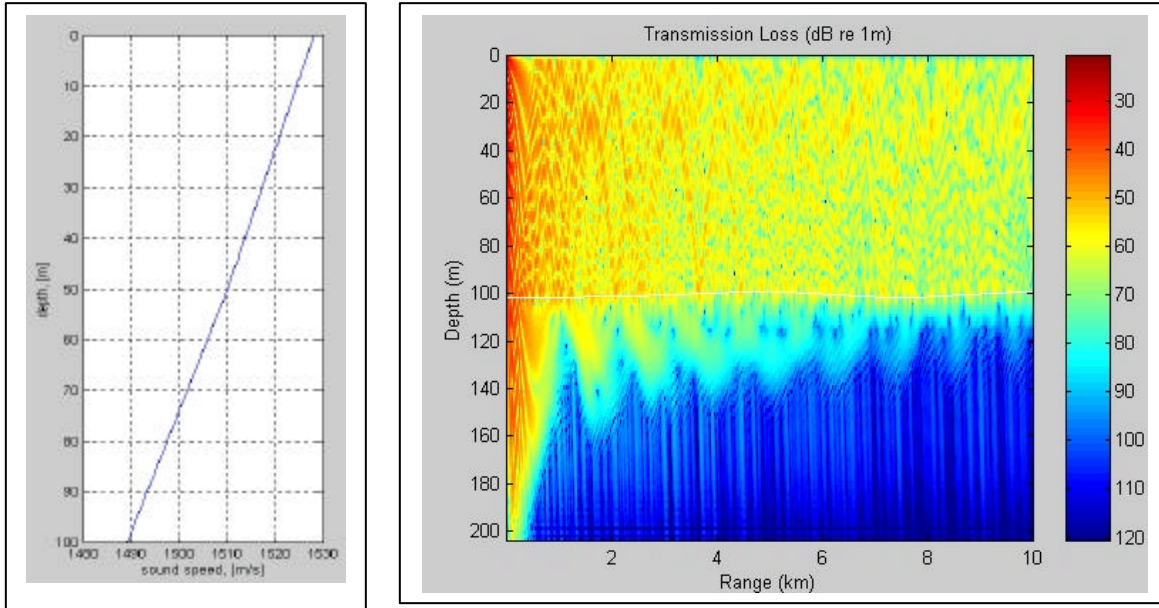


Figure 3.10.(a) Negative SSP (b) Sound Propagation at Frequency 400 Hz, Source 30 m.

3. Case 3: Negative SSP Gradient Below Surface Duct

For this case, the source is again located at a range of 0 m and at a depth of 5 m. The sound speed is range-independent with a negative, bi-linear gradient sound speed profile with surface duct of 1492 m/s at the surface and 1500 m/s at a depth of 40m, and 1489 m/s at the depth of 100 m. The density of water is assumed to be 1.0 g/cm^3 . The bottom is chosen to be a ‘bumpy’ bottom with the same depths as in the previous cases. Its compressional sound speed is 1700 m/s, the sound speed gradient 1 s^{-1} , density 1.5 g/cm^3 , and compressional attenuation 0.1 dB/km/Hz . Figure 3.11 shows the positive sound speed within the surface duct, the negative sound speed profile below the surface duct, and the sound transmission loss for a source at depth 5 m and frequency of 400 Hz.

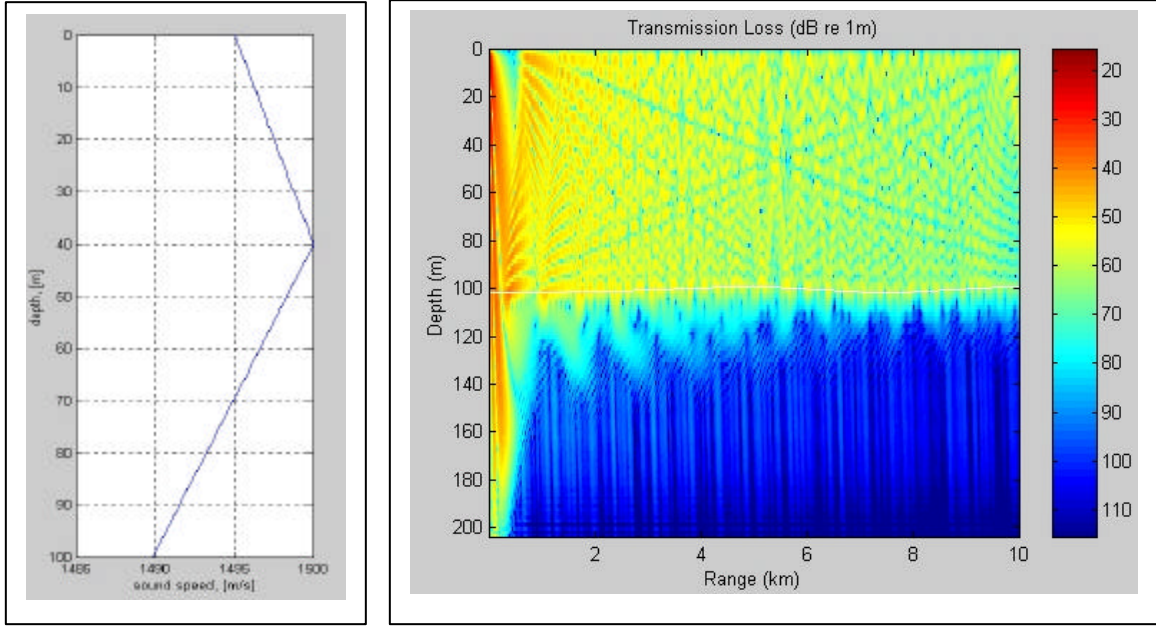


Figure 3.11. (a) SSP (b) Sound Propagation at Frequency 400 Hz, Source 5 m.

D. BPSK DEMODULATION AND DETECTION

At the receiver location, the received signal waveforms arrive distorted due to noise and intersymbol interference in the underwater communication channel. We need to demodulate the received signal in order to recover the transmitted signal and recover the binary data. Figure 3.12 shows two basic steps in the demodulation and detection process. Step 1, the waveform-to-sample transformation, consists of the demodulator followed by a sampler. At the end of each symbol time duration T_b , the sampler produces an output $z(T_b)$ which in the absence of noise is proportional to the energy of the received symbol. Step 2 is a decision process where $z(T_b)$ is compared to a threshold g_o to decide if the received data represents a binary 1 or binary 0.

1. Correlation Receiver

As mentioned in Chapter II, there are two main types of degradation factors in the performance of underwater communication, namely noise and dispersion introduced by the ocean channel with its multipath environment. In this section, we ignore the degrading factor produced by the ocean impulse response and assume that the only

performance degradation is due to AWGN with zero mean. In next section, the effect of the ocean impulse response will be added to the received signal.

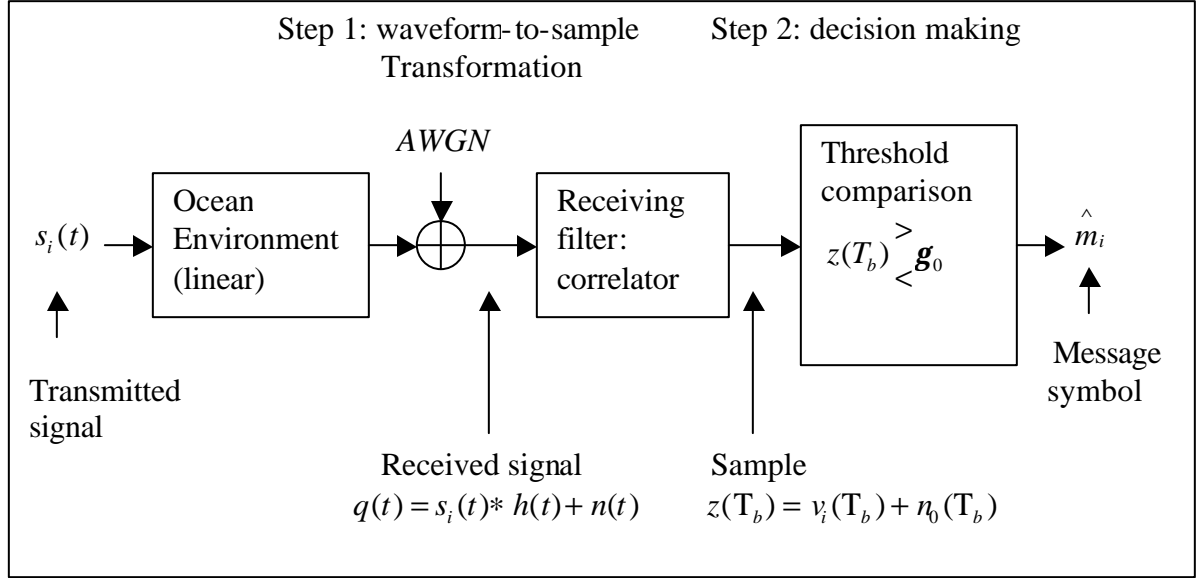


Figure 3.12. Two Basic Steps in the Demodulation/Detection of the Received Signal.

In the process of demodulation, the received signal is reduced to a single random variable $z(T_b)$ sometimes called a “detection statistic”. In the absence of distortion due to the ocean, the received signal can be expressed as:

$$q(t) = s(t - \tau) + n(t) \quad 0 \leq t \leq T \quad (3.37)$$

where $q(t)$ represents the received signal, $s(t - \tau)$ is the transmitted delayed BPSK signal, and $n(t)$ is AWGN with zero mean and variance, σ_n^2 .

As shown in Figure 3.13, the recovered signal is formed by multiplying the input signal by two local sinusoidal carriers $s_1(t)$ and $s_2(t)$, assumed synchronized with the received signal to obtain

$$y_1(t) = q(t) \cdot s_1(t) = q(t) \cdot \cos(2\pi f_c t) \quad (3.38)$$

and

$$y_2(t) = q(t) \cdot s_2(t) = -q(t) \cdot \cos(2\pi f_c t) \quad (3.39)$$

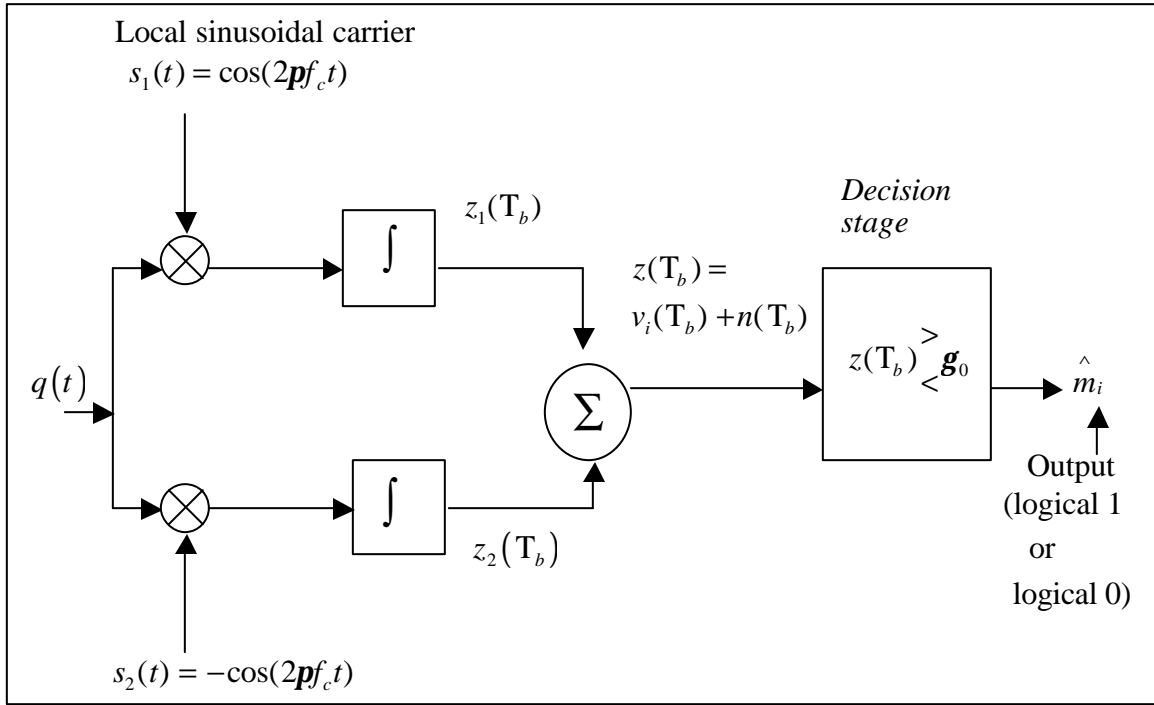


Figure 3.13. Correlator Receiver.

The recovered signals $y_1(t)$ and $y_2(t)$ are integrated over the bit interval to obtain

$$z_i(T_b) = \int y_i(t) dt = \int q(t) s_i(t) dt \quad i = 1, 2 \quad (3.40)$$

and the outputs of the integrations are subtracted to form the detection statistic

$$z(T_b) = z_1(T_b) - z_2(T_b) \quad (3.41)$$

In the decision stage, $z(T_b)$ is compared to an optimum threshold as follows

$$z(T_b) \begin{matrix} > \\ < \end{matrix} \frac{v_1 + v_2}{2} = g_o \quad (3.42)$$

where v_1 is the signal component of $z(T_b)$ when $s_1(t)$ is transmitted, and v_2 is the signal component of $z(T_b)$ when $s_2(t)$ is transmitted. The threshold level g_o defined by $g_o = (v_1 + v_2)/2$ is the optimum threshold for minimizing the probability of bit error [Ref 1]. For equal energy, equally likely antipodal signals, where $s_1(t) = -s_2(t)$ and $v_1 = -v_2$, the decision rule becomes

$$z(T_b) \begin{matrix} > \\ < \end{matrix} g_o = 0 \quad (3.43a)$$

Assuming that $s_1(t)$ corresponds to binary 1 and $s_2(t)$ is binary 0, the decision rule thus reduces to

$$\begin{aligned} &\text{decide binary 1} && \text{if } z_1(T_b) > z_2(T_b) \\ &\text{decide binary 0} && \text{otherwise} \end{aligned} \quad (3.43b)$$

E. MULTIPATH MITIGATION

In this section, we assume the received signal is further distorted by intersymbol interference due at least in part to multipath propagation in the channel. We need to use some multipath mitigation technique to compensate for the degraded signal. One such technique is time reversal. In this method the received signal is convolved with the time-reversed impulse response of the ocean before applying it to the demodulation. As shown in Figure 3.14, the received signal has the following form

$$q(t) = s(t) * h(t) + n(t) \quad (3.44)$$

where $h(t)$ is the ocean impulse response in the time-domain.

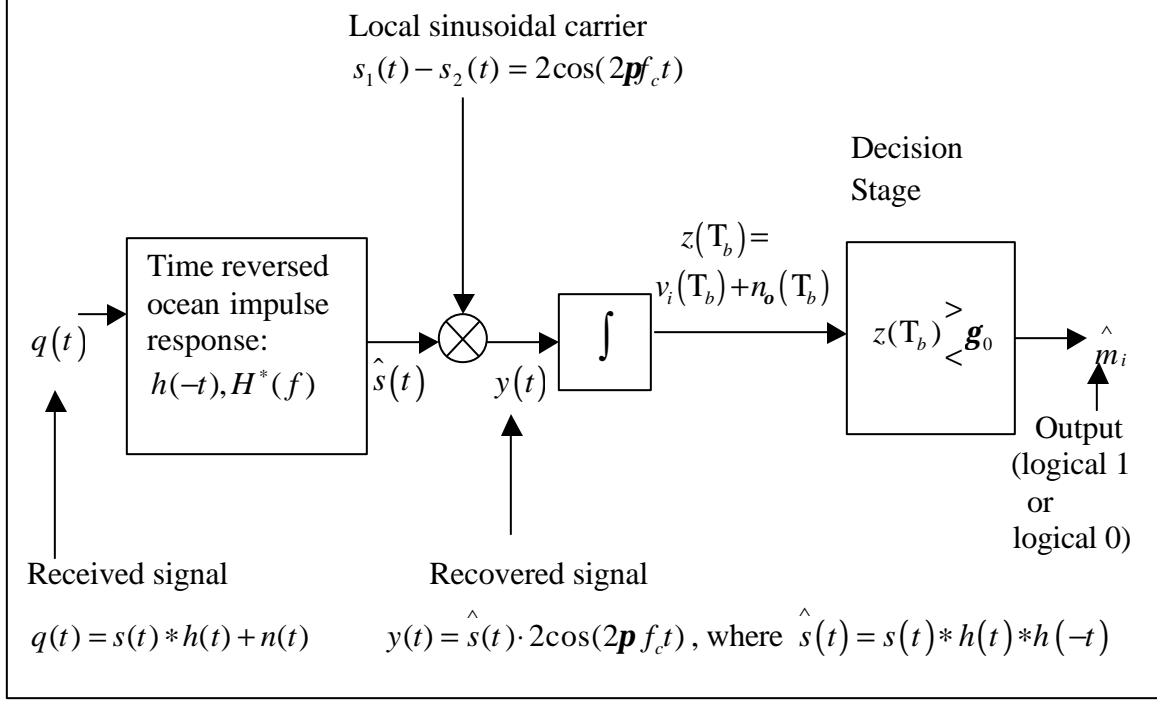


Figure 3.14 Multipath Mitigation for the Distorted Signal in Underwater Environment.

The distortion in the signal (represented by the convolution $s(t) * h(t)$) is mitigated by applying the time-reversed ocean impulse response to the received signal. In the absence of noise, the resulting mitigated signal is

$$\hat{s}(t) = q(t) * h(-t) = s(t) * h(t) * h(-t) \quad (3.45)$$

The convolution of $h(t)$ with $h(-t)$ produces an impulse-like signal. Hence the result of Eq. (3.45) is a tendency to restore the distorted signal to its original condition. The recovered signal is then formed by multiplying the mitigated signal by the two local sinusoidal carriers $s_1(t)$ and $s_2(t)$ to obtain

$$y(t) = \hat{s}(t) \cdot (s_1(t) - s_2(t)) = \hat{s}(t) \cdot 2\cos(2\pi f_c t) \quad (3.46)$$

The recovered signals $y(t)$ are integrated over the bit time duration to form the detection statistic. This is compared to a threshold as before to produce the recovered binary data.

THIS PAGE INTENTIONALLY LEFT BLANK

IV. SIMULATION RESULTS

A. EVALUATION OF BIT ERROR PROBABILITY FOR BPSK SIGNAL

In this section, the parameters (bandwidth, sampling frequency, bit rate, samples per bit, interpolation factor and up-sampling frequency) for the BPSK signal and a Finite Impulse Response (FIR) filter are defined, and the effect of the AWGN on the bit error performance is evaluated.

1. Evaluation for BPSK Parameters

An important theorem of communication is based on the assumption of a strictly bandlimited channel, i.e. one in which no signal power whatever is allowed outside the band of interest. For our work, we need to define the bandwidth for the BPSK signal transmission. The single-sided power spectral density for the BPSK signal (also known as the analytic signal) is given by

$$P_{BPSK}^+(f) = \frac{A_c^2 T_b}{4} \left[\frac{\sin \mathbf{p}(f - f_c) T_b}{\mathbf{p}(f - f_c) T_b} \right]^2 \quad (4.1)$$

This follows from Eq. (3.8) by dropping the terms for negative frequencies. This power spectral density is depicted in Figure 4.1 and is seen to consist of a main lobe and smaller sidelobes. Although there are many criteria for measuring bandwidth, for our digital communication, we are constrained to two bandwidth criteria namely Null-to-null bandwidth and Power bandwidth.

The *Null-to-null bandwidth* is given by $W = 2R = 2/T_b$ where R is the position of the first null relative to the center frequency (see Figure 4.1). The sampling frequency corresponding to this definition of bandwidth is given by

$$f_s = 2R = 2/T_b \quad (4.2)$$

Thus, the bit rate for this bandwidth definition is $R = W/2 = 1/T_b$ and the number of samples per bit is $N_{sb} = f_s T_b = 2$.

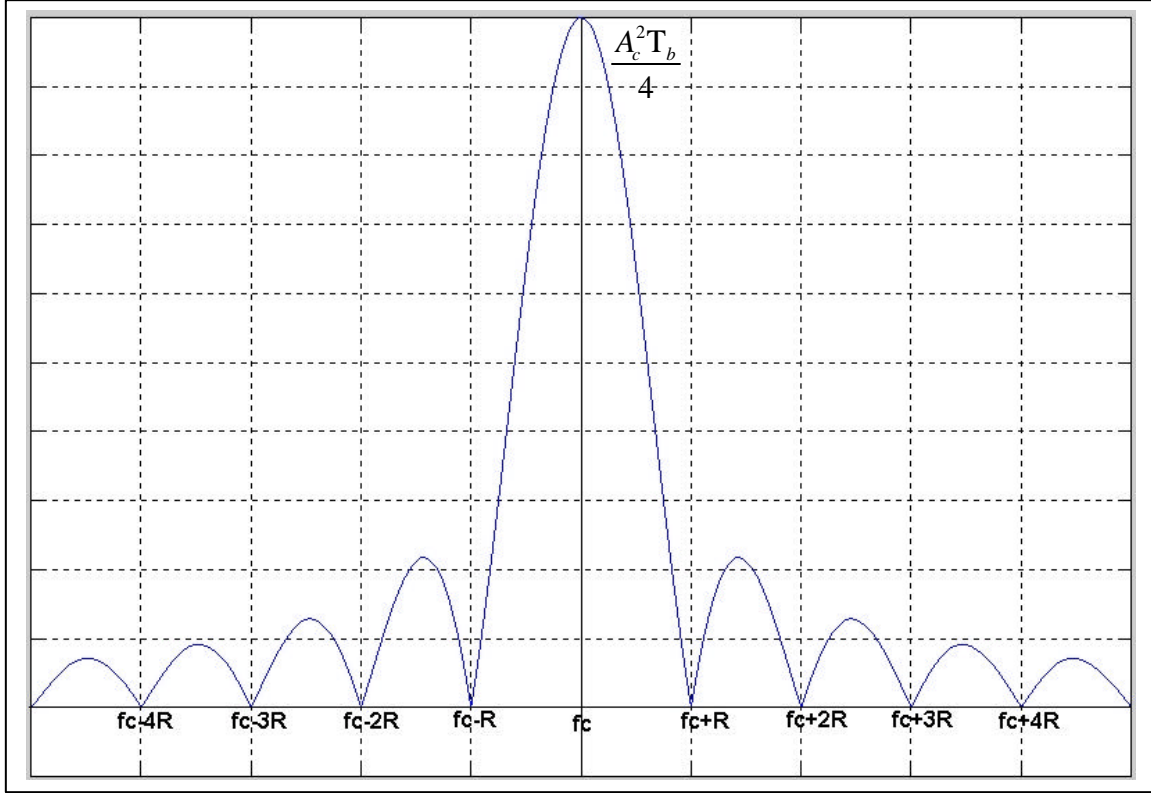


Figure 4.1. The Power Spectral Density for BPSK Signal.

The *Power bandwidth* defines the frequency band in which 99% of the total power resides. This bandwidth has been adopted by the Federal Communication Commission (FCC Rules and Regulations Section 2.202) and states that the occupied bandwidth is the band that leaves exactly 0.5% of the signal power above the upper band limit and exactly 0.5% of the signal power below the lower band limit. Thus for this definition 99% of the signal power is inside the band. For the BPSK signal this bandwidth is given by $W = 20.56R = 20.56/T_b$. The sampling frequency for the power bandwidth is given by

$$f_s = 20.56R = 20.56/T_b \quad (4.3)$$

Thus, the bit rate for this bandwidth is $R = W/20.56 = 1/T_b$ and the number of samples per bit is $N_{sb} = f_s T_b = 20.56$.

Since the carrier frequency is generally much higher than the bandwidth of the baseband signal, a random binary signal must be interpolated to reconstruct a bandlimited waveform without error. The interpolation factor is determined as

$$I = \text{ceil} \left[\frac{2(f_c + W)}{f_s} \right] \quad (4.4)$$

where I represents the interpolation factor and ceil rounds towards plus infinity. The increased sampling rate is then

$$f'_s = If_s \quad (4.5)$$

where f'_s represents the up-sampling frequency.

The interpolated random binary signal must then be filtered to remove the unwanted spectral energy above the band. A digital Finite Impulse Response (FIR) filter is used. The FIR filter is designed using a Hamming window with the following parameters.

$$\begin{aligned} w_p &= \frac{1.0(2pW/2)}{f'_s} \equiv \text{passband digital frequency} \\ w_s &= \frac{2.0(2pW/2)}{f'_s} \equiv \text{stopband digital frequency} \\ N_h &= \frac{8p}{w_s - w_p} \equiv \text{filter order (number of coefficients is } N_h + 1) \end{aligned}$$

The filter parameters are shown for a general FIR filter designed using the Hamming window method in Figure 4.2. The variable w , is the digital frequency defined as

$$w = \frac{2\pi f}{f_s} \quad (4.6)$$

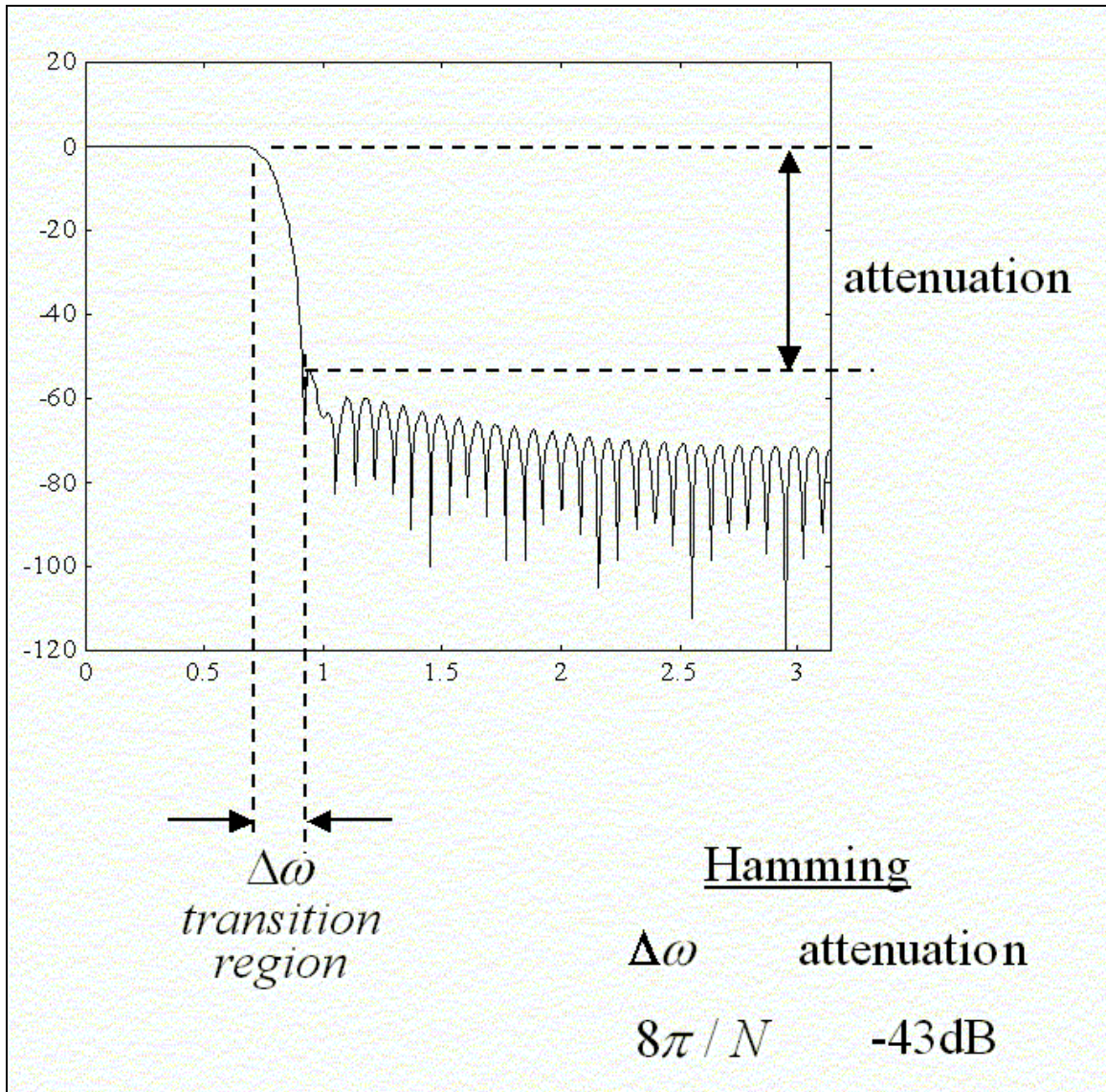


Figure 4.2. General FIR Filter (Hamming Window Design).

In the following experiments, the frequency response of the BPSK signal for the Null-to-null bandwidth and Power bandwidth is shown. Figure 4.3 shows the frequency response for 1000 bits of a BPSK signal which is sampled according to the Null-to-null bandwidth and has parameters $R=100$ bits/sec, $f_c=400$ Hz, $f_s=200$ Hz, $N_{sb}=2$, $I=6$ and $f'_s=1200$ Hz. Figure 4.4 shows the frequency response for 1000 bits of a BPSK signal which is sampled according to the Power bandwidth criterion with parameters $R=100$ bits/sec, $f_c=4000$ Hz, $f_s=2100$ Hz, $I=6$, $f'_s=12600$ Hz and $N_{sb}=21 = \text{ceil}(20.56)$. The complete procedures to generate the BPSK signal are explained in Appendix B.

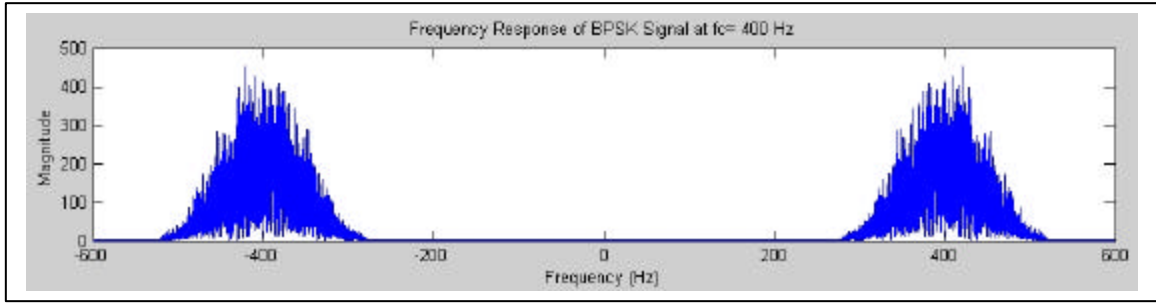


Figure 4.3. Frequency Response for BPSK Signal Sampled by Null-to-null Bandwidth.

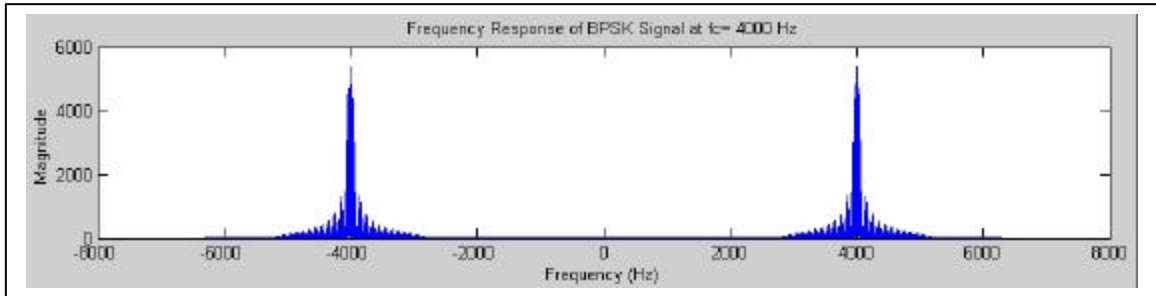


Figure 4.4. Frequency Response for BPSK Signal Sampled by Power Bandwidth.

As shown in Figure 4.3 and Figure 4.4, sampling according to the Power bandwidth is more reliable than the Null-to-null bandwidth since 99% of the signal power is within the bandwidth. However, since the most energy is contained within the Null-to-null bandwidth, it is sufficient to work with the Null-to-null bandwidth for our work. In

the next subsection, the bit error performance under AWGN for BPSK signal having Null-to-null bandwidth is evaluated.

2. Influence of AWGN on Bit Error Probability

For evaluation of the bit error performance under AWGN, the bit error probability was tested for various values of the average signal power to average noise power ratio (SNR). The average signal power was kept constant.

The average signal power to average noise power ratio is defined as $SNR = \frac{E_b}{\mathbf{s}_o^2 \Delta t}$

where $E_b = \frac{A_c^2 T_b}{2}$ is the average signal power, \mathbf{s}_o^2 is the white Gaussian noise variance,

and $\Delta t = \frac{T_b}{N_{sb}}$. The SNR is thus given by

$$SNR = \frac{A_c^2 T_b}{2 \mathbf{s}_o^2 \Delta t} \quad (4.7)$$

or in decibels as

$$SNR_{(dB)} = 10 \log (SNR) = 10 \log \left(\frac{A_c^2 T_b}{2 \mathbf{s}_o^2 \Delta t} \right) \quad (4.8)$$

The theoretical value of the bit error probability P_B from Eq. (2.19) is:

$$P_B = Q \left(\sqrt{\frac{2E_b}{N_o}} \right) = Q(\sqrt{SNR}) = Q \left(\sqrt{\frac{A_c^2 T_b}{2 \mathbf{s}_o^2 \Delta t}} \right) \quad (4.9)$$

In the following experiment, the parameters for the simulation to evaluate the bit error performance under AWGN for a BPSK signal are as follows: $N_{bit}=10000$ bits, $R=100$ bits/sec, $W=200$ Hz, $f_c=400$ Hz, $f_s=200$ Hz, $N_{sb}=2$. The noise variance σ_o^2 is varied from 0.01 to 2 in increments of 0.1 and from 3 to 60 in increments of 2.

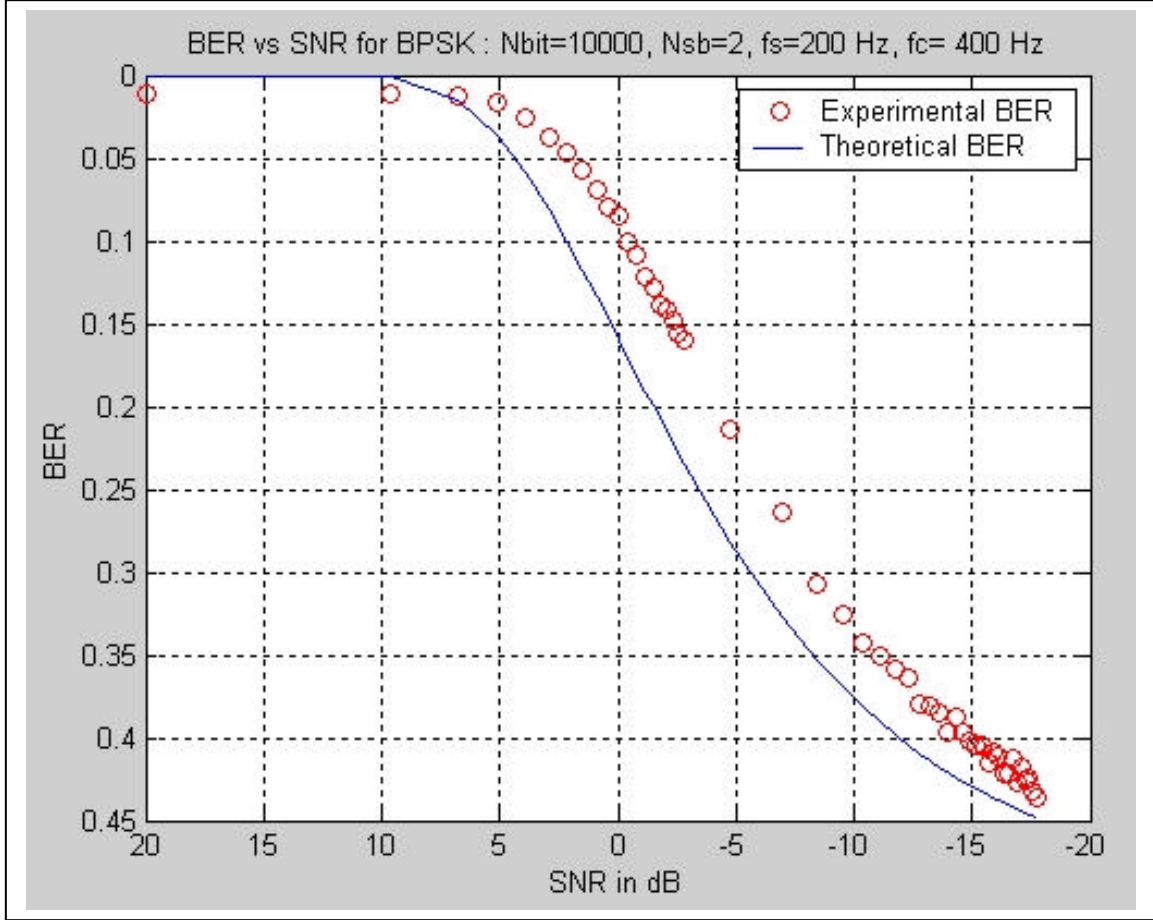


Figure 4.5. BER versus SNR (dB).

The experimental bit error rate estimates for various values of SNR for the Null-to-null bandwidth is shown in Figure 4.5. It can be seen that the experimental values follow the theoretical values given by Eq. (4.9) but are over all slightly lower. This is due to the effect of the FIR filter which removes some of the noise. Since the effect of AWGN on BER for BPSK signal is consistent with the theoretical values, our concern in

ocean communication will be now with the degradation due to ocean impulse response and the multipath than the degradation due to the additive noise.

B. BIT ERROR DEGRADATION AND MULTIPATH MITIGATION FOR BPSK SIGNAL IN A SHALLOW WATER ENVIRONMENT

In this final section, the bit error performance degradation due to the ocean impulse response is evaluated. This impulse response is generated from the MMPE model in the three different ocean environments as described in Chapter III. In all three of these cases, we used the same bandwidth (200 Hz) and center frequency (400 Hz) for the BPSK signal. In all cases the performance is compared for two situations. First, the received signal is applied directly to the demodulation with no prior mitigation steps and the BER is evaluated as a function of range and depth from the transmitter. Secondly, the received signal is convolved with the time-reversed ocean impulse response before applying it to the demodulation. This mitigation step tends to compress the spreading caused by the ocean impulse response. The BER is then evaluated and compared to that of the unmitigated situation.

1. Bit Error Performance Results for a Positive SSP Gradient

The parameters of this environment are given in Chapter III (see Figure 3.9). First, by choosing an ocean impulse response extracted from the MMPE model at a chosen depth of 50 m and range 5 km, the influence of the ocean impulse response on the bit error rate at this chosen depth and range is evaluated. Then the time-reversed ocean impulse response is convolved with the received signal to compensate for the distorted signal and the bit error rate is evaluated again. In the following, we describe this one specific case in detail. Later, in section B the evaluation is performed at many chosen depths and ranges of this ocean environment.

a. Investigation Of The One Specific Case

The parameters of the generated random binary data are as follows: $N_{bit}=20$ bits, $R=100$ bits/sec, $N_{sb}=24$, $f_s=2400$ Hz. This discrete random binary data $b[n]$ is filtered to remove an unwanted signal (i.e., above bandwidth, $W=200$ Hz) by a FIR filter. The filtered random binary data is $b_f[n]=b[n]*h_{LPF}[n]$ (see Appendix B). This filtered random binary data $b_f[n]$ is modulated by cosine modulating signal,

$\cos\left(\frac{2\pi f_c n}{f_s}\right)$, having a carrier frequency of $f_c=400$ Hz and the sampling interval

$\Delta t = 1/f_s$. This entire procedure simulates the sampling of an analog BPSK waveform (which is what would actually be present in the water) at 2400 samples/sec. The modulated BPSK signal, as shown in Figure 4.6 in time and frequency domains, is

$$s[n] = b_f[n] \cdot \cos\left[\frac{2\pi f_c n}{f_s}\right].$$

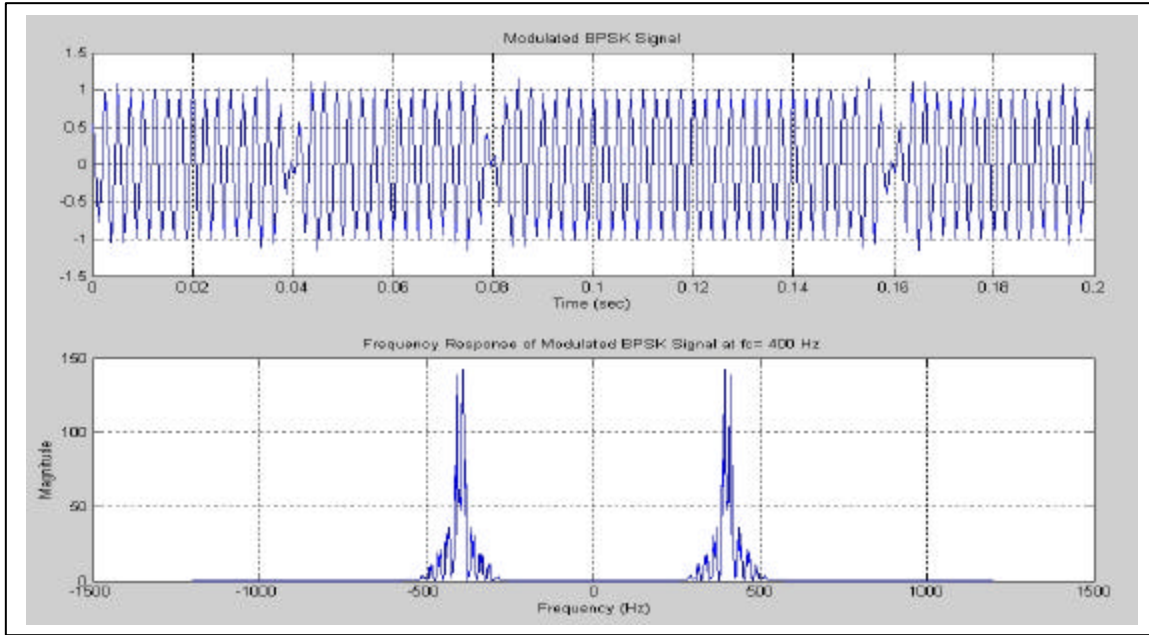


Figure 4.6. BPSK Signal in Time Domain and Frequency Domain.

The modified ocean frequency response $H'(f)$ extracted from the MMPE model at a chosen depth of 50 m and range 5 km corresponds to a center frequency of $f_c = 400$ Hz, a bandwidth of $W=300$ Hz and a sampling frequency of $f_{s_{ocean}} = 300$ Hz. To obtain the ocean impulse response at the same sampling rate and bandwidth as the BPSK signal, the ocean impulse response from MMPE is up-sampled by a factor of 8, $I = \frac{2(3 \times f_c)}{f_{s_{ocean}}} = 8$, and filtered to remove an unwanted signal (i.e., above bandwidth, 200 Hz) by a FIR filter (see Appendix C). Figure 4.7 shows the passband

ocean frequency response $H_b(f)$ (magnitude and phase) and ocean impulse response $h_b[n]$. The complete procedure to generate the passband ocean impulse response at this high sampling frequency is explained in Appendix C.

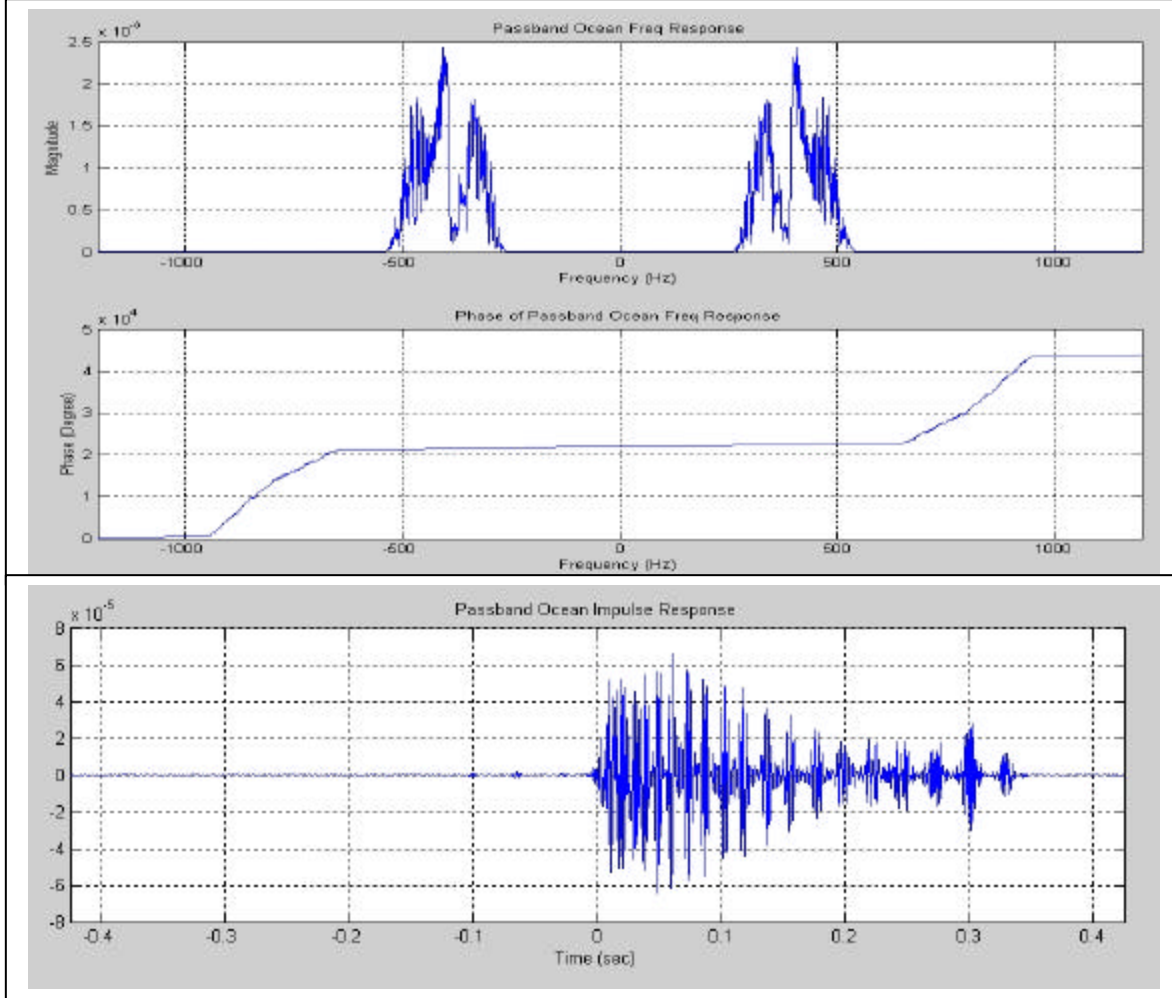


Figure 4.7. Passband Ocean Frequency Response (Magnitude and Phase) and Ocean Impulse Response.

The BPSK signal $s[n]$ is convolved with the ocean impulse response $h_b[n]$ by linear convolution in the time domain. The received signal is $q[n] = s[n] * h_b[n]$. This simulates the distortion caused by propagation through the

ocean. Figure 4.8 shows the distorted received signal in time and frequency domains at the chosen receiver location.

The recovered signal is obtained by multiplying the received signal $q[n]$ by the cosine modulating signal, $\cos\left(\frac{2pf_c n}{f_s}\right)$. Thus, the recovered signal is $y[n] = q[n] \cdot \cos\left[\frac{2pf_c n}{f_s}\right]$. This recovered signal is filtered to remove unwanted frequency components above the bandwidth by a FIR filter and integrated over the bit time duration to form the detection statistic. This is compared to a threshold to produce the recovered binary data. Figure 4.9 shows that the recovered binary data has a very high bit error rate (55 %) due to the ocean impulse response when compared to the transmitted binary data.

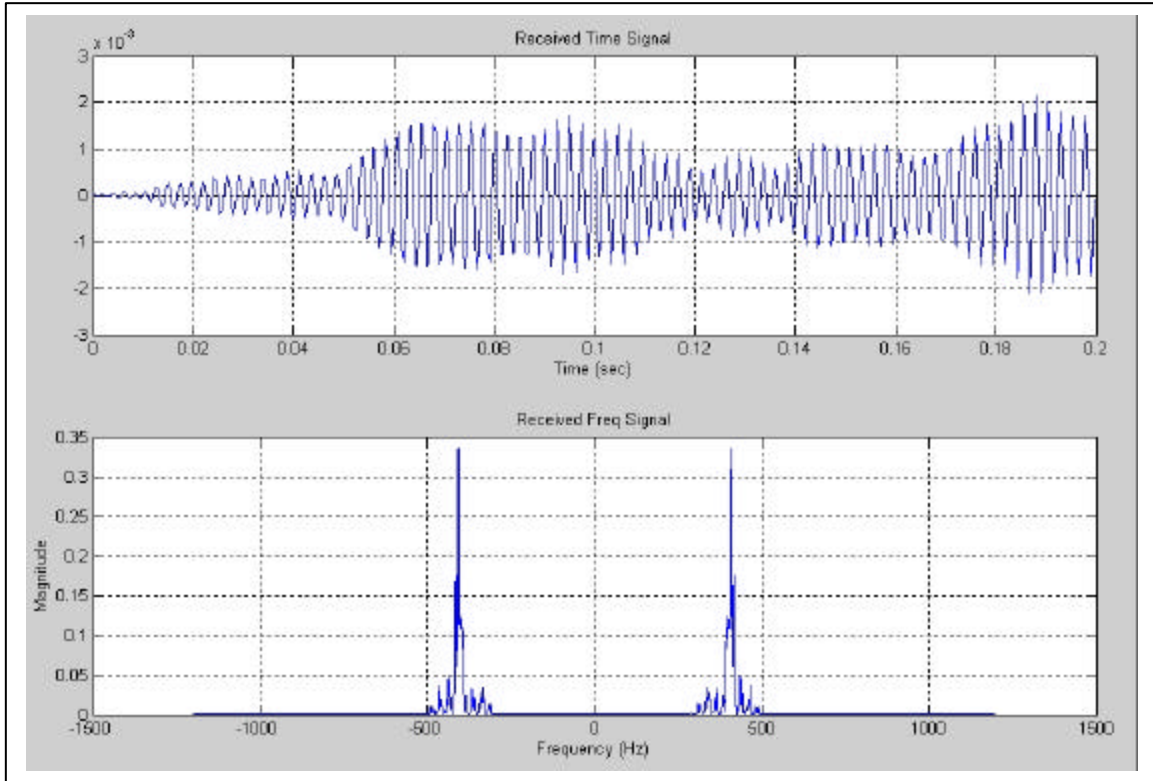


Figure 4.8. Received Signal in Time Domain and Frequency Domain.

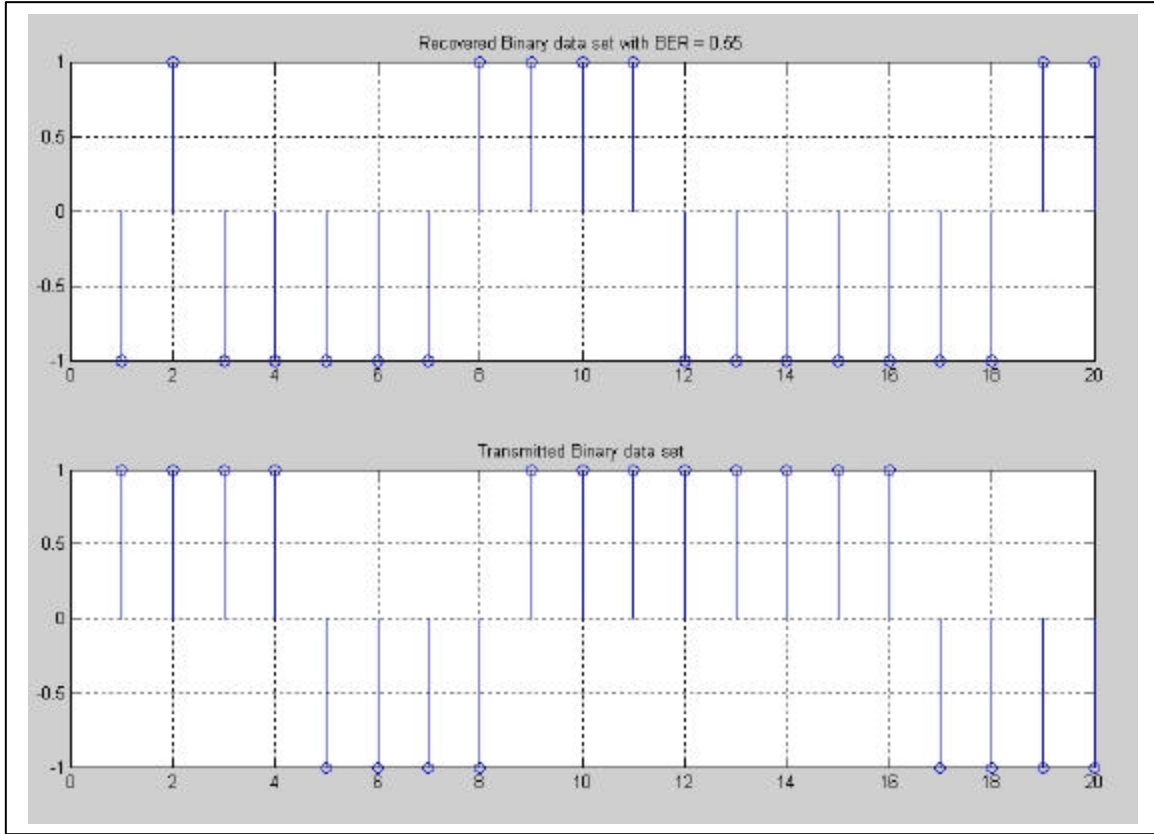


Figure 4.9. Comparison of Recovered Binary Data with Transmitted Binary Data for the Received Signal (55 % error rate).

To mitigate this high bit error rate due to the ocean impulse response, the time-reversed ocean impulse response is applied to the received signal. The time-reversed ocean impulse $h_t[n]$ is obtained by reversing the passband ocean impulse response $h_b[n]$ in time (i.e. $h_t[n] = h_b[-n]$). Figure 4.10 shows the passband time-reversed ocean frequency response (magnitude and phase) and ocean impulse response. The phase is the negative of the phase in Figure 4.7.

To show the mitigated ocean impulse response, the time-reversed ocean impulse response is convolved with the ocean impulse response. The mitigated ocean impulse response is thus given by $h_m = h_b[n] * h_t[n] = h_b[n] * h_b[-n]$. Figure 4.11 shows that in the absence of noise the mitigated ocean impulse produces an impulse-like signal.

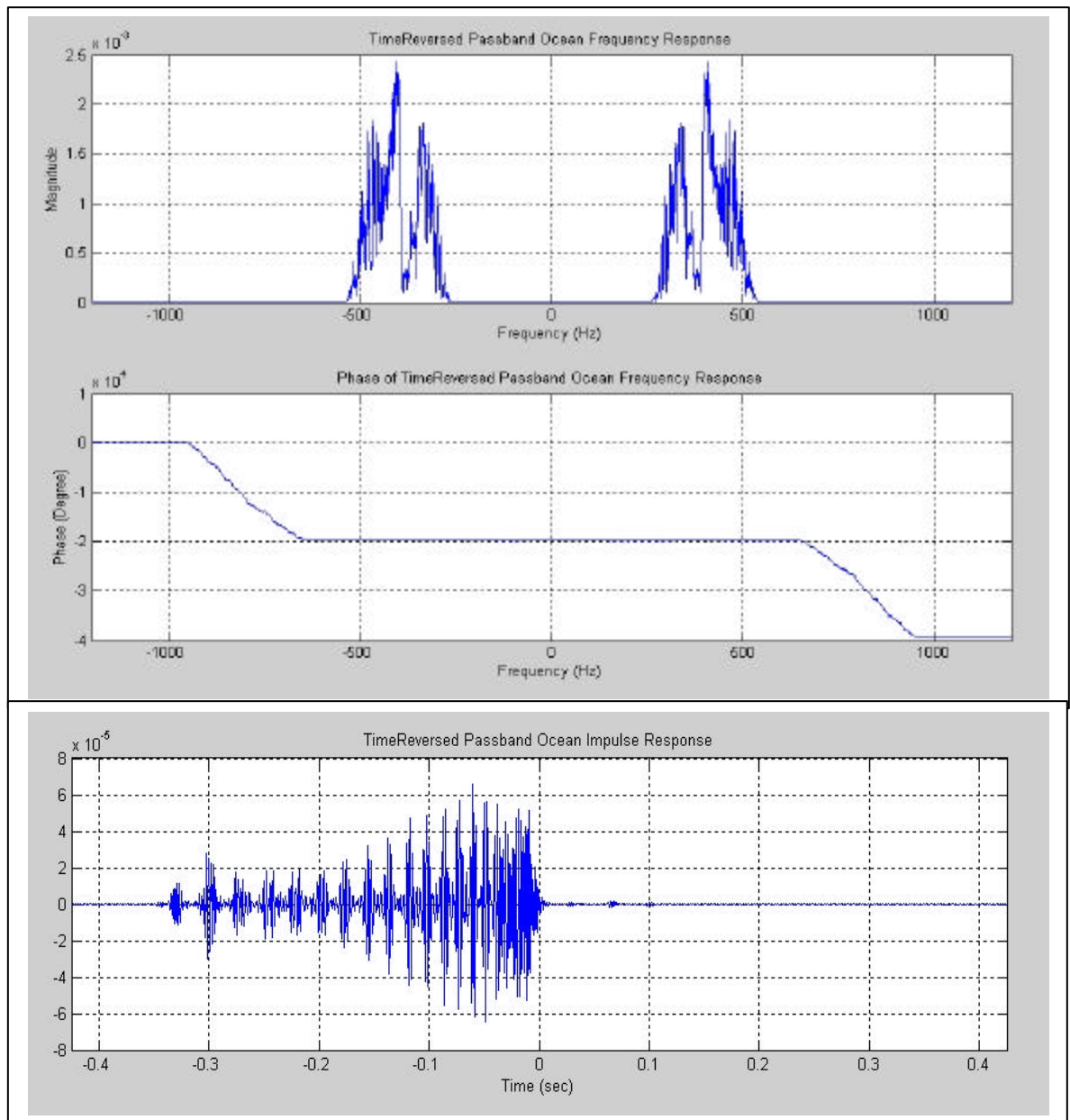


Figure 4.10. Time Reversed Ocean Frequency Response (Magnitude and Phase) and Ocean Impulse Response.

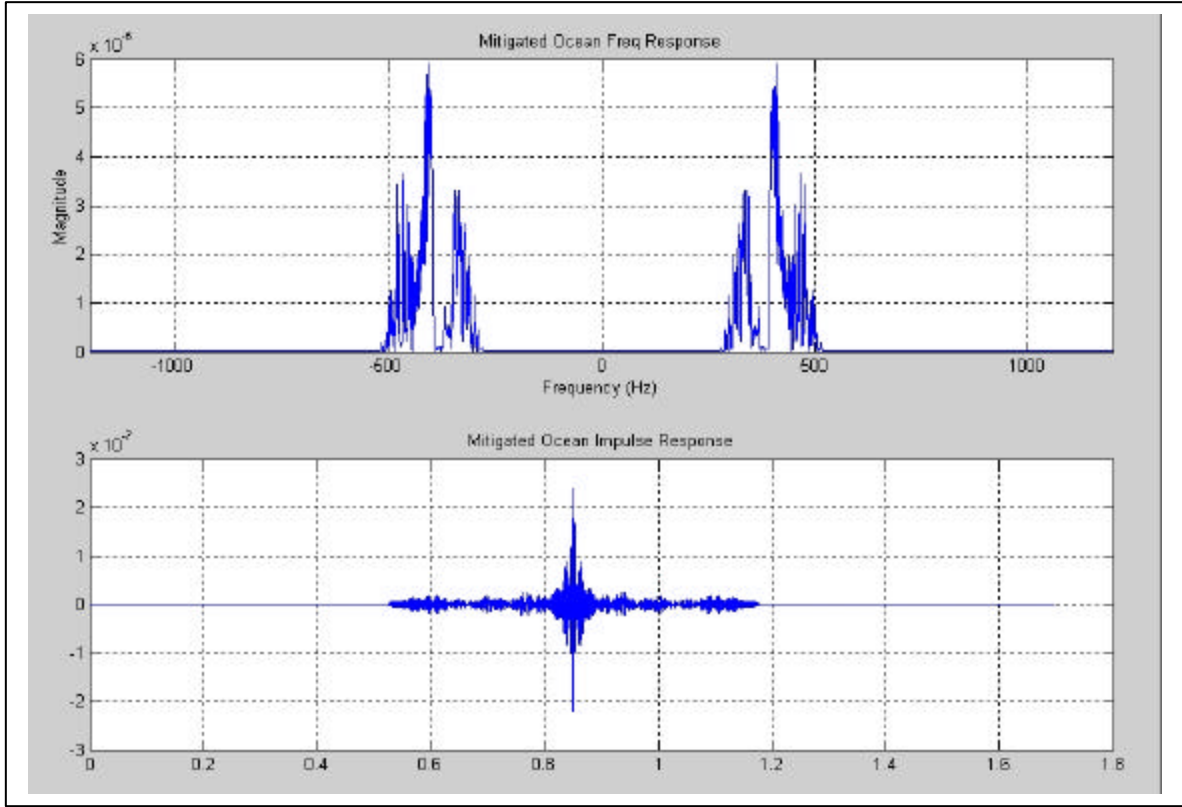


Figure 4.11. Mitigated Ocean Impulse Response and Frequency Response.

The mitigated signal is obtained by convolving $h_b[-n]$ with the received signal to obtain $\hat{s}[n] = q[n] * h_b[-n]$. The recovered signal is obtained by multiplying the mitigated signal $\hat{s}[n]$ by cosine to obtain $y[n] = \hat{s}[n] \cdot \cos\left[\frac{2p f_c n}{f_s}\right]$ and following the same procedures to recover the transmitted binary data described before. The recovered binary data is compared to the transmitted binary data to compute BER. Figure 4.12 shows the mitigated signal in time and frequency domains obtained by convolving the time-reversed ocean impulse response with the received signal. Figure 4.13 shows that the mitigated procedure was able to reduce the bit error rate from 0.55 % to 0 %.

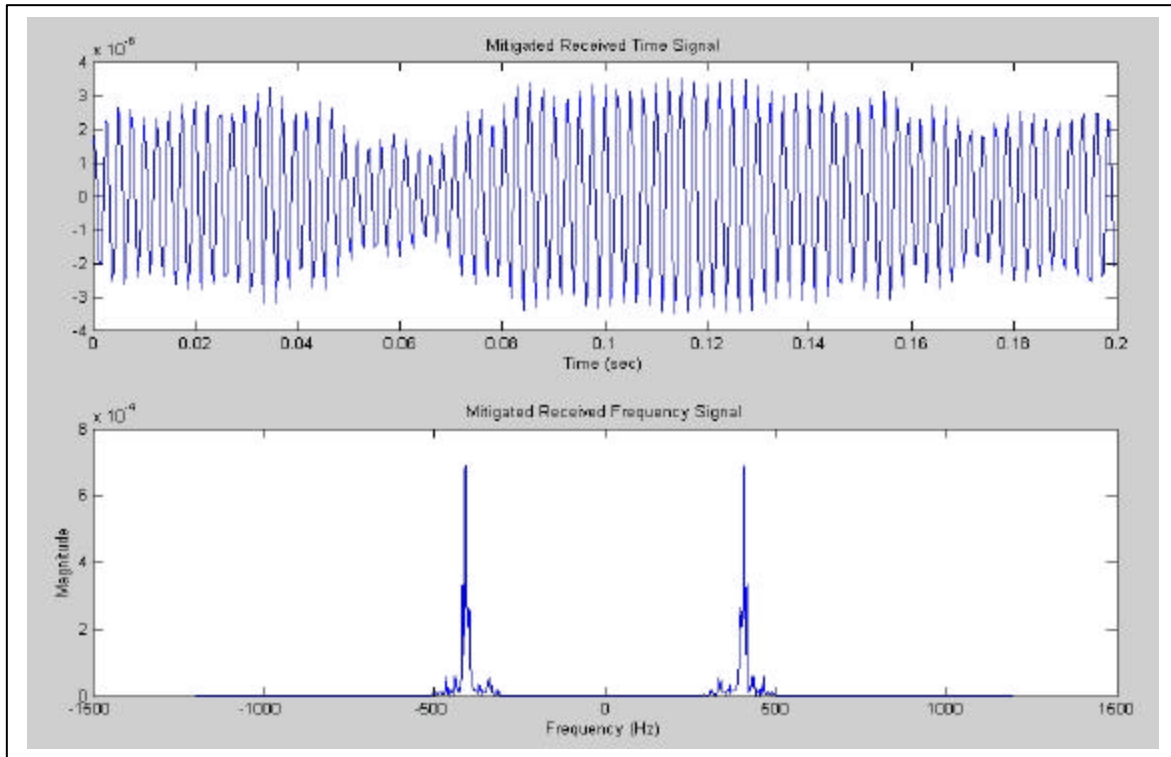


Figure 4.12. Mitigated Signal in Time and Frequency Domain.

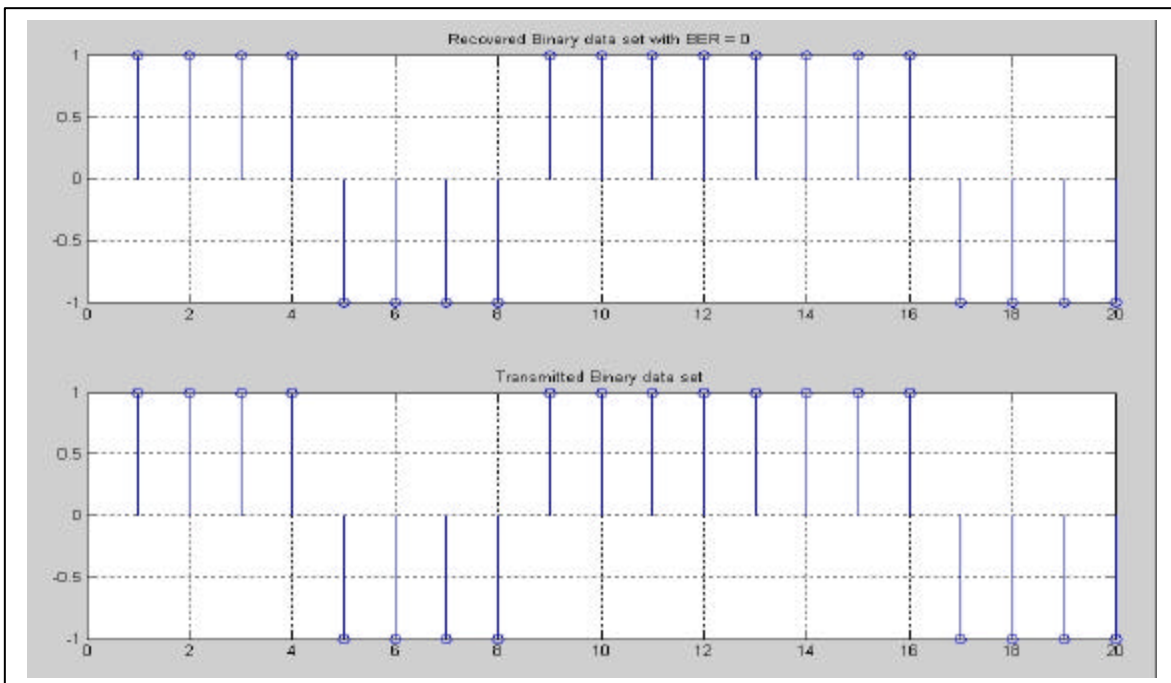


Figure 4.13. Comparison of Recovered Binary Data with Transmitted Binary Data for Mitigated Signal Showing Zero Error.

b. Results For Many Chosen Ranges and Depths

In the following experiment, to obtain more complete results of simulation in this ocean environment, the simulation was performed for the received signal and the mitigated signal to evaluate the bit error performance for many chosen depths and ranges. The parameters for this simulation are the same as in the previous section except the number of bits was increased from 20 to 10,000 ($N_{bit}=10,000$). The ocean frequency responses $H'(f)$ were extracted from the MMPE model at depths of 5 m to 95 m in increments of 5 m and ranges of 0.5 km to 9.5 km in increments of 0.5 km with a sampling frequency $f_{s_{ocean}} = 300$ Hz, bandwidth $W = 300$ Hz and center frequency $f_c = 400$ Hz. The experimental procedures followed were as described before.

As shown in Figure 4.14, the recovered binary data set for the received signals at chosen depths and ranges as described above has a high bit error rate (average=0.4946) due to the distortion of the transmitted BPSK signal due to the multipath propagation resulting from the positive SSP gradient. Figure 4.15 however shows that the recovered binary data set for the mitigated signals obtained by convolving the time-reversed ocean impulse response with the received signal has a low bit error rate (average=0.0451) compared to the bit error rate of the unmitigated received signals. The results of this simulation at many chosen depths and ranges is consistent with the result of simulation at the former chosen depth of 50 m and range 5 km. We conclude therefore that by using the time-reversed ocean impulse response, we can compensate for the degradation in the bit error performance due to the multipath propagation in this simulated ocean environment.

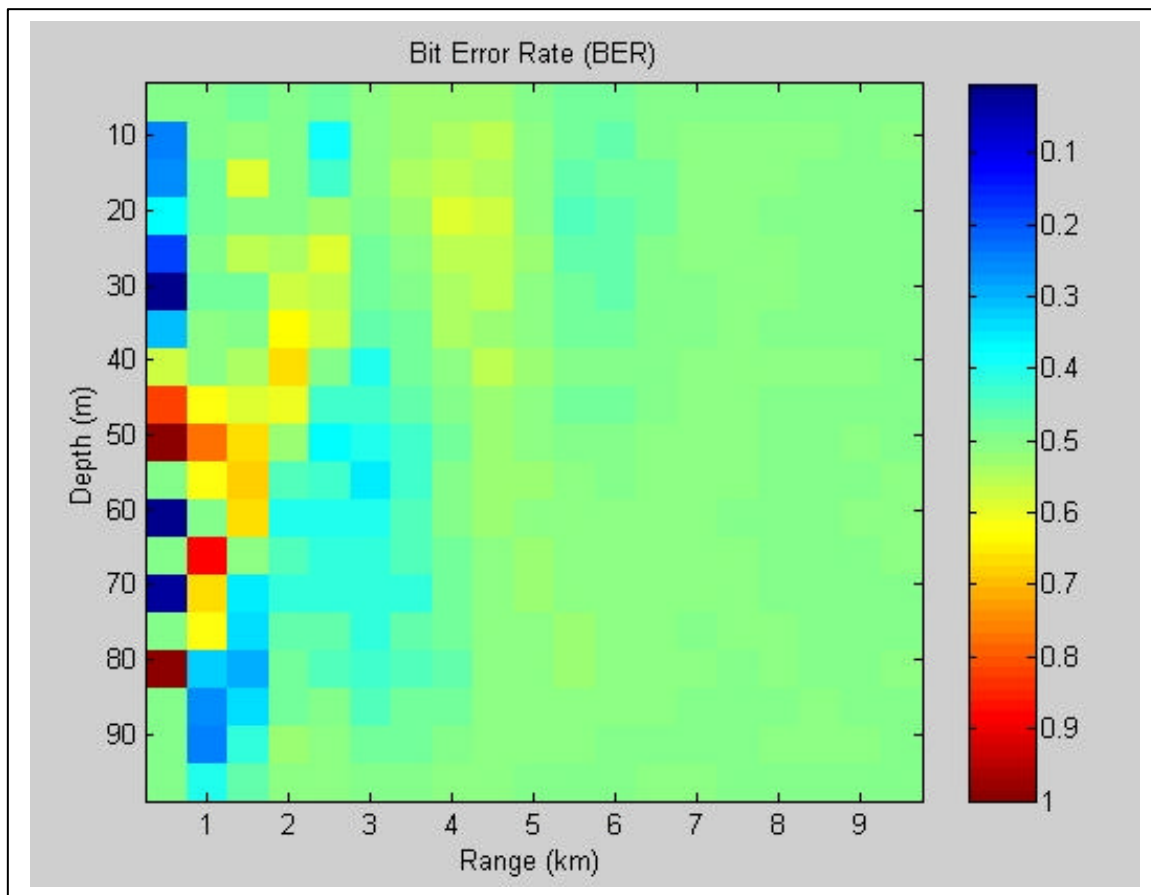


Figure 4.14. Bit Error Performance for Received Signal at Chosen Depths 5 to 95 m and Ranges 0.5 to 9.5 km for a Positive SSP Gradient.

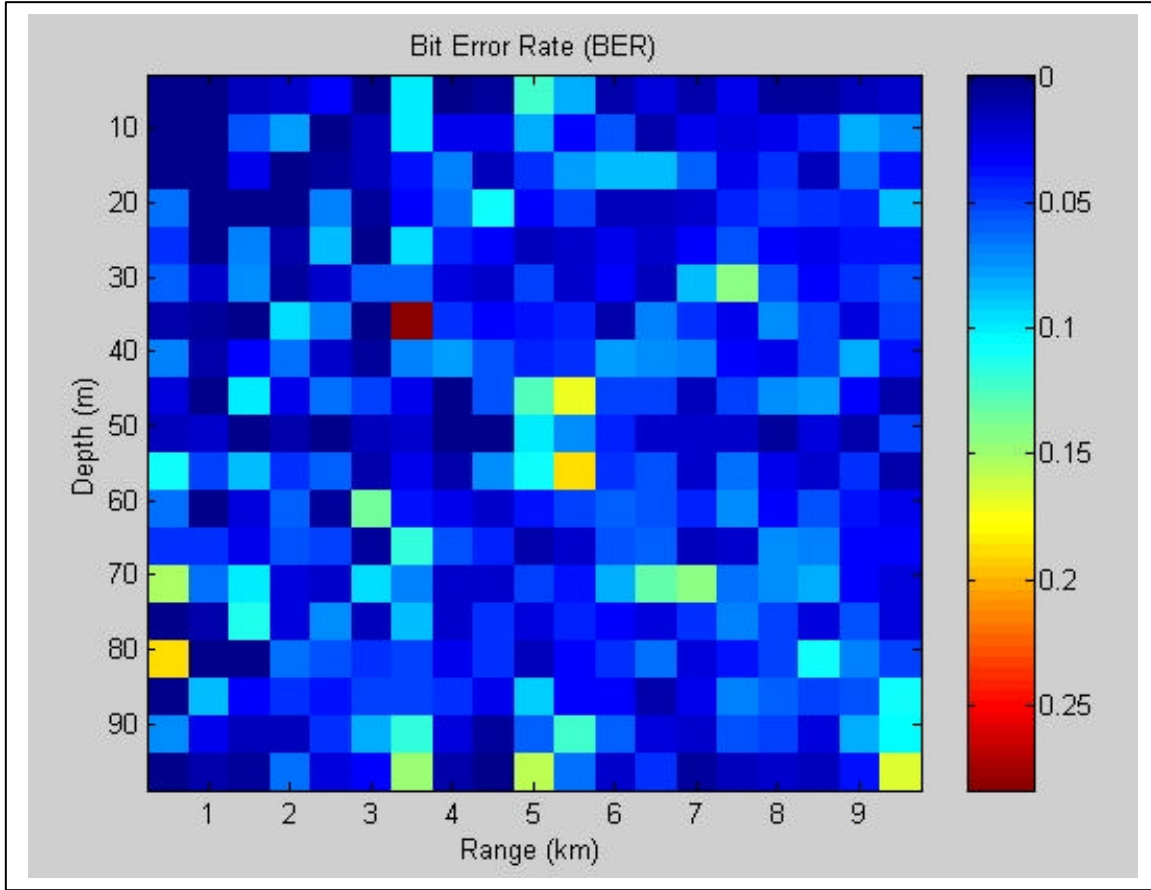


Figure 4.15. Bit Error Performance for Mitigated Signal at Chosen Depths 5 to 95 m and Ranges 0.5 to 9.5 km for a Positive SSP Gradient.

2. Bit Error Performance Results for a Strong Negative SSP Gradient

In the following experiment, for a shallow water acoustic channel of having a strong negative SSP gradient, the simulation was performed for the received signal and the mitigated signal to evaluate the bit error performance for many chosen depths and ranges. The SSP and TL plots are shown in Figure 3.10a and 3.10b. The signal parameters and grid of range and depth values were the same as for the previous case and the experimental procedures followed were as described before. As shown in Figure 4.16, the recovered binary data set for the received signals at chosen depths and ranges as described above has a high bit error rate (average=0.4981) due to the distortion of the ISI resulting from the strong negative sound speed profile. Figure 4.17 shows that the recovered binary data set for the mitigated signals however has a low bit error rate

(average=0.0415) compared to the bit error rate of the unmitigated received signals. We conclude therefore that by using the time-reversed ocean impulse response, we can compensate for the degradation in the bit error performance due to the multipath propagation in this ocean environment as well.

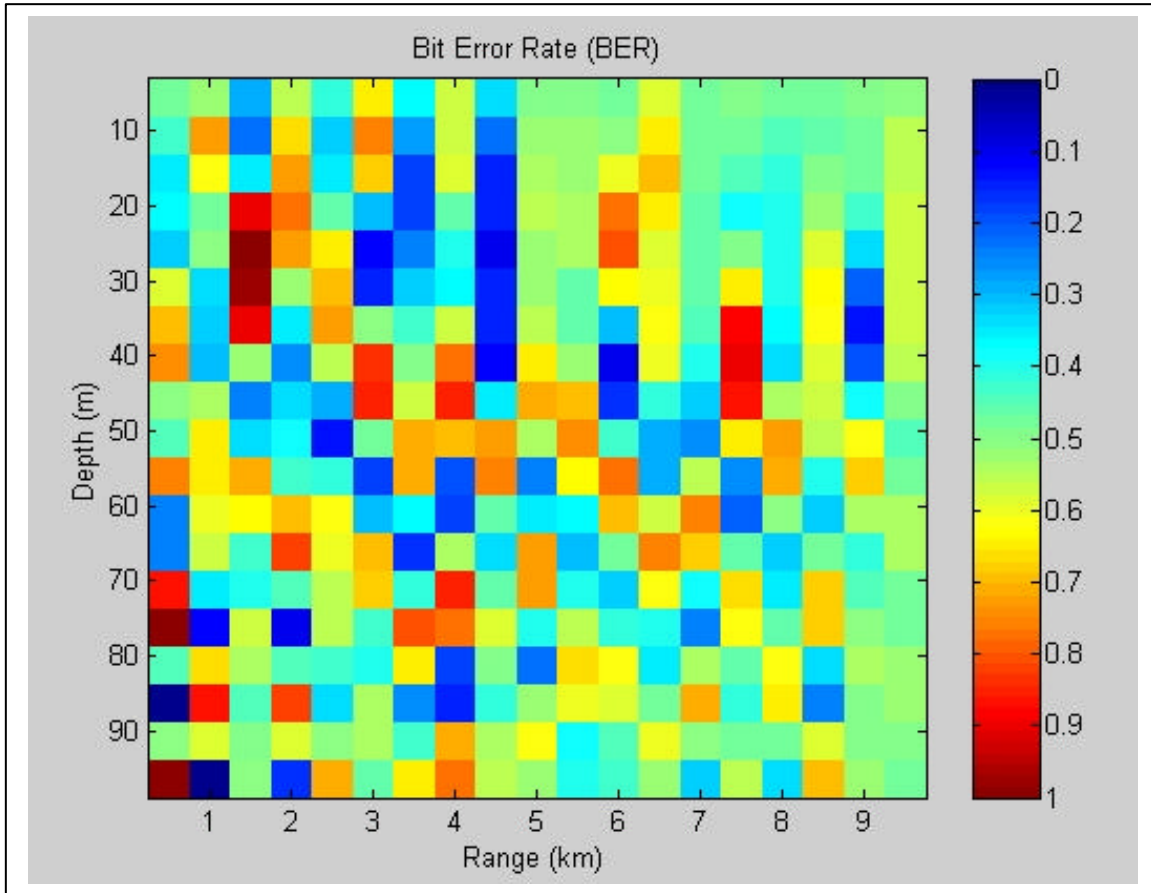


Figure 4.16. Bit Error Performance for Received Signal at Chosen Depths 5 to 95 m and Ranges 0.5 to 9.5 km for a Strong Negative SSP Gradient.

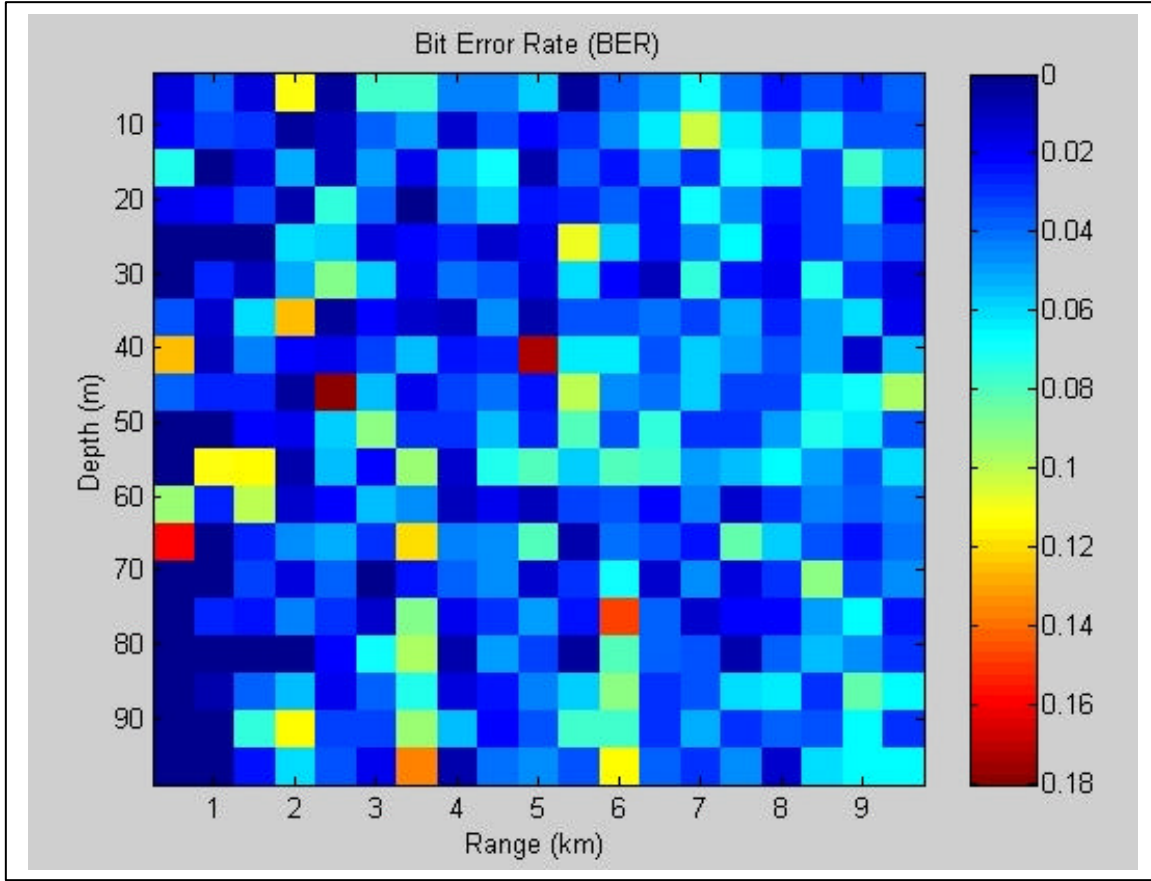


Figure 4.17. Bit Error Performance for Mitigated Signal at Chosen Depths 5 to 95 m and Ranges 0.5 to 9.5 km for a Strong Negative SSP Gradient.

3. Bit Error Performance Results for a Negative SSP Gradient below Surface Duct

In the following experiment, for a shallow water acoustic channel having a negative SSP gradient below surface duct, the simulation was performed for the received signal and the mitigated signal to evaluate the bit error performance for many chosen depths and ranges. The SSP and TL plots for this environment are shown in Figure 3.11a and 3.11b. The signal parameters and grid of range and depth values were the same as in the previous case and the experimental procedures followed were as described before. As shown in Figure 4.18, the recovered binary without mitigation has a high bit error rate (average=0.4989) due to the multipath and the resulting ISI. Figure 4.19 shows that the recovered binary data set for the mitigated signals however has a low bit error rate

(average=0.0398) compared to the bit error rate of the unmitigated received signals. We conclude that for this environment as well, by using the time-reversed ocean impulse response, we can compensate for the degradation in the bit error performance due to the multipath propagation.

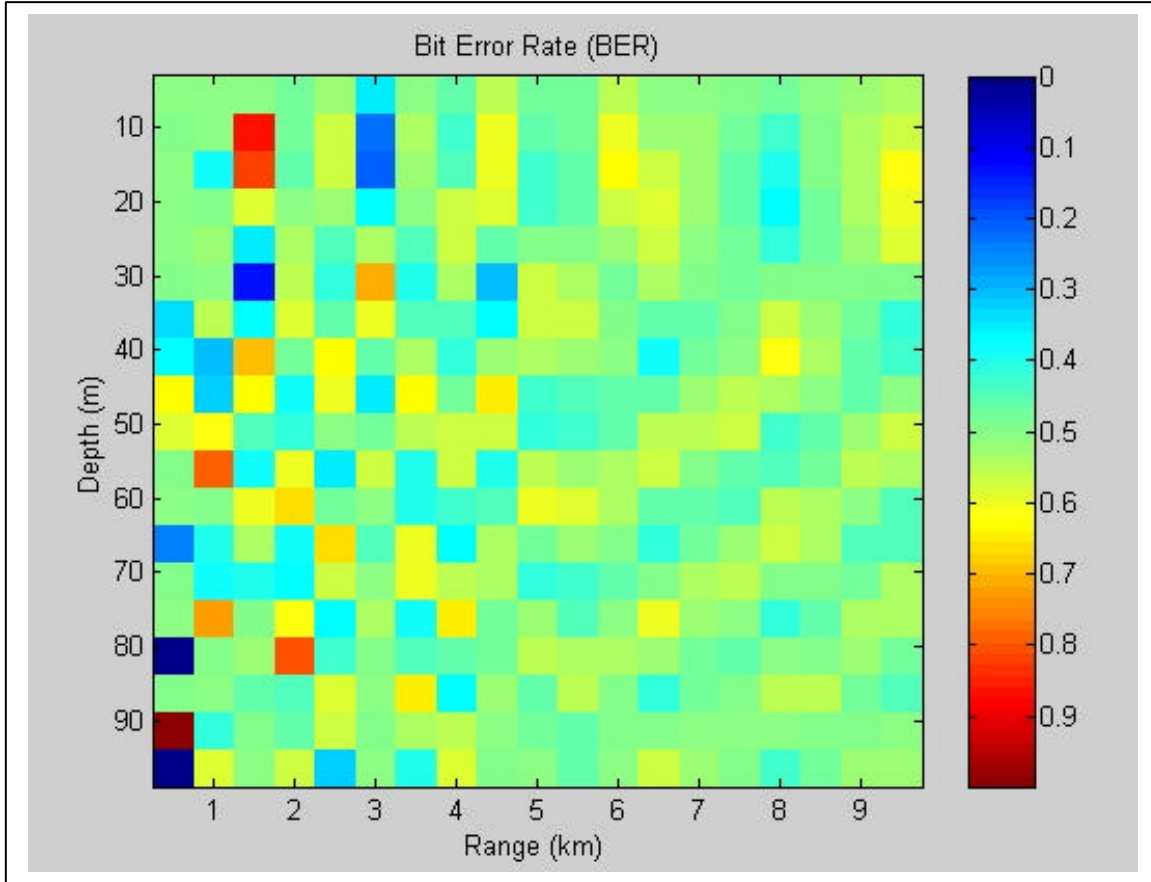


Figure 4.18. Bit Error Performance for Received Signal at Chosen Depths 5 to 95 m and Ranges 0.5 to 9.5 km for a Negative SSP Gradient below Surface Duct.

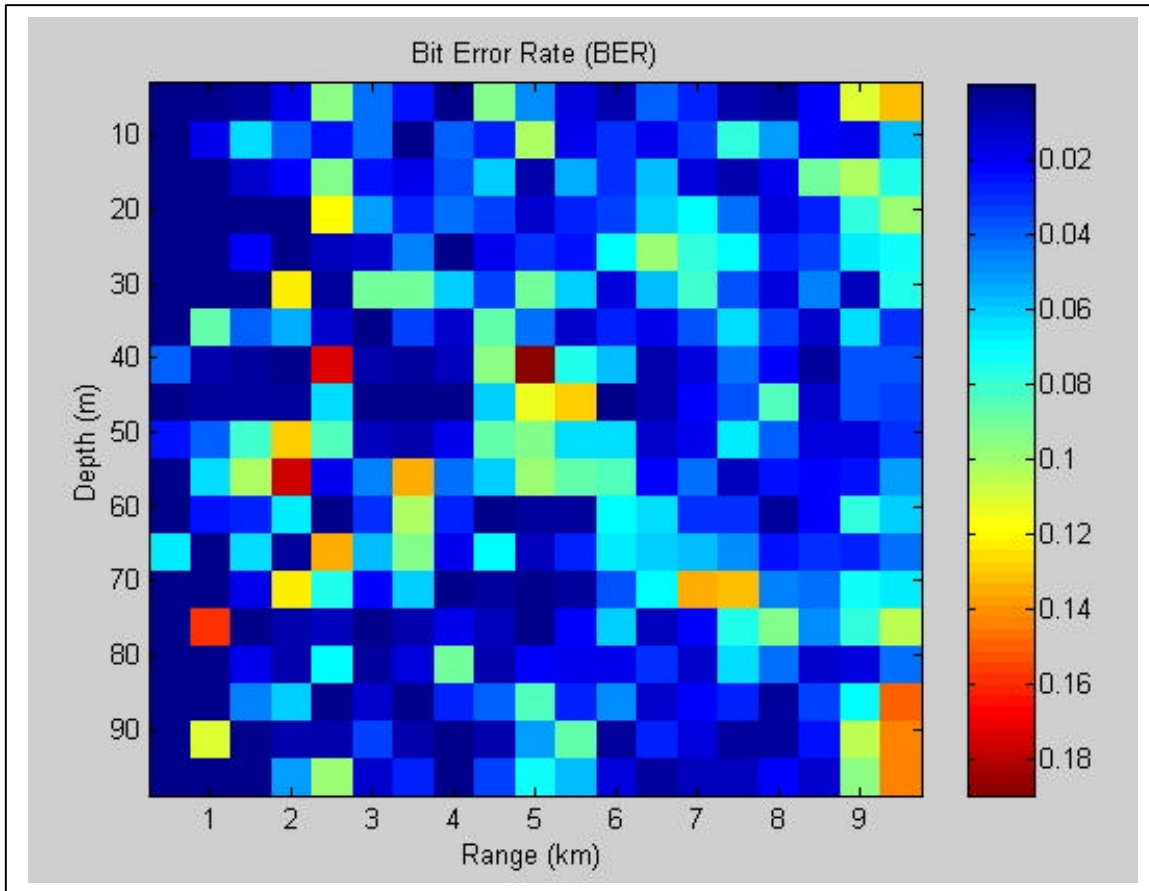


Figure 4.19. Bit Error Performance for Mitigated Signal at Chosen Depths 5 to 95 m and Ranges 0.5 to 9.5 km for a Negative SSP Gradient below Surface Duct.

V. CONCLUSIONS AND RECOMMENDATIONS

A. CONCLUSIONS

The primary goal of this thesis was to investigate mitigating the degradation on the bit error performance of the BPSK signal by convolving the time-reversed ocean impulse response with the received signal distorted by the multipath propagation in three different shallow water acoustic channels. The simulation was validated by a comparison of the results of the bit error performance from the received signal and those from the mitigated signal. In our experiments, it was possible to reduce the high bit error rate as follows. For a positive SSP gradient, the average bit error rate decreased from 0.4946 to 0.0451. For a strong negative SSP gradient, the average bit error rate decreased from 0.4981 to 0.0415. For a negative SSP gradient below the surface duct, the average bit error rate decreased from 0.4989 to 0.0398. Thus, it was possible to improve the bit error performance of a BPSK signal by using the time-reversed ocean impulse response.

The experiments assumed that the correct ocean impulse response was used at each position of the receiver. The sensitivity to range and depth or incorrect ocean impulse response was not investigated in any quantitative manner. There were some indications, however, of a fair amount of sensitivity to change in position.

B. RECOMMENDATIONS

Although our experiment was not able to produce a sufficiently low bit error rate needed to achieve an effective underwater communication in the ocean environment, the algorithm may be of some use if appropriate error correction coding is employed to reduce the bit error rate. Experiments with a time-reversed ocean impulse response showed reasonable success in reducing the bit error rate of the distorted BPSK signal due to the intersymbol interference. The combination of appropriate other filtering and coding/decoding with this time-reversed ocean impulse response may therefore be worthy of further investigation.

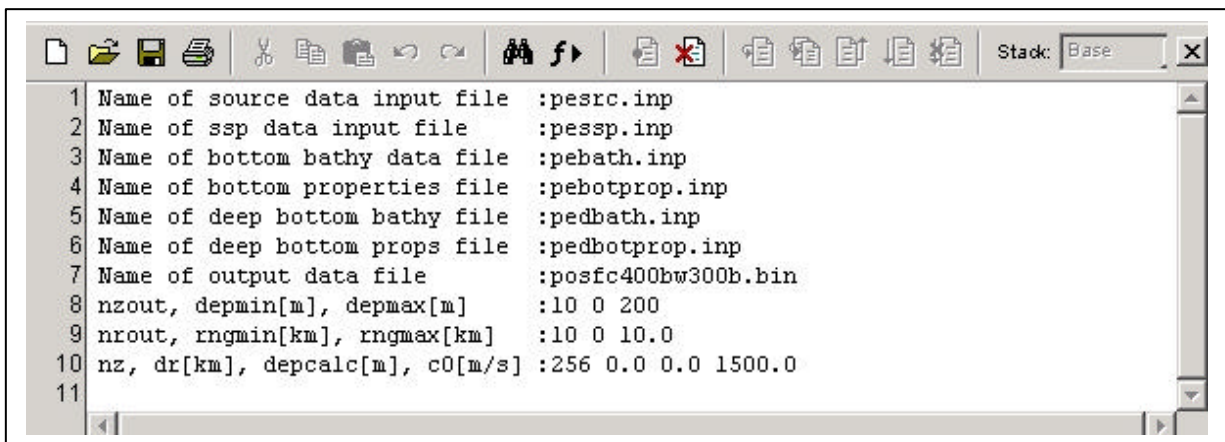
THIS PAGE INTENTIONALLY LEFT BLANK

APPENDIX A. MMPE INPUT FILES FOR THREE DIFFERENT OCEAN ENVIRONMENTAL CASES

This appendix gives the complete set of MMPE input files for three different ocean environmental cases as described in Chapter III. The MMPE input files of the environmental data except the input file of the sound speed profile and `pesrc.inp` file of the source data are same for three cases.

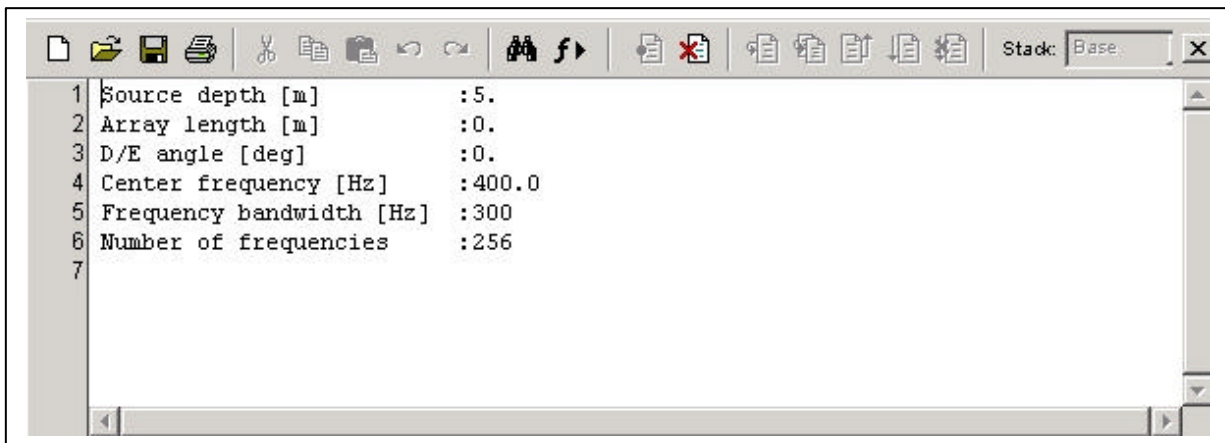
A. MMPE INPUT FILES FOR POSITIVE SSP GRADIENT

1. `pefiles.inp` File of the Main Input File



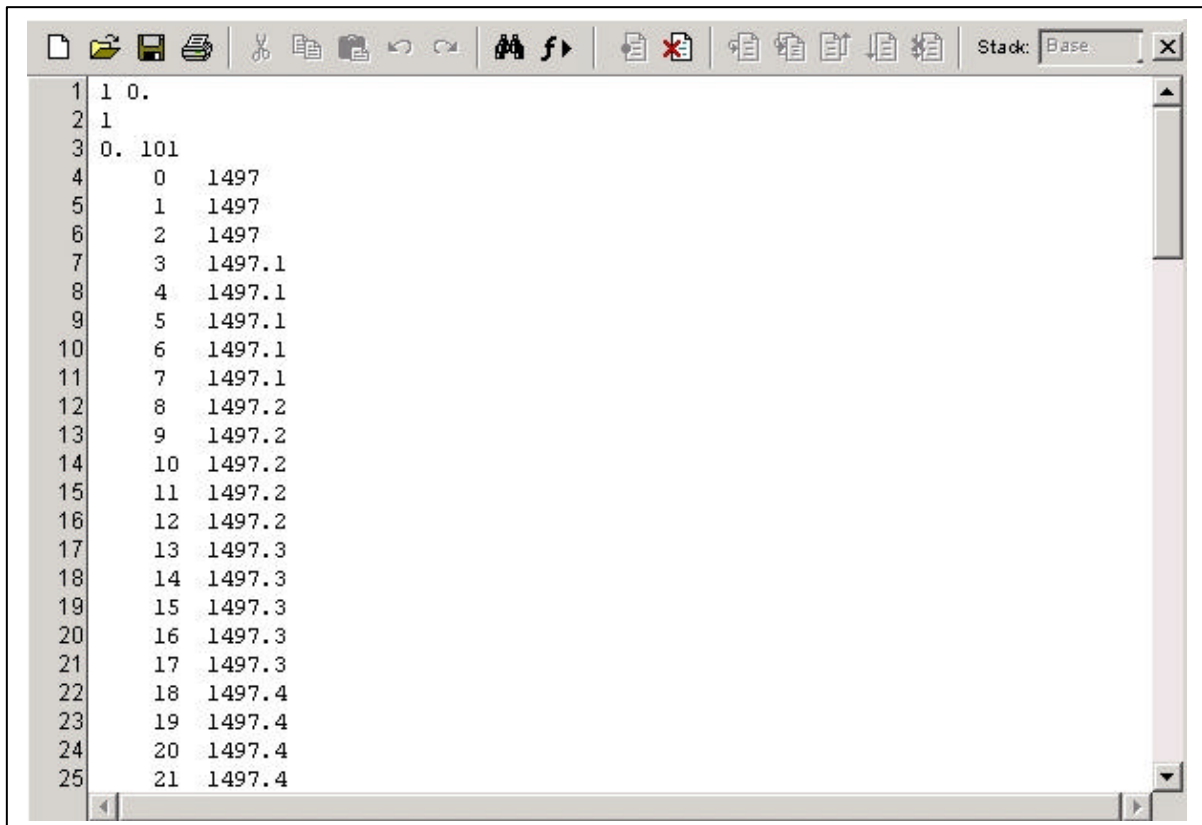
```
1 Name of source data input file :pesrc.inp
2 Name of ssp data input file :pessp.inp
3 Name of bottom bathy data file :pebath.inp
4 Name of bottom properties file :pebotprop.inp
5 Name of deep bottom bathy file :pedbath.inp
6 Name of deep bottom props file :pedbotprop.inp
7 Name of output data file :posfc400bw300b.bin
8 nzout, depmin[m], depmax[m] :10 0 200
9 nrout, rngmin[km], rngmax[km] :10 0 10.0
10 nz, dr[km], depcalc[m], c0[m/s] :256 0.0 0.0 1500.0
11
```

2. `pesrc.inp` File of the Source Data



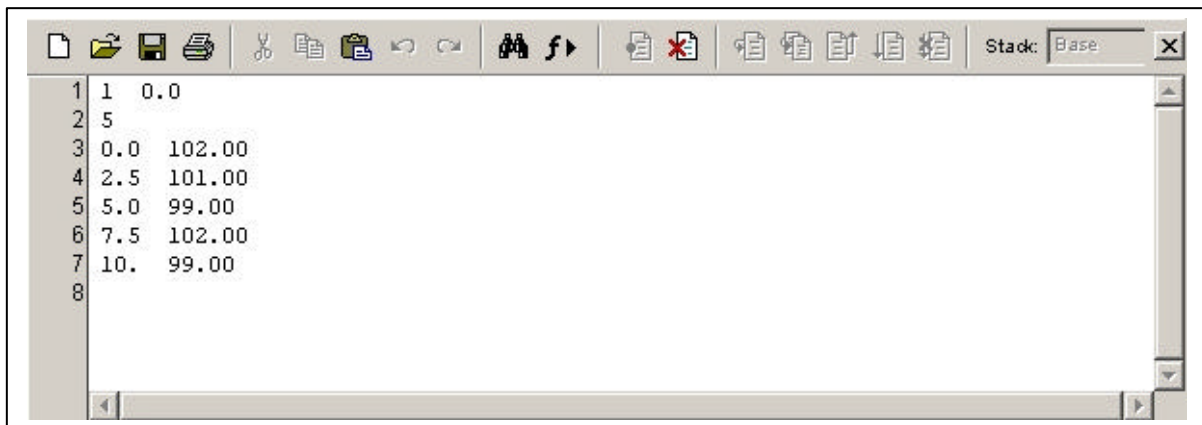
```
1 Source depth [m] :5.
2 Array length [m] :0.
3 D/E angle [deg] :0.
4 Center frequency [Hz] :400.0
5 Frequency bandwidth [Hz] :300
6 Number of frequencies :256
7
```

3. `pessp.inp` File of the Environmental Data



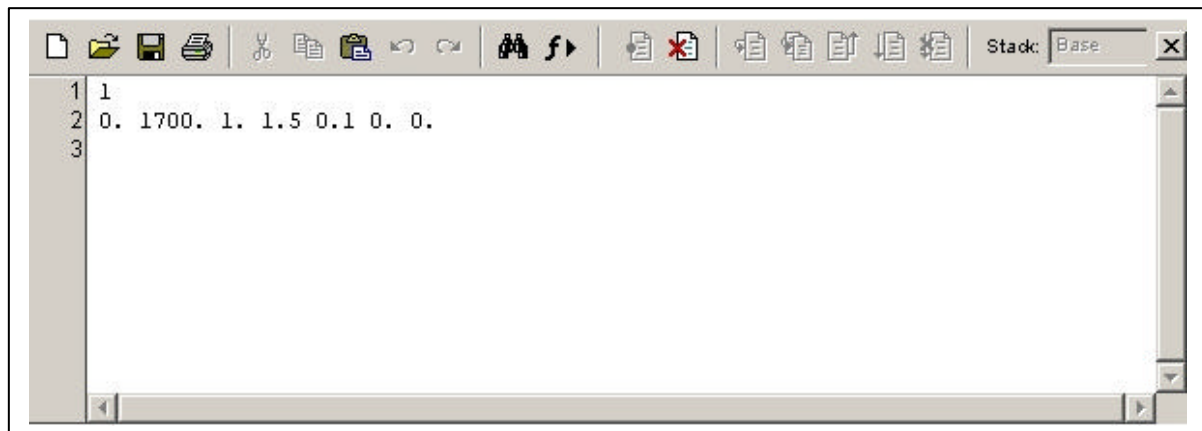
1	1	0.
2	1	
3	0.	101
4	0	1497
5	1	1497
6	2	1497
7	3	1497.1
8	4	1497.1
9	5	1497.1
10	6	1497.1
11	7	1497.1
12	8	1497.2
13	9	1497.2
14	10	1497.2
15	11	1497.2
16	12	1497.2
17	13	1497.3
18	14	1497.3
19	15	1497.3
20	16	1497.3
21	17	1497.3
22	18	1497.4
23	19	1497.4
24	20	1497.4
25	21	1497.4

4. `pebath.inp` File of the Environmental Data

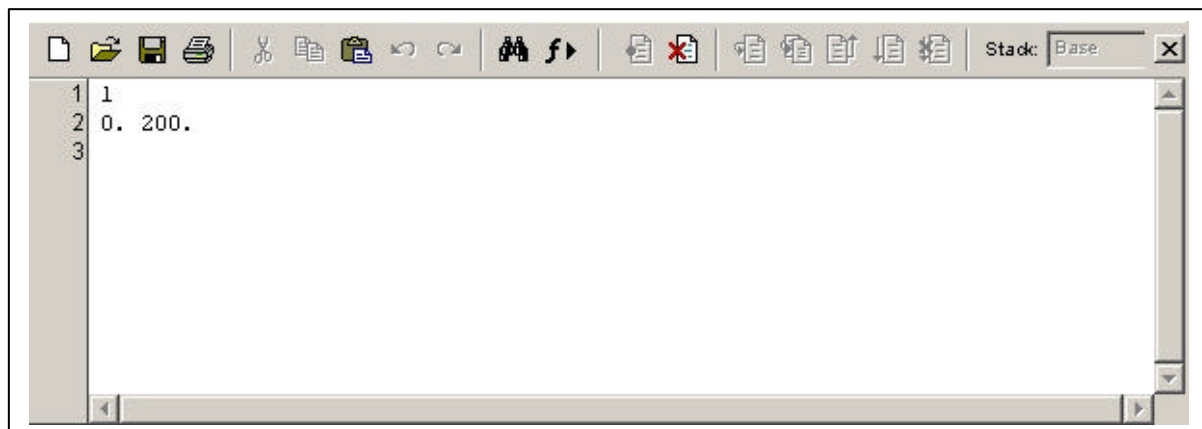


1	1	0.0
2	5	
3	0.0	102.00
4	2.5	101.00
5	5.0	99.00
6	7.5	102.00
7	10.	99.00
8		

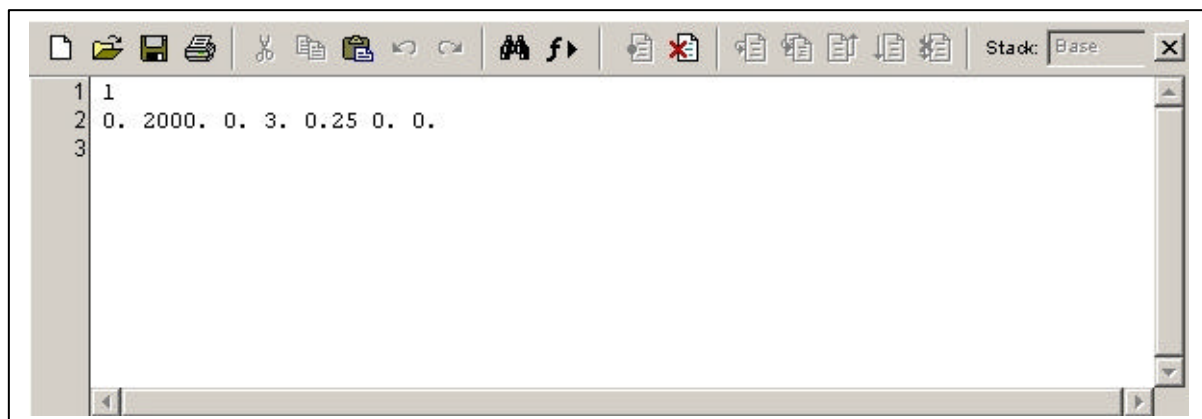
5. pebotprop.inp File of the Environmental Data



6. pedbath.inp File of the Environmental Data

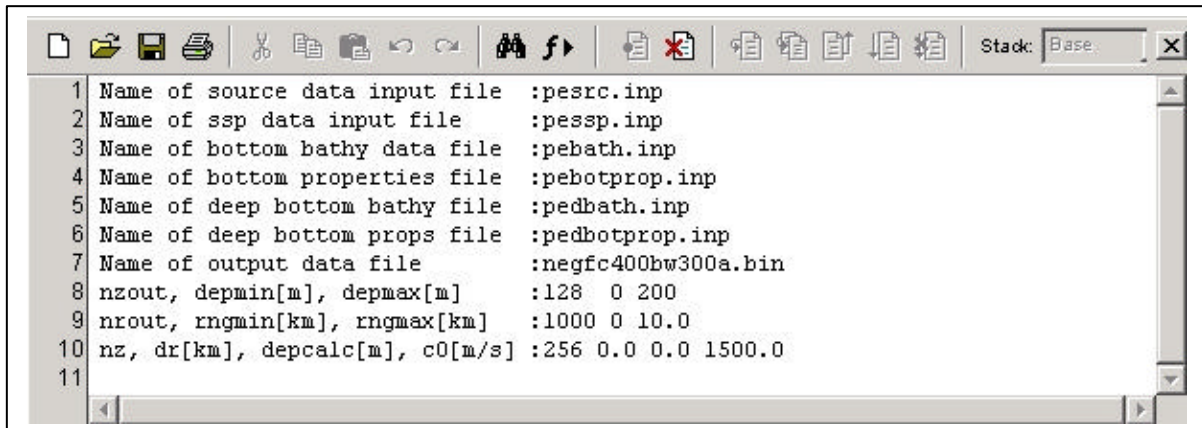


7. pefiles.inp File of the Environmental Data



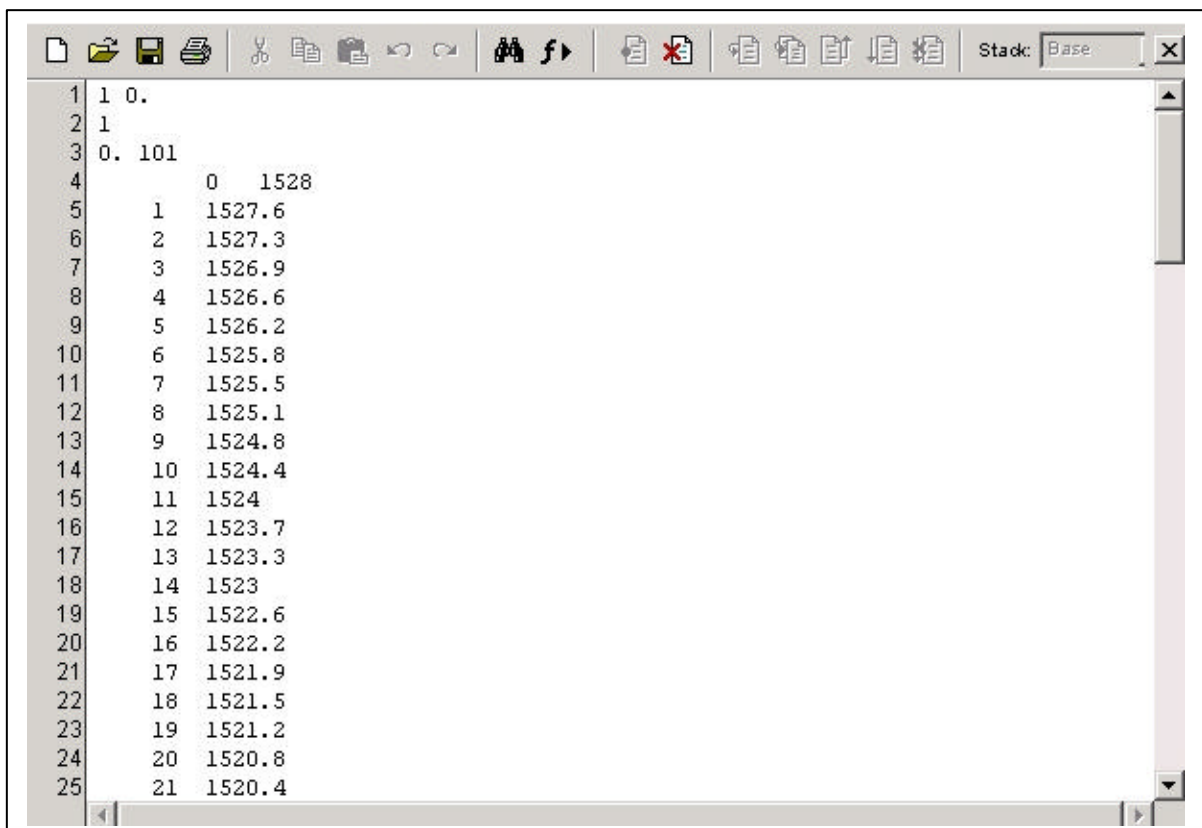
B. MMPE INPUT FILES FOR STRONG NEGATIVE SSP GRADIENT

1. pefiles.inp File of the Main Input File



```
1 Name of source data input file :pesrc.inp
2 Name of ssp data input file :pessp.inp
3 Name of bottom bathy data file :pebath.inp
4 Name of bottom properties file :pebotprop.inp
5 Name of deep bottom bathy file :pedbath.inp
6 Name of deep bottom props file :pedbotprop.inp
7 Name of output data file :negfc400bw300a.bin
8 nzout, depmin[m], depmax[m] :128 0 200
9 nrout, rngmin[km], rngmax[km] :1000 0 10.0
10 nz, dr[km], depcalc[m], c0[m/s] :256 0.0 0.0 1500.0
11
```

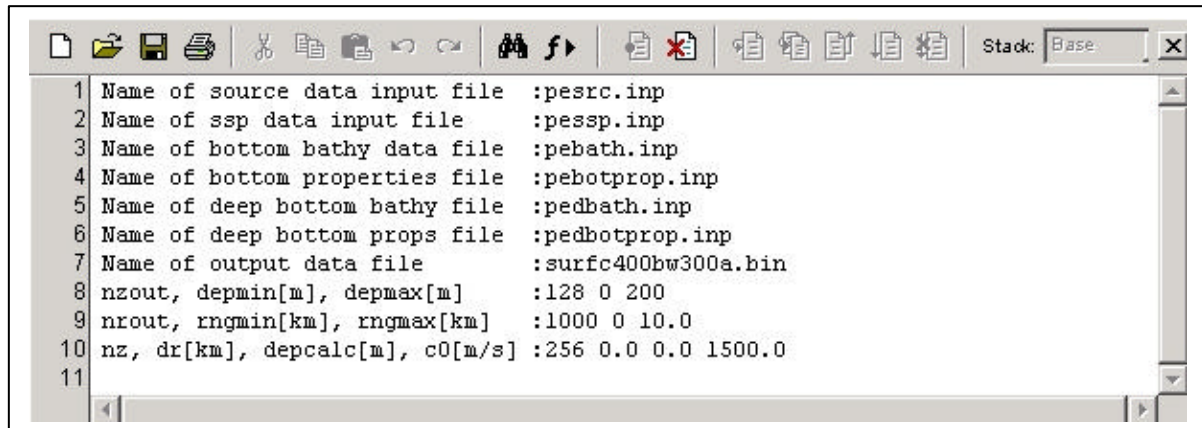
2. pessp.inp File of the Environmental Data



```
1 1 0.
2 1
3 0. 101
4 0 1528
5 1 1527.6
6 2 1527.3
7 3 1526.9
8 4 1526.6
9 5 1526.2
10 6 1525.8
11 7 1525.5
12 8 1525.1
13 9 1524.8
14 10 1524.4
15 11 1524
16 12 1523.7
17 13 1523.3
18 14 1523
19 15 1522.6
20 16 1522.2
21 17 1521.9
22 18 1521.5
23 19 1521.2
24 20 1520.8
25 21 1520.4
```

C. MMPE INPUT FILES FOR NEGATIVE SSP GRADIENT BELOW SURFACE DUCT

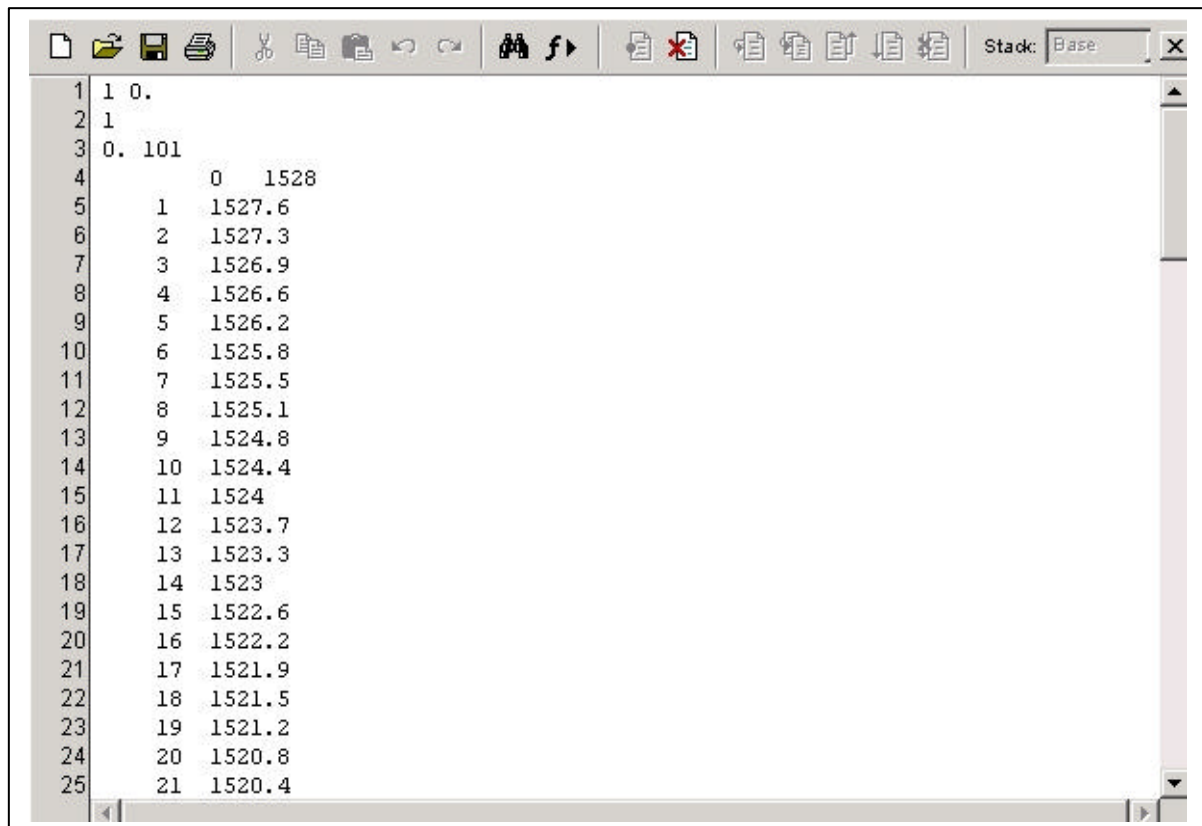
1. pefiles.inp File of the Main Input File



A screenshot of a text editor window titled 'Stack: Base'. The editor displays the content of the 'pefiles.inp' file. The text is as follows:

```
1 Name of source data input file :pesrc.inp
2 Name of ssp data input file :pessp.inp
3 Name of bottom bathy data file :pebath.inp
4 Name of bottom properties file :pebotprop.inp
5 Name of deep bottom bathy file :pedbath.inp
6 Name of deep bottom props file :pedbotprop.inp
7 Name of output data file :surfc400bw300a.bin
8 nzout, depmin[m], depmax[m] :128 0 200
9 nrout, rngmin[km], rngmax[km] :1000 0 10.0
10 nz, dr[km], depcalc[m], c0[m/s] :256 0.0 0.0 1500.0
11
```

2. pessp.inp File of the Environmental Data



A screenshot of a text editor window titled 'Stack: Base'. The editor displays the content of the 'pessp.inp' file. The text is as follows:

```
1 1 0.
2 1
3 0. 101
4      0 1528
5      1 1527.6
6      2 1527.3
7      3 1526.9
8      4 1526.6
9      5 1526.2
10     6 1525.8
11     7 1525.5
12     8 1525.1
13     9 1524.8
14    10 1524.4
15    11 1524
16    12 1523.7
17    13 1523.3
18    14 1523
19    15 1522.6
20    16 1522.2
21    17 1521.9
22    18 1521.5
23    19 1521.2
24    20 1520.8
25    21 1520.4
```

THIS PAGE INTENTIONALLY LEFT BLANK

APPENDIX B. DETAILED SIGNAL PROCESSING STEPS

This appendix gives the complete procedures from the generation of the BPSK signal to the demodulation of the received signal for an ideal digital communication channel (i.e., without any distortion)

A. RANDOM BINARY DATA GENERATION

The generated random binary data $b[n]$ has parameters $N_{bit} = 20$ bits, $R = 100$ bit/sec, $N_{sb} = 24$, $f_s = 2400$ Hz and $T_b = 0.01$ sec. Figure B-1 shows the random binary data in time and frequency domains.

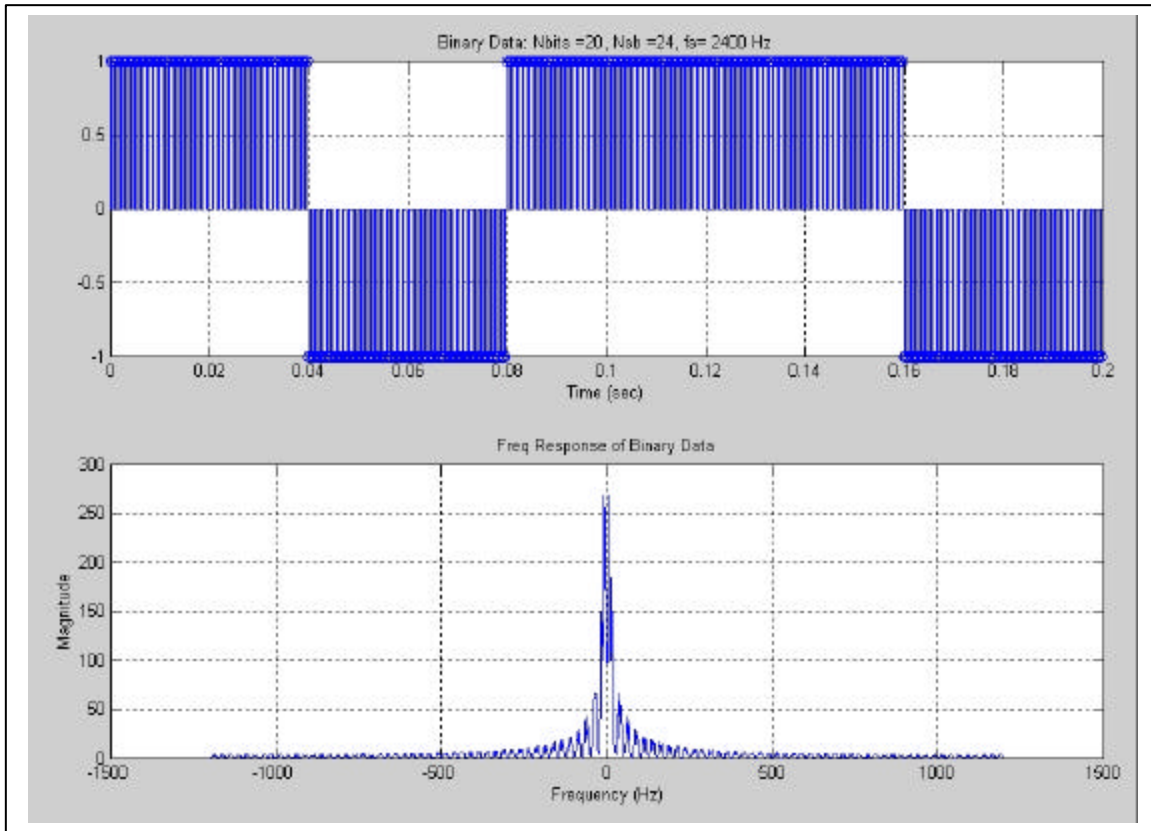


Figure B-1. Random Binary Data in Time Domain and Frequency Domain.

B. FILTERING

This random binary data is filtered to remove an unwanted spectral energy above bandwidth ($W = 200$ Hz). The FIR filter $h_{LPF}[n]$ is designed using a Hamming window as described in chapter 4. The filtered binary data is $b_f[n] = b[n] * h_{LPF}[n]$. Figure B-2 shows the frequency response of FIR filter $h_{LPF}[n]$ and the filtered binary data $b_f[n]$.

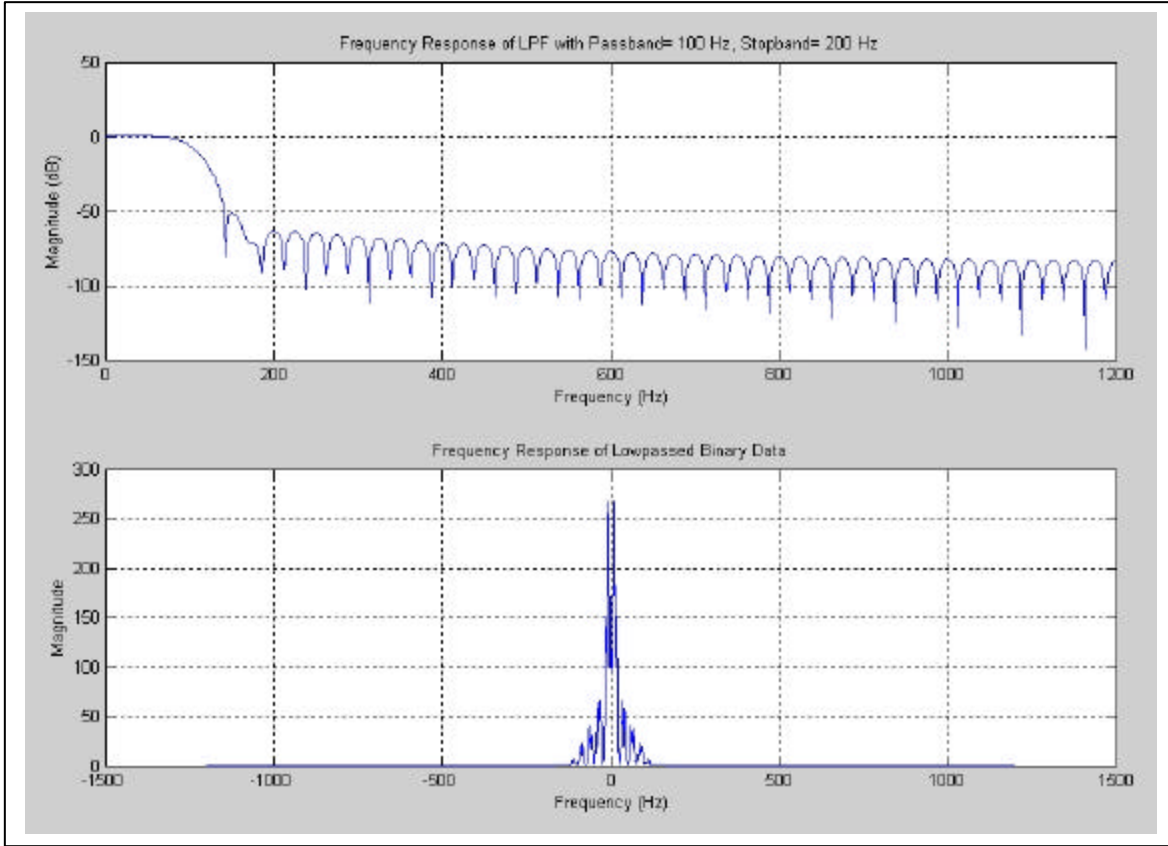


Figure B-2. Frequency Response of the FIR Filter and the Filtered Binary Data.

C. GENERATION OF BPSK SIGNAL

The filtered binary data $b_f[n]$ is modulated by a cosine modulating signal, $k[n] = \cos\left[\frac{2\pi f_c n}{f_s}\right]$ having a carrier frequency of $f_c = 400$ Hz. The modulated BPSK signal is $s[n] = b_f[n] \cdot k[n]$. Figure B-3 shows the modulated BPSK signal in the time and frequency domains.

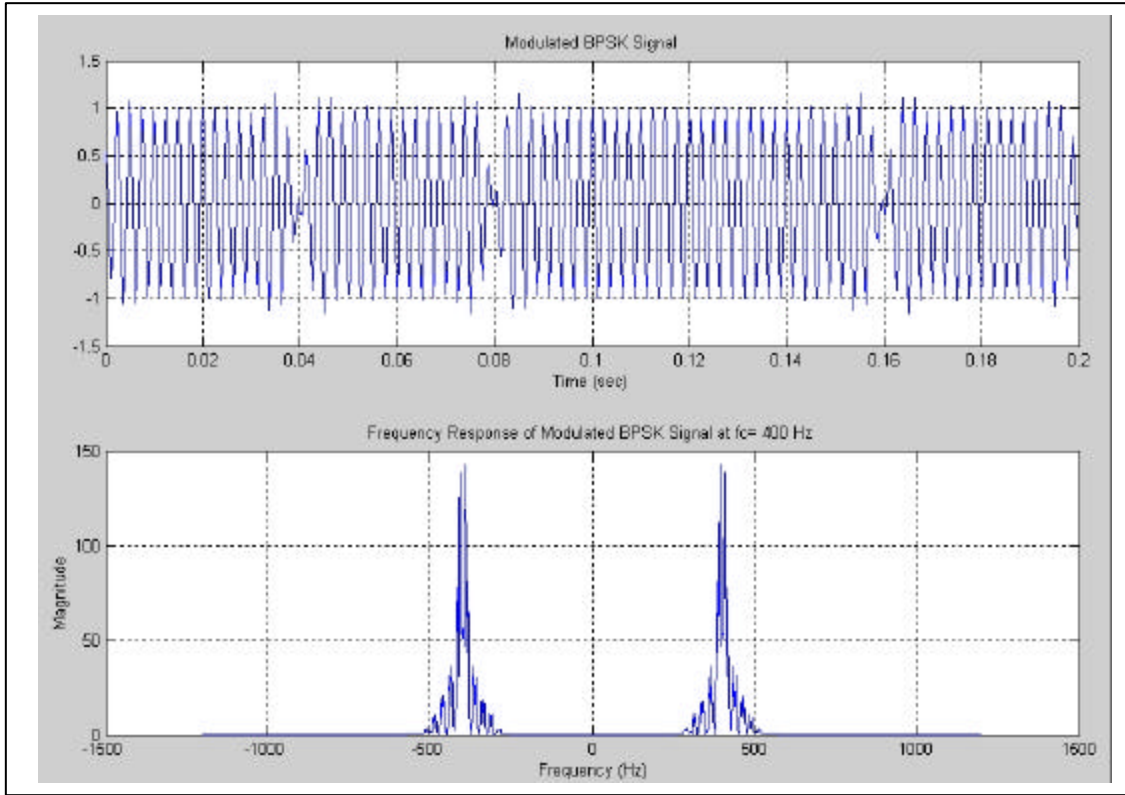


Figure B-3. BPSK Signal $s[n]$ in Time Domain and Frequency Domain.

D. DEMODULATION OF BPSK SIGNAL, FILTERING

The transmitted BPSK signal $s[n]$ is demodulated by multiplying by a cosine demodulating signal, $d[n] = \cos\left[\frac{2p f_c n}{f_s}\right]$. The demodulated signal is given by $y[n] = s[n] \cdot d[n]$ and produces a double frequency component centered at ± 800 Hz as shown in Figure B-4. The signal $y[n]$ is filtered again to remove unwanted spectral energy outside bandwidth by using same FIR filter described above. The demodulated and filtered signal is $y_f[n] = y[n] * h_{LPF}[n]$. Figure B-4 shows the frequency response of the demodulated BPSK signal $y[n]$ before lowpass filtering. Figure B-5 shows the demodulated and filtered signal $y_f[n]$ in time and frequency domains.

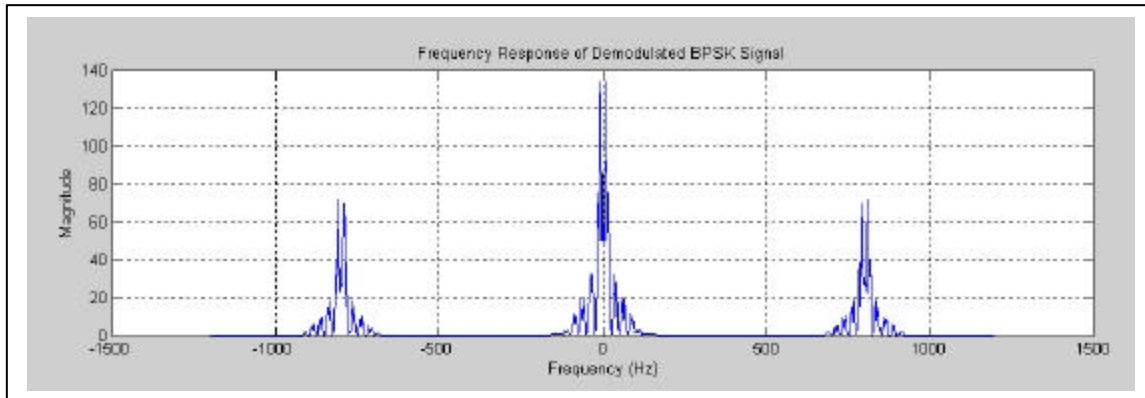


Figure B-4. Demodulated BPSK Signal $y[n]$ in Frequency Domain.

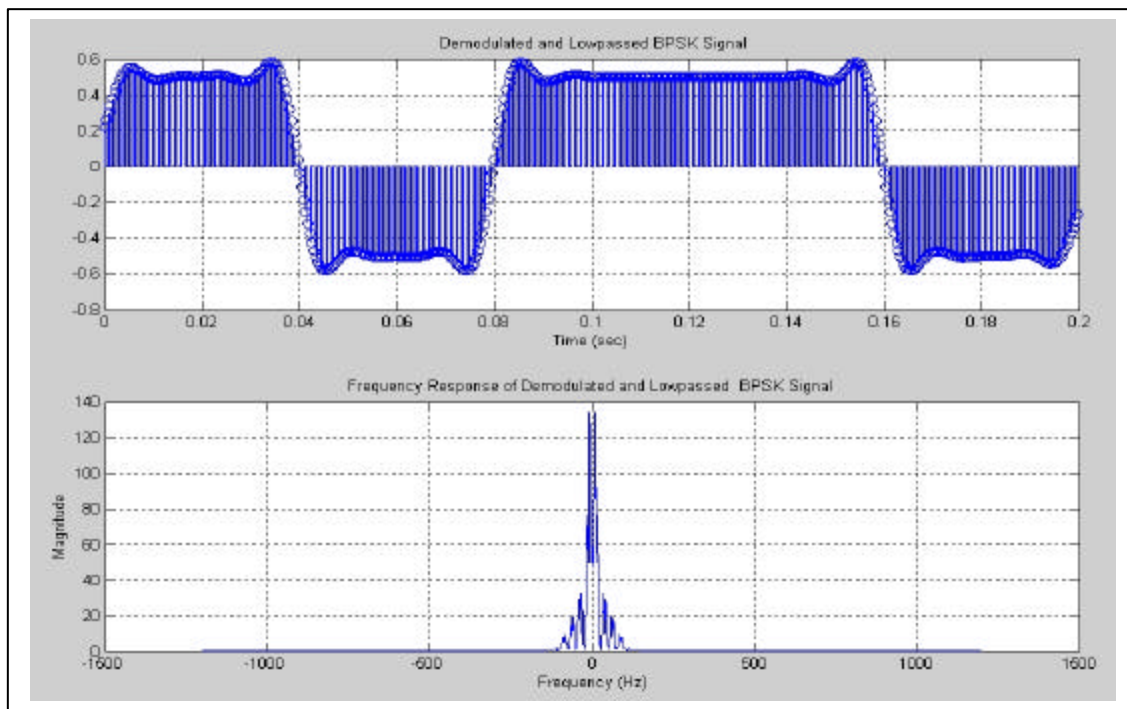


Figure B-5. Demodulated and Filtered BPSK Signal in Time and Frequency Domain.

E. BER COUNTING

This demodulated and filtered signal $y_f[n]$ is integrated over the bit time duration to form the detection statistic and then compared to an optimum threshold as described in Eq. (3.43a) of Chapter III and by this decision rule, we decide binary 1 or 0. Thus, the recovered binary data is compared to the transmitted binary data. Figure B-6

shows that the bit error rate of the recovered binary data for an ideal digital communication signal goes to zero.

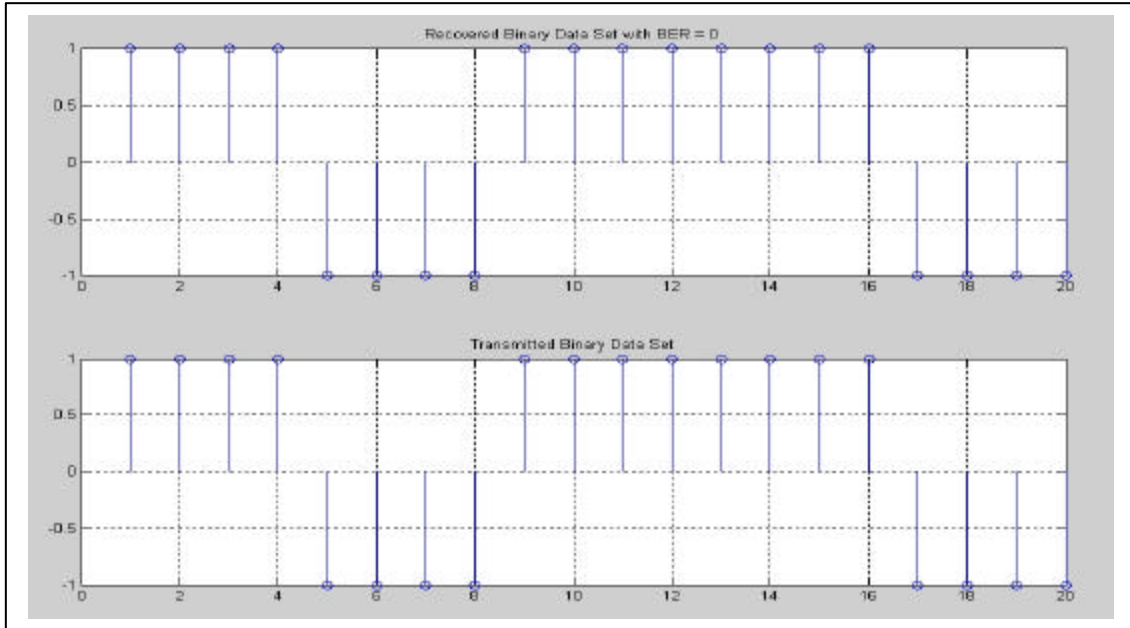


Figure B-6. Comparison between Recovered Binary Data and Transmitted Binary Data.

THIS PAGE INTENTIONALLY LEFT BLANK

APPENDIX C. COMPLETE PROCEDURES TO GENERATE THE PASSBAND OCEAN IMPULSE RESPONSE AND FREQUENCY RESPONSE FROM THE MMPE MODEL

This appendix gives the complete procedures to generate the passband ocean impulse response and frequency response at a high sampling frequency from the modified ocean frequency response $H'(f)$ extracted from MMPE model.

A. MODIFIED OCEAN FREQUENCY RESPONSE AND OCEAN IMPULSE RESPONSE FROM MMPE MODEL

The modified ocean frequency response $H'(f)$ extracted from MMPE model as mentioned in Eq. (3.31) of Chapter III has $W = 300$ Hz, $f_c = 400$ Hz, $f_{s_{ocean}} = 300$ Hz and $n_f = 256$, where n_f represents the number of frequency components or FFT size. Let us consider a chosen depth of 50 m and range 5 km in the ocean environment having a positive SSP gradient. Figure C-1 shows the modified ocean frequency response $H'(f)$ and ocean impulse response $h'[n]$ obtained by taking the inverse DFT of $H'(f)$.

B. BASEBAND OCEAN IMPULSE RESPONSE BY PADDING ZEROS

To obtain the ocean impulse response at the same sampling frequency as the BPSK signal, we need to pad zeros between lower part and upper part of the modified ocean frequency response $H'(f)$. In this case, to obtain 8 times sampling frequency ($f'_{s_{ocean}} = 8f_{s_{ocean}}$) of the original sampling frequency of $f_{s_{ocean}} = 300$ Hz, we need to pad zeros between $-3f_c$ and $3f_c$, except for the interval $-\frac{W}{2} \leq f \leq \frac{W}{2}$. These zeros should be equally spaced as $\Delta f = \frac{W}{n_f - 1} = 1.1765$ Hz. Figure C-2 shows the baseband ocean frequency response $H_o(f)$ and ocean impulse response $h_o[n]$.

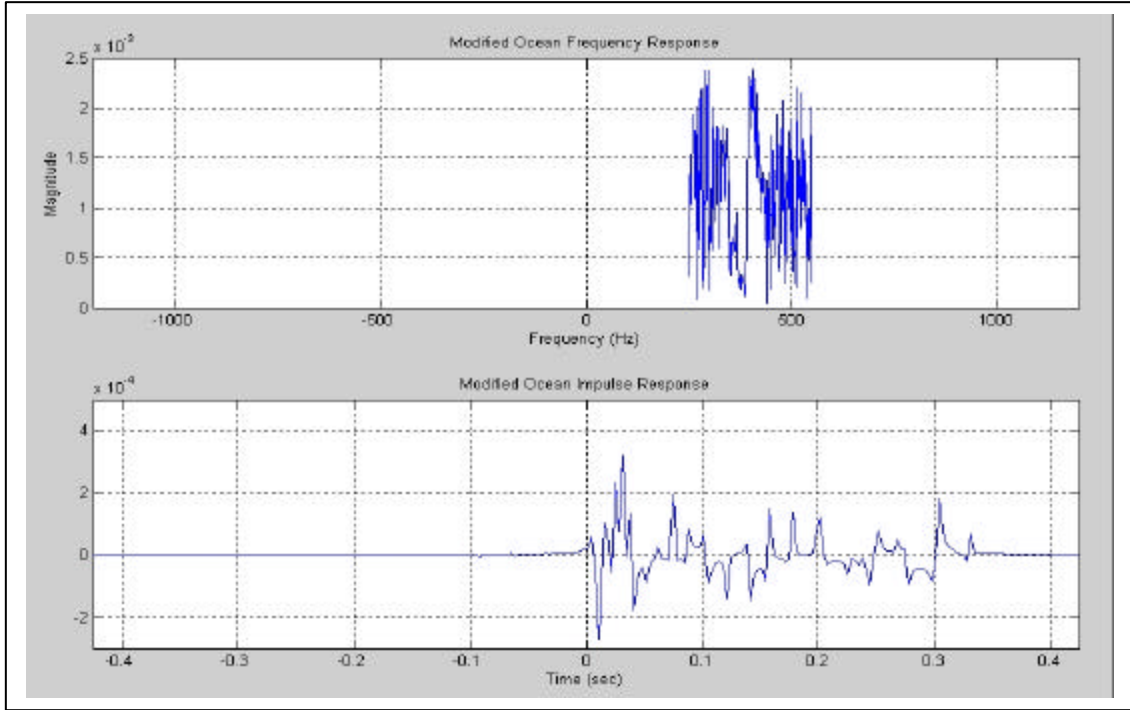


Figure C-1. Modified Ocean Frequency Response $H'(f)$ and Impulse Response $h'[n]$.

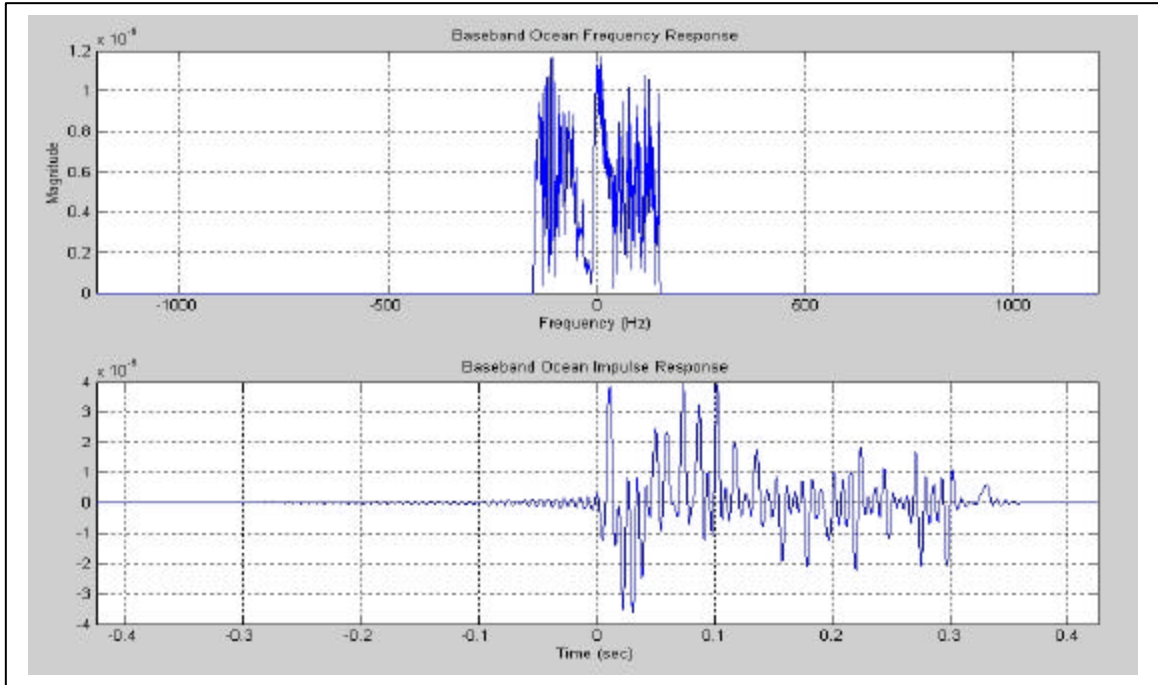


Figure C-2. Baseband Ocean Frequency Response $H_o(f)$ and Impulse Response $h_o[n]$.

C. FILTERING AND PRE-ENVELOPE OF THE OCEAN IMPULSE RESPONSE

Since the baseband ocean response $W = 300$ Hz, we need to filter it to have the same bandwidth as the BPSK signal (200 Hz). The FIR filter $h_{LPF}[n]$ is designed using a Hamming window as described in chapter 4. Figure C-3 shows the frequency response of the FIR filter and the filtered baseband ocean frequency response.

The filtered baseband ocean impulse response $h_{f,o}[n]$ is multiplied by $\exp(-j2\pi f_c t)$ to obtain the pre-envelope of the passband ocean impulse response, $h_p[n] = h_{f,o}[n] \cdot \exp(-j2\pi f_c t)$. Figure C-4 shows the frequency response of the pre-envelope of the ocean impulse response $H_p(f)$.

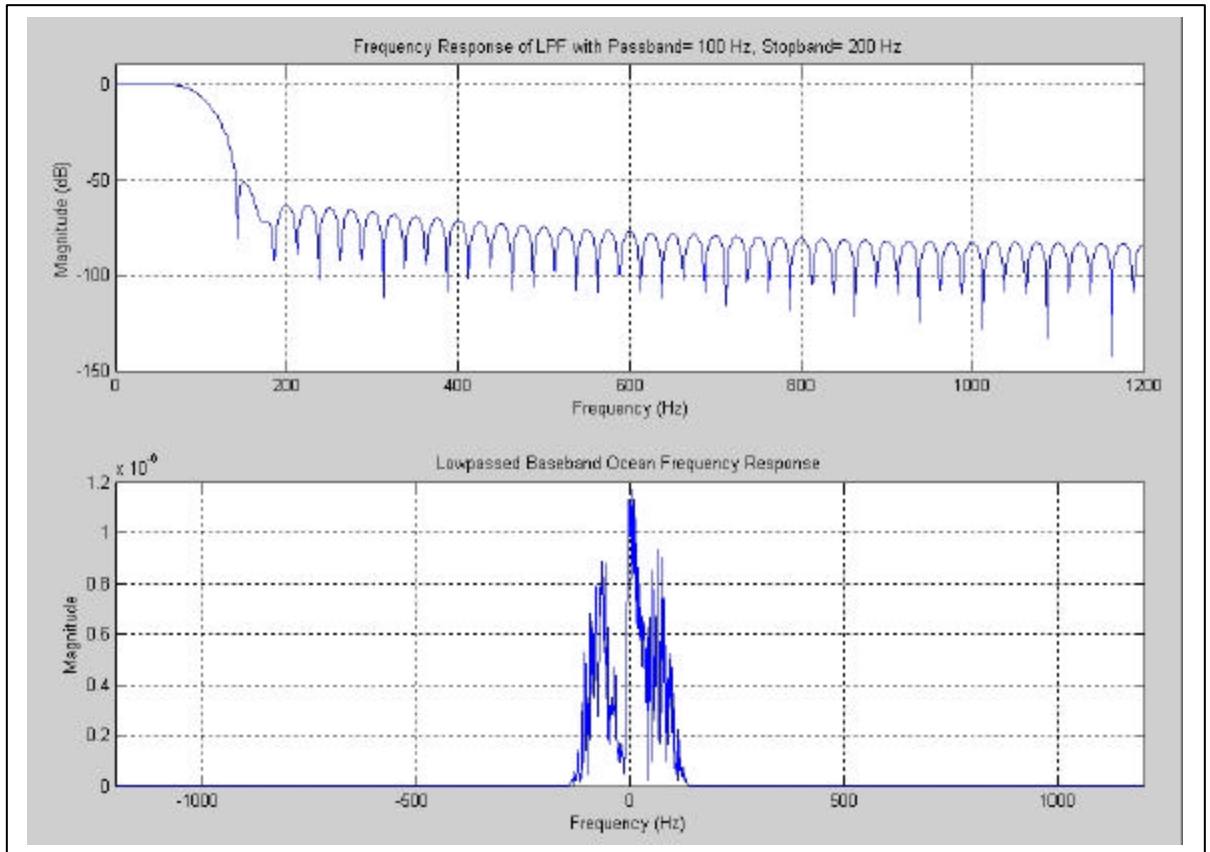


Figure C-3. Frequency Response of FIR Filter and Filtered Baseband Ocean Frequency Response.

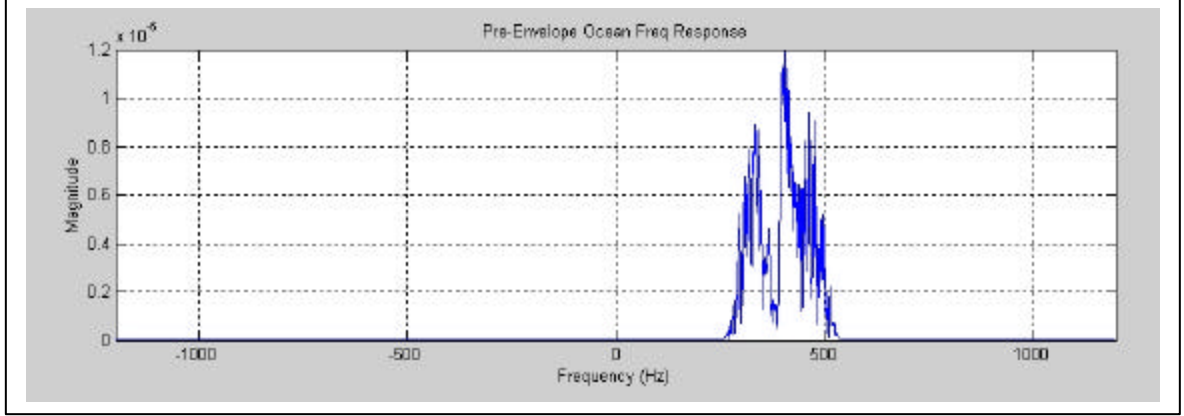


Figure C-4. Pre-Envelope Ocean Frequency Response $H_p(f)$.

D. PASSBAND OCEAN IMPULSE RESPONSE

Since the pre-envelope of the passband ocean impulse response is $h_p[n] = h_b[n] + j\hat{h}_b[n]$ where $h_b[n]$ is the passband ocean impulse response and $\hat{h}_b[n]$ is the Hilbert transform of $h_b[n]$ (see Ref 13). The passband ocean impulse response is obtained by taking the real part of $h_p[n]$ and by scaling by a factor of 2. The passband ocean impulse response is defined as $h_b[n] = 2\text{Re}(h_p[n])$. The passband frequency response $H_b(f)$ is obtained by doing the Fourier transform of $h_b[n]$. Figure C-5 shows the passband ocean frequency response.

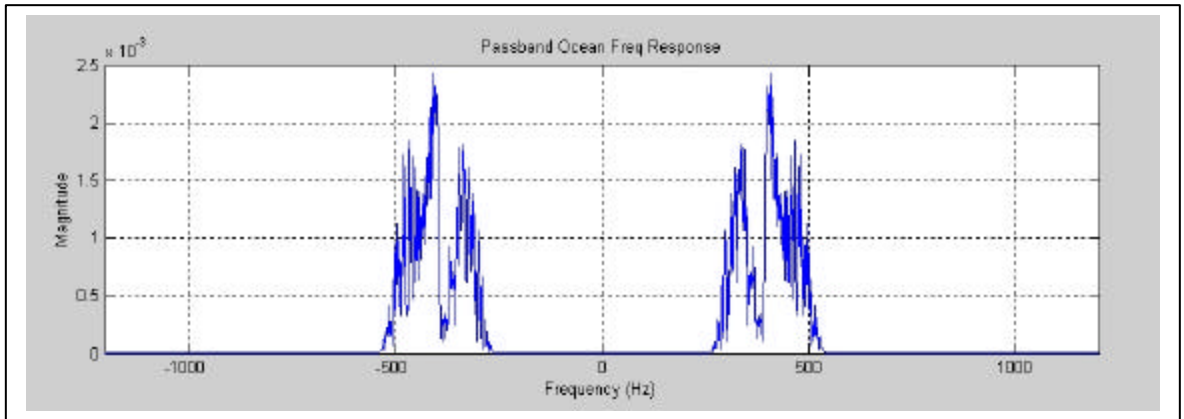


Figure C-5. Passband Ocean Frequency Response $H_b(f)$.

LIST OF REFERENCES

1. Sklar, Bernard, Digital Communications Fundamentals and Applications, 2nd Edition, Prentice- Hall, Inc., New Jersey, 2001.
2. Proakis, John G., Digital Communications, 4th Edition, McGraw-Hill, Inc., New York, 2001.
3. Couch, Leon W. II, Digital and Analog Communication Systems, 2nd Edition, Macmillan, Inc., New York, 1987.
4. Pittman III, Gell Tiger L., Simulation of an Orthogonal Frequency Division Multiplexing Based Underwater Communication System Using a Physics Based Model for the Underwater Acoustic Sound Channel, Master's Thesis, Naval Postgraduate School, September 2001.
5. Veyesl, Erdogan, A Simulation of MPSK Communications System Performance in the Presence of Wideband Noise and Co-Channel Interference, Master's Thesis, Naval Postgraduate School, December 1998.
6. Hsu, Hwei P., Schaum's Outline of Theory and Problems of Analog and Digital Communications, McGraw-Hill, Inc., 1993.
7. Kinsler, Lawrence E., Frey, Austin R., Coppens, Alan B., Sanders, James V., Fundamentals of Acoustics, John Wiley & Sons, Inc., New York, 2000.
8. Tappert, F. D. "The Parabolic Approximation Method," in Lecture Notes in Physics, Vol. 70, Wave Propagation and Underwater Acoustics, edited by J. B. Keller and J. S. Papadakis, Springer-Verlag, New York, 1977.
9. Smith, Kevin B., "Convergence, Stability, and Variability of Shallow Water Acoustic Predictions Using a Split-Step Fourier Parabolic Equation Model," *J. Comp. Acoust.*, Vol. 9, No. 1, June 2001.
10. Hardin, R. H. and Tappert, F. D., "Applications of the Split-Step Fourier Method to the Numerical Solution of Nonlinear and Variable Coefficient Wave Equations," *SIAM Rev.* 15, 1973.
11. Thomson, D. J. and Chapman, N. R. "A Wide-Angle Split-Step Algorithm for the Parabolic Equation," *J. Acoust. Soc. Am.*, Volume 74, 1983.
12. Therrien, Charles W., Discrete Random Signals and Statistical Signal Processing, Prentice-Hall, Inc., 1992.

13. Ziomek, L. J., Fundamentals of Acoustic Field Theory and Space Time Signal Processing, CRC Press, Boca Raton, Fl, 1995.

INITIAL DISTRIBUTION LIST

1. Defense Technical Information Center
Ft. Belvoir, Virginia
2. Dudley Knox Library
Naval Postgraduate School
Monterey, California
3. Prof. Kevin B. Smith, Code PH/SK
Department of Physics
Naval Postgraduate School
Monterey, California
4. Chairman, Code EC
Department of Electrical and Computer Engineering
Naval Postgraduate School
Monterey, California
5. Prof. Charles W. Therrien
Department of Electrical and Computer Engineering
Naval Postgraduate School
Monterey, California
6. Prof. Murali Tummala
Department of Electrical and Computer Engineering
Naval Postgraduate School
Monterey, California
7. LT Jung, Du San
Naval Postgraduate School
Monterey, California